PHOTOSYNTHETIC WATER OXIDATION AND PROTON-COUPLED ELECTRON TRANSFER

A Dissertation
Presented to
The Academic Faculty

by

Ian Blake Cooper

In Partial Fulfillment
of the Requirements for the Degree
Doctor of Philosophy in the
School of Chemistry and Biochemistry

Georgia Institute of Technology
December 2008

PHOTOSYNTHETIC WATER OXIDATION AND PROTON-COUPLED ELECTRON TRANSFER

Approved by:

Dr. Bridgette Barry, Advisor
School of Chemistry and Biochemistry
Georgia Institute of Technology

Dr. Mostafa El-Sayed
School of Chemistry and Biochemistry
Georgia Institute of Technology

Dr. Christoph Fahrni
School of Chemistry and Biochemistry
Georgia Institute of Technology

Dr. Nils Kröger
School of Chemistry and Biochemistry
Georgia Institute of Technology

Dr. Nael McCarty
School of Biology
Georgia Institute of Technology

Date Approved: November 6, 2008

ACKNOWLEDGMENTS

First and foremost, I wish to thank Dr. Bridgette Barry for her unending support and interest in my development as a scientist. I wish to thank Dr. Mostafa El-Sayed, Dr. Christoph Fahrni, Dr. Nils Kröger, and Dr. Nael McCarty for their participation as members of my thesis committee. I wish to thank Dr. Jun Chen, Dr. Antonio de Riso, Dr. Sascha Rexroth, Dr. Ilya Vassiliev, Shana Bender, Tina Dreaden, David Jenson, James Keough, Adam Offenbacher, Brandon Polander, and Robin Sibert for their discussion and support during my research efforts. I wish to thank the Petit Institute for Bioengineering and Bioscience for providing facilities in which to perform research. I wish to thank Dr. Brian Dyer, Dr. Scott Brewer, and Dr. Dung Vu at Los Alamos National Lab for being gracious hosts during my visits to LANL and for help in data collection and interpretation. I wish to thank my family and friends for their support and love during this period of my life. I especially wish to thank my wife, Robyn, for her undying love and support. Finally, I wish to thank God for giving me the mind and strength to succeed in science.

TABLE OF CONTENTS

Page

ACKNOWLEDGMENTS iii

LIST OF TABLES vii

LIST OF FIGURES viii

LIST OF ABBREVIATIONS x

LIST OF SYMBOLS xii

SUMMARY xiii

CHAPTERS

1 INTRODUCTION 1

Structure of Photosystem II 1

Function and Kinetics of Photosystem II 5

Inorganic Cofactors of the OEC 7

Redox-Active Tyrosines 9

Proton-Coupled Electron Transfer 10

Vibrational Spectroscopy 12

Electron Paramagnetic Resonance (EPR) Spectroscopy 17

Thesis Overview 19

References 20

2 TIME-RESOLVED VIBRATIONAL SPECTROSCOPY DETECTS PROTEIN-BASED INTERMEDIATES IN THE PHOTOSYNTHETIC OXYGEN-EVOLVING CYCLE 34

Abstract 34

Introduction 35

Materials and Methods 38

Results 39

Discussion 44

References 46

3 PROTON COUPLED ELECTRON TRANSFER REACTIONS AND TYROSINE Z OF THE PHOTOSYNTHETIC WATER OXIDIZING COMPLEX 51

Abstract 51

Introduction 52

Materials and Methods 55

Results and Discussion 56

References 70

4 PERTURBATIONS AT THE CHLORIDE SITE DURING THE PHOTOSYNTHETIC OXYGEN-EVOLVING CYCLE 76

Abstract 76

Introduction 77

Materials and Methods 80

Results 82

Discussion 97

Summary 101

References 101

5 AZIDE AS A PROBE OF PROTON TRANSFER REACTIONS IN PHOTOSYNTHETIC OXYGEN EVOLUTION 109

Abstract 109

Introduction 110

Materials and Methods 113

Results 114

Discussion 126

References 129

6 CONCLUSIONS 136

VITA 141

LIST OF TABLES

Page

Chapter 2

Table 1 44

Chapter 3

Table 1 58

Table 2 63

Table 3 65

Chapter 4

Table 1 83

Table 2 84

Chapter 5

Table 1 115

LIST OF FIGURES

Page

Chapter 1

Figure 1 2

Figure 2 3

Figure 3 4

Figure 4 6

Figure 5 9

Figure 6 11

Figure 7 13

Figure 8 14

Chapter 2

Figure 1 36

Figure 2 41

Figure 3 43

Chapter 3

Figure 1 57

Figure 2 59

Figure 3 61

Figure 4 62

Figure 5 64

Figure 6 67

Chapter 4

Figure 1 85

Figure 2 87

Figure 3 89

Figure 4 91

Figure 5 93

Figure 6 95

Figure 7 96

Chapter 5

Figure 1 116

Figure 2 117

Figure 3 120

Figure 4 123

Figure 5 125

LIST OF ABBREVIATIONS

AU	Absorbance Units
CcO	Cytochrome *c* Oxidase
Chl	Chlorophyll
CP43	Chlorophyll binding polypeptide subunit of PSII
CP47	Chlorophyll binding polypeptide subunit of PSII
CPET	Coupled proton-electron transfer
D1	Reaction center binding polypeptide subunit of PSII
D2	Reaction center binding polypeptide subunit of PSII
DCBQ	2,6-dichlorobenzoquinone
DCMU	3-(3,4-dichlorophenyl)-1,1-dimethylurea
ENDOR	Electron-nuclear double resonance
EPR	Electron paramagnetic resonance
ESEEM	Electron spin-echo envelope modulation
ET	Electron transfer
ETPT	Electron transfer proton transfer
EXAFS	Extended X-ray absorption fine structure
FT-IR	Fourier-transform infrared
HAT	Hydrogen atom transfer
HEPES	4-(2-hydroxyethyl)-1-piperazineethanesulfonic acid
KIE	Kinetic isotope effect
kDa	kilo-Dalton
MCT	Mercury-cadmium-telluride
MES	2-(*N*-morpholino)ethanesulfonic acid

MSP	Manganese stabilizing protein
Nd:YAG	Neodymium:yttrium aluminum garnet
OEC	Oxygen-evolving complex
PCET	Proton-coupled electron transfer
Pheo	Pheophytin
PGHS-1	Prostaglandin H synthase-1
PPBQ	Phenylparabenzoquinone
PSII	Photosystem II
PT	Proton transfer
PTET	Proton transfer electron transfer
RC	Reaction center
RNR	Ribonulceotide reductase
Tris	Tris(hydroxymethyl)aminomethane
UV	Ultraviolet
XANES	X-ray absorption near edge structure
YAG	Ytrrium aluminum garnet

LIST OF SYMBOLS

B_0	Magnetic field strength
g	Constant characterizing the magnetic moment of an electron
h	Planck's constant
K_i/K_i'	Inhibitor disassociation constants
K_m	Michaelis constant
μ_B	Bohr magneton
v	Frequency
P_{680}	Special pair chlorophyll
Q	Plastoquinone
S_n	OEC oxidation states where n = 0 - 4
V_{max}	Maximum enzymatic activity
Y_D, D	Y160 of the D2 polypeptide subunit
Y_Z, Z	Y161 of the D1 polypeptide subunit

SUMMARY

Photosystem II (PSII) is the membrane-bound oxidoreductase peptide complex responsible for the oxidation of water to molecular oxygen and reduction of plastoquinone to plastoquinol. Primary electron transfer is initiated upon absorption of a photon by the primary donor chl resulting in electron transfer and production of a $P_{680}^{+}Q_A^{-}$ charge separated state. P_{680}^{+} is reduced by Y_Z (Y161 of the D1 polypeptide subunit), one of two redox-active tyrosine residues found in PSII. This produces a neutral tyrosyl radical ($Y_Z^{\bullet}$) which is subsequently reduced by electrons derived from water at the oxygen-evolving complex (OEC). The OEC is composed of four manganese, one calcium ion, and one chloride ion. Four photons are required to convert water to O_2, each photon advancing the OEC through successive oxidation states or S states. The exact chemical mechanism of water oxidation in PSII is not known. However, proton-coupled electron transfer (PCET) is thought to be one of the fundamental steps in driving the extraction of electrons and protons from water. Here, the mechanism of water oxidation is investigated with focus on PCET events using vibrational spectroscopy. Vibrational spectroscopy is sensitive to changes in protein structure, charge, and hydrogen bonding, and is ideal for the study of fast events coupled with light-induced electron transfer. The results presented here demonstrate the utility of time-resolved infrared spectroscopy in the detection of intermediates of photosynthetic water oxidation. We suggest that proton transfer may precede manganese oxidation during water oxidation based on time-resolved infrared and difference FT-IR spectroscopic results. The mechanism of PCET associated with $Y_Z^{\bullet}$ reduction is

investigated. Using reaction-induced difference FT-IR spectroscopy, the identity of the chloride binding site is speculated through the use of bromide exchange at the OEC. Also, proton transfer reactions at the OEC are investigated using azide as a vibrational probe. The advances in the understanding of photosynthetic water oxidation gained in this work will aid in the elucidation of the chemical mechanism of this important reaction. Understanding the details of photosynthetic water oxidation will assist in the development of technology aimed at harnessing the energy of the sun for the benefit of humankind.

CHAPTER 1

INTRODUCTION

Structure of Photosystem II

The reduction equivalents required for carbon fixation in plants, algae, and cyanobacteria are provided by the water splitting reactions of the oxidoreductase complex photosystem II (PSII). PSII is composed of 20 polypeptide subunits and contains 36 chlorophyll (Chl) molecules, 7 β-carotene molecules, 2 pheophytin (Pheo) molecules, 2 plastoquinone (Q) molecules, 1 heme molecule, 1 non-heme Fe^{+2}, 4 variable oxidation state Mn, 1 Ca^{+2}, and 1 Cl^{-} (figure 1) [1-6]. The oxidation of water is carried out by the reaction center (RC) complex. The RC consists of 4 Chl, 2 Pheo, 2 Q (Q_A and Q_B), 2 redox-active tyrosines (Y_Z and Y_D), 4 Mn, 1 Ca^{+2}, and 1 Cl^{-} (figure 2; Cl^{-} not shown). The components of the RC are ligated by the D1 and D2 polypeptide subunits, with important amino acids thought to be involved in water oxidation provided by the CP43 polypeptide subunit. The Mn_4Ca complex, along with Cl^{-} and Y_Z, constitute the oxygen-evolving complex (OEC). Figure 3 shows the OEC from a recent crystal structure [6]. In this figure, nearby amino acids are shown which may ligate Mn or may play direct and indirect roles in water oxidation chemistry. Electron density has not been assigned to Cl^{-} in recent crystal structures. Though the lack of Cl^{-} is not addressed, Cl^{-} loss may be a consequence of the crystallization process or a result of X-ray damage [7].

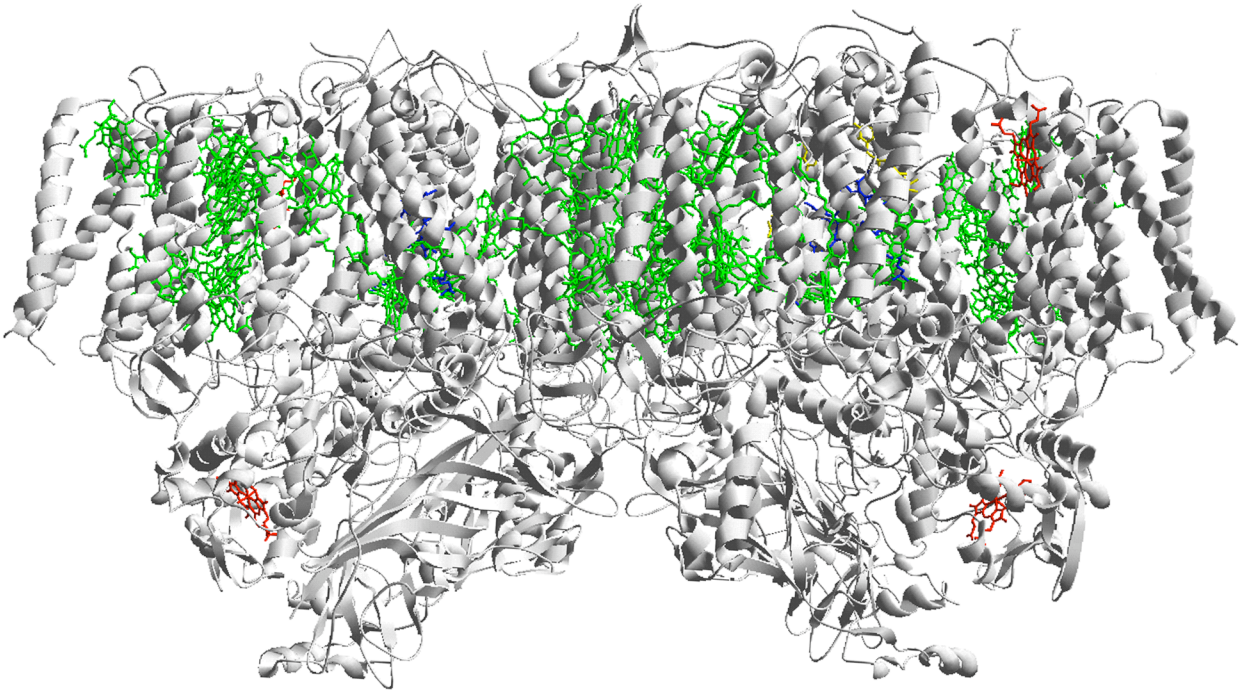

Figure 1. X-ray crystal structure of dimeric PSII from *Thermosynechococcus elongatus* solved to 3.0 Å resolution [6]. Figure generated using Deep View/Swiss PDB Viewer 3.7 and Brookhaven Protein Data Bank file 2AXT. Peptide secondary and tertiary structure is shown as gray ribbons, chlorophyll is green, heme is red, pheophytin is blue, and plastoquinone is yellow.

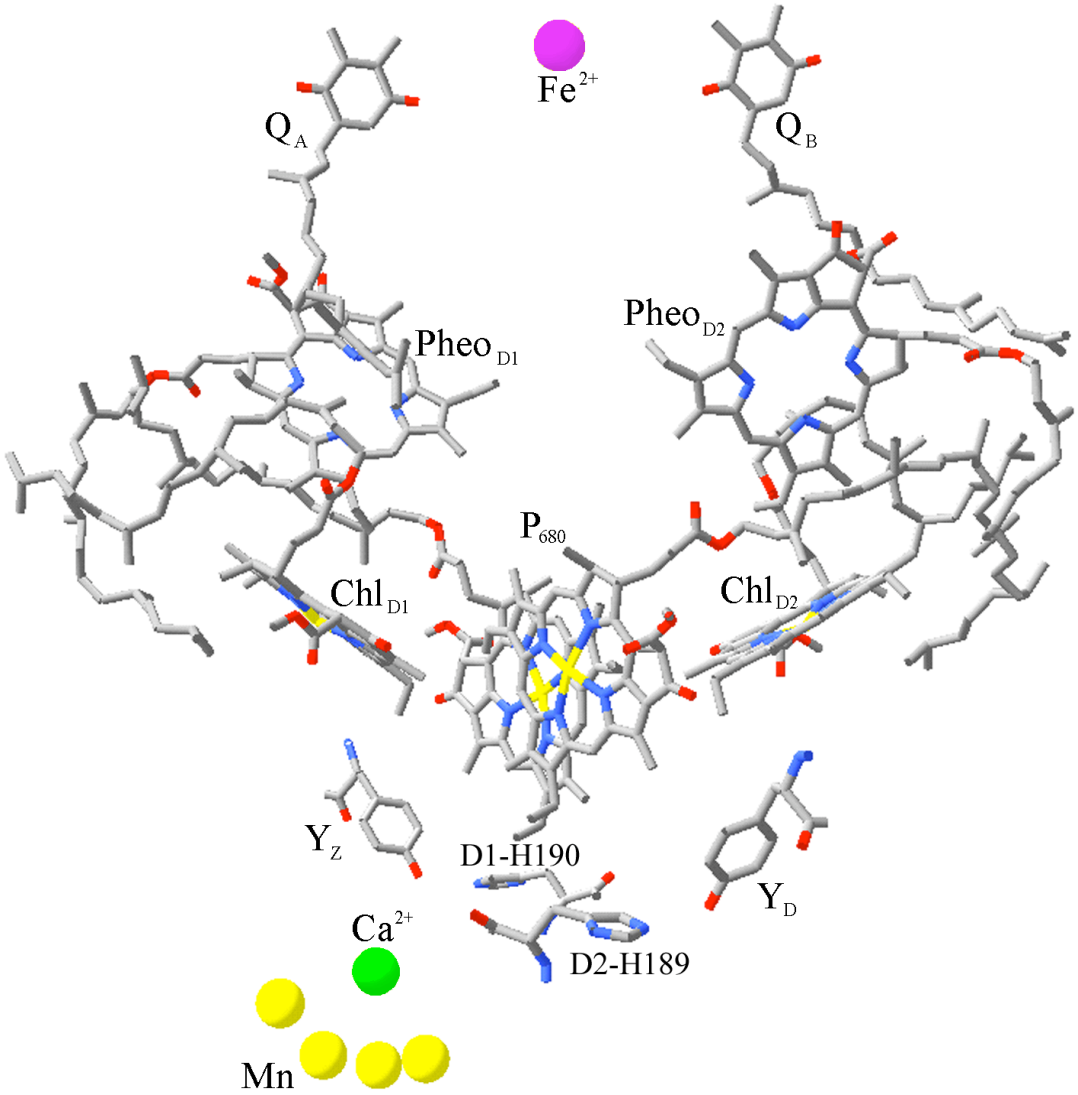

Figure 2. Arrangement of electron transfer cofactors of PSII [6]. Figure generated using Deep View/Swiss PDB Viewer 3.7 and Brookhaven Protein Data Bank file 2AXT. Calcium is green, carbon is gray, iron is purple, manganese is yellow, nitrogen is blue, and oxygen is red.

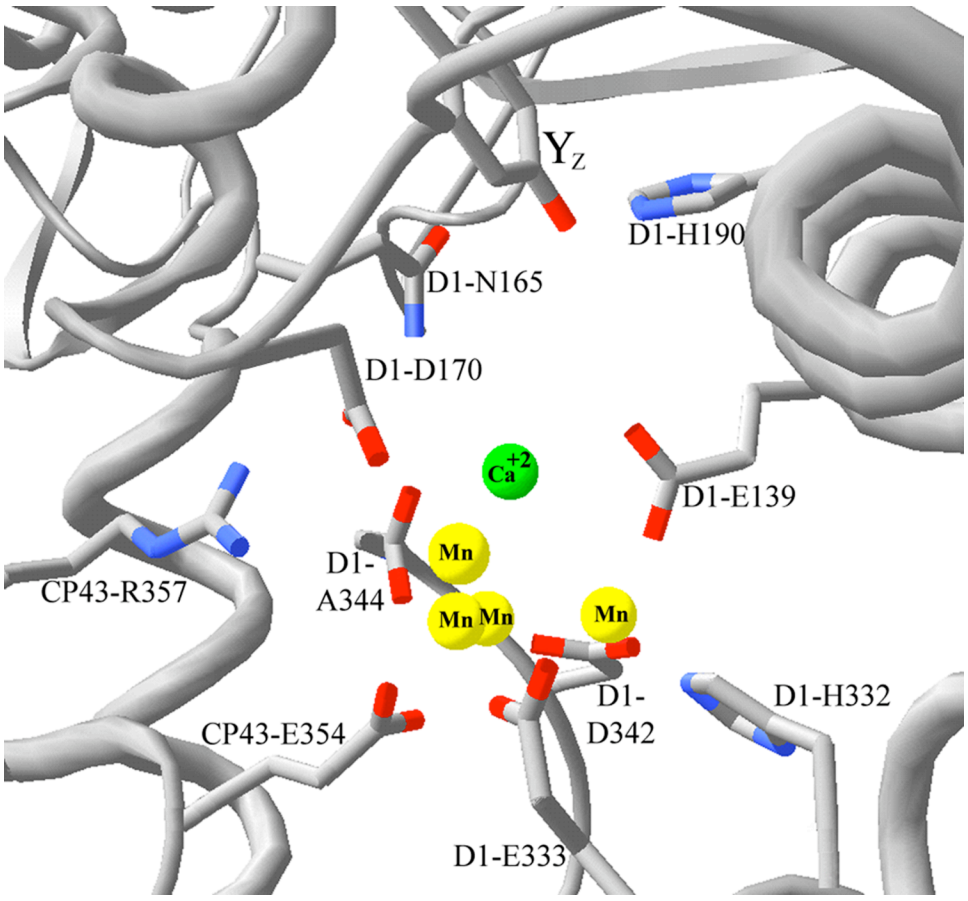

Figure 3. View of the OEC and neighboring amino acids [6]. Figure generated using Deep View/Swiss PDB Viewer 3.7 and Brookhaven Protein Data Bank file 2AXT. Calcium is green, carbon is gray, manganese is yellow, nitrogen is blue, and oxygen is red. Local secondary structure elements are displayed as gray ribbons.

Function and Kinetics of Photosystem II

PSII derives reduction equivalents required for carbon fixation from the light-driven oxidation of water to O_2, protons, and electrons and reduction of plastoquinone to plastoquinol. The kinetics of electron transfer in PSII varies widely between sub-nanosecond and millisecond timescales (figure 4). The primary step in water oxidation is charge separation between the primary donor Chl and Pheo upon absorption of visible light of sufficient wavelength and intensity [8, 9]. Some controversy exists surrounding the identity of the primary electron donor to Pheo in this initial event. Primary charge separation is thought to occur between Chl_{D1} and Pheo [8-10]. The positive hole left by electron transfer from Chl_{D1} after light-induced charge separation is proposed to migrate to P_{680}, the chl dimer composed of P_{D1} and P_{D2} at the D1/D2 polypeptide subunit interface [11]. $Pheo^-$ is oxidized by Q_A with a time constant of 250-500 ps [12, 13]. P_{680}^+ will oxidize D1-Y161 (Y_Z) to produce a neutral tyrosyl radical ($Y_Z^\bullet$). In O_2 evolving PSII complexes, with an intact OEC, this event occurs on the nanosecond timescale [14, 15]. However, in Mn-depleted PSII, the kinetics of P_{680}^+ reduction is slowed to the microsecond timescale [16, 17]. The reaction between P_{680}^+ and Y_Z is in competition with charge recombination ($P_{680}^+Q_A^- \rightarrow P_{680}Q_A$). Charge recombination between Q_A^- and P_{680}^+ occurs with a time constant of 150-200 μs [16, 18]. $Y_Z^\bullet$ is reduced by the Mn_4Ca cluster on the microsecond to millisecond timescale with electrons derived from the oxidation of water [19]. The reduction of $Y_Z^\bullet$ is slowed as the number of oxidizing equivalents stored at the Mn_4Ca cluster increases [19]. An electron is passed from Q_A^- to Q_B on the microsecond timescale [20]. A second charge separation will

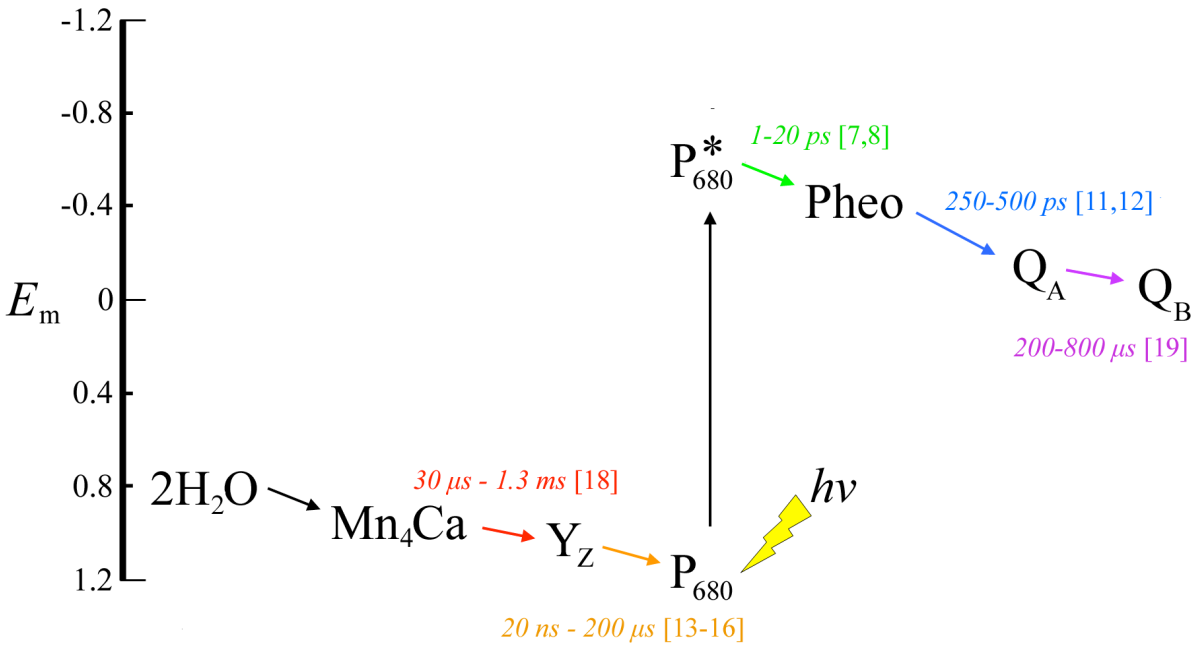

Figure 4. Diagram of the electron transfer cofactors of PSII with approximate electron transfer times color-coded to each event. Arrows starting at water and ending at Q_B indicate forward electron flow. The placement of electron transfer cofactors relative to the vertical axis indicates the approximate midpoint potential (E_m) in volts at pH 6.5 ([151] and references therein).

result in a doubly reduced plastoquinol (Q_BH_2) which then diffuses from the Q_B active site, allowing a fully oxidized Q to bind. Each round of charge separation advances the OEC through oxidation states known as S_n states (S_0 - S_4). The subscript denotes the number of oxidizing equivalents stored at the OEC. Molecular oxygen is liberated during the $S_3 \rightarrow [S_4] \rightarrow S_0$ transition in which the transient S_4 state is formed. Information about the transient S_4 state has been collected using transient UV [21], EPR [22], X-ray absorption [23], and transient infrared [24] spectroscopies.

Inorganic Cofactors of the OEC

Calcium

The quantum efficiency of PSII is dependent on the integrity of the RC and associated polypeptides. Removal of extrinsic 18 and 24 kDa polypeptides from the lumenal side of PSII results in loss of Ca^{+2} and/or Cl^- binding affinity at the OEC, depending on the method of polypeptide depletion [25-27]. Loss of Ca^{+2} and Cl^- leads to diminished oxygen-evolving capabilities. Ca^{+2} can be replaced with Sr^{+2} to restore oxygen evolution [25, 28]. However, the $S_3 \rightarrow [S_4] \rightarrow S_0$ transition is retarded in the presence of Sr^{+2} [29, 30]. Cd^{+2} will also bind at the OEC Ca^{+2} binding site but will not restore oxygen evolution [31-34]. Other cations have been shown to compete with Ca^{+2} for binding at the OEC including Cs^+, K^+, and La^{3+} ([35] and references therein). Some of the proposed roles that Ca^{+2} may play in water oxidation include maintenance of Mn reduction potential [36], maintenance of a hydrogen-bonded network [37, 38], and activation of substrate water [32, 39]. Ca^{+2} may also play a role in assembly of the Mn_4Ca cluster [34].

Chloride

Cl^- is known to bind near the OEC [40, 41], and previous studies have identified one Cl^- per OEC [40]. In the absence of Cl^-, other anions have been found to activate oxygen evolution to varying degrees: $Br^- >> NO_3^- > NO_2^- > I^-$ [42, 43]. Other anions such as F^- [44, 45], SO_4^{-2} [26, 46], and N_3^- [47, 48] inhibit oxygen evolution by binding at the Cl^- site in the OEC. Although electron density has been assigned to Ca^{+2}, X-ray crystal structures have not identified the specific location of Cl^- [2-6]. Cl^- has been proposed to have a role as a ligand to Mn in the OEC [49], in maintaining a hydrogen-

bonded network, which facilitates proton transfer [50], in maintaining the potential of the Mn cluster [51], or in activation of substrate water [52]. Cl^- may associate with amino acids [53, 54], or Cl^- may be bound to Mn [49].

Manganese

Four Mn are present in the OEC [55]. The oxidizing equivalents necessary to drive oxygen production from water are stored at this cluster of Mn. The structure and orientation of Mn in the OEC is hinted at in recent crystal structures [5, 6], though X-ray damage during data collection cannot be discounted [56]. Many different structures have been proposed based on extended X-ray absorption fine structure (EXAFS) measurements [57, 58], ^{55}Mn electron-nuclear double resonance (ENDOR) spectroscopy [59, 60], electron spin-echo envelope modulation (ESEEM) [61], EPR [60] spectroscopy, the crystal structures [5], and quantum mechanical/molecular mechanical density functional theory calculations [62-64]. Some of the proposed structures derived from EXAFS, X-ray crystal structures, and computer modeling are shown in figure 5. In addition to speculation about the structure of the Mn cluster, the oxidation states of Mn at each S state have been proposed. Information about Mn oxidation states has been collected using X-ray absorption near-edge structure (XANES) and magnetic resonance techniques (reviewed in [65]). Various experiments conducted over many years have lead to the consensus that, for oxidation states S_0 - S_3 of the Mn cluster, the oxidation states of the four Mn ions are (II, III, IV, IV or III, III, III, IV), (III, III, IV, IV), (III, IV, IV, IV), and (IV, IV, IV, IV), respectively. Removal of the Mn cluster leads to complete loss of oxygen evolution [66, 67]. Various methods have been developed to remove Mn from the OEC including treatment with Tris [66], NH_2OH [68], and high pH [69].

A.

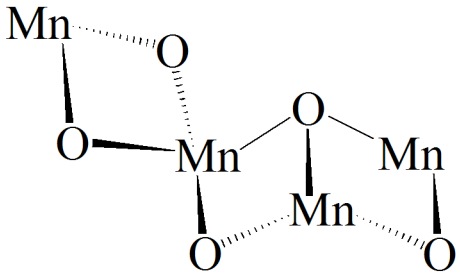

B.

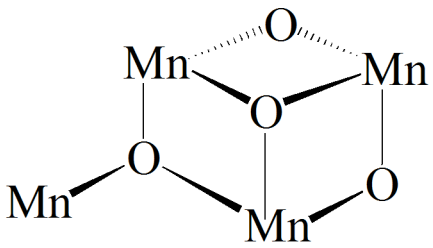

Figure 5. Mn cluster models derived from X-ray absorption experiments, X-ray crystal structures, and computer modeling. A. Model derived from single crystal EXAFS [152]. B. The cuboid-type model derived from an X-ray crystal structure and density functional theory calculations [5, 62].

Redox-Active Tyrosines

Redox-active tyrosines play a role in many biological systems. In prostaglandin H synthase-1 (PGHS-1), Y385$^{\bullet}$ oxidizes bound arachidonic acid to form a fatty acyl radical prior to the cyclooxygenase step in the production of prostaglandin G_2 [70, 71]. In class IA ribonucleotide reductase (RNR), a cysteinyl radical necessary for ribonucleotide reduction in the R1 subunit active site is generated by Y122$^{\bullet}$ of the R2 subunit. The electron is proposed to travel the 35 Å distance between Y122 and C439 via transient amino acid radical intermediates [72, 73]. In cytochrome *c* oxidase (CcO),

Y244, covalently linked to H240, becomes a tyrosyl radical when providing reduction equivalents necessary for O-O bond breakage during the formation of intermediate P [74, 75]. Galactose oxidase is another example of an enzyme that employs a covalently linked tyrosine. Y272 is attached to C228 via a thioether linkage and aids in the oxidation of primary alcohols at the mononuclear Cu site via radicalization [76].

In PSII, two tyrosine residues play redox-active roles, Y161 of the D1 subunit (Y_Z) and Y160 of the D2 subunit (Y_D) [77-79]. Each residue is within hydrogen bonding distance of nearby histidines, D1-H190 and D2-H189 for Y_Z and Y_D, respectively. Though both tyrosines can reduce P_{680}^+, Y_Z is most directly involved in electron transfer reactions associated with water oxidation at the Mn cluster. Y_D is a dark stable radical and is thought to play a role in Mn cluster assembly [80] and photoprotection [81].

Proton-Coupled Electron Transfer

Proton-coupled electron transfer (PCET) is employed in biology to facilitate charge transport and catalysis in metabolism. In enzymes, the coupling of proton transfer (PT) and electron transfer (ET) occurs with tight control over kinetics and thermodynamic driving forces. Collinear PCET arises when ET occurs via hydrogen bond pathways or through hydrogen atom transfer (HAT) [73]. Orthogonal PCET is also common in which ET and PT occur along different coordinates. Due to the greater mass of a proton, PT is limited to relatively short distances compared to ET. The emergence of orthogonal PCET in enzymes may mitigate this difference in transport distances [73]. PCET can be further subdivided into concerted proton-electron transfer (CPET) where ET and PT proceed through one kinetic step, ET followed by PT (ETPT), or PT followed

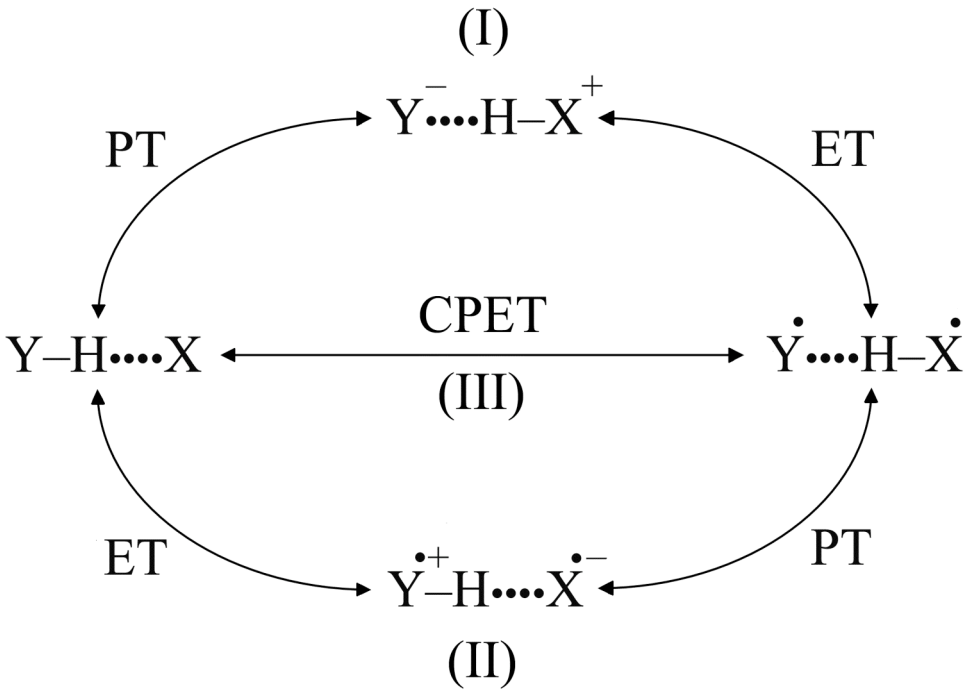

Figure 6. Illustration of the possible pathways for proton-coupled electron transfer (PCET) to occur. PTET (path I) involves proton transfer followed by electron transfer. ETPT (path II) involves electron transfer followed by proton transfer. CPET (path III) involves transfer of both proton and electron in one kinetic step.

by ET (PTET) (figure 6). Each mechanism can be distinguished kinetically by sensitivity to pH and solvent isotope exchange as demonstrated through the use of model systems [82-87].

As a result of light-induced charge separation, electrons are removed from the OEC. The positive charge that accumulates at the OEC with S state advancement may be alleviated by proton release. If positive charge were allowed to grow and persist, redox potentials would increase and high-energy intermediates would be unavoidable [87]. Two examples of PCET proposed to occur during water oxidation (oxidation/reduction of

Y_Z and Mn cluster oxidation) are both considered orthogonal PCET reactions. Upon oxidation of Y_Z by P_{680}^+, the phenolic proton of Y_Z may move to D1-H190 ([88-90], but see [91]). Once reduced by the Mn cluster, Y_Z is thought to reaccept the proton from D1-H190 (figure 7). Oxidation of the Mn cluster via electron transfer to $Y_Z^\bullet$ has been proposed to be coupled to deprotonation of substrate water to CP43-R357 (figure 8) [52, 92-94]. As part of this deprotonation mechanism, D1-D61 accepts a proton from CP43-R357 and may form the entrance to a proton exit pathway to the lumen of the thylakoid [63, 87, 93, 95, 96].

Vibrational Spectroscopy

Vibrational spectroscopy is concerned with the detection and identification of normal vibrational modes of polyatomic molecules. Normal vibrational modes of a molecule arise from the dynamical behavior associated with the motions of the atomic nuclei [97]. Spectroscopic detection of normal vibrational modes is dependent on the transition from one vibrational energy level to another. Vibrational energy transitions can occur only when the molecular dipole moment is modulated by the motion of a normal mode within a normal coordinate of a molecule [97]. Normal coordinates refers to the molecular coordinates representing the equilibrium geometry of a molecule. If the dipole moment varies within a given normal coordinate, then the molecule can exchange energy with an oscillating electromagnetic field of frequency matching a particular normal mode vibration [97]. The energy absorption that results from the interaction of normal mode vibrations with an electromagnetic field can be observed spectroscopically

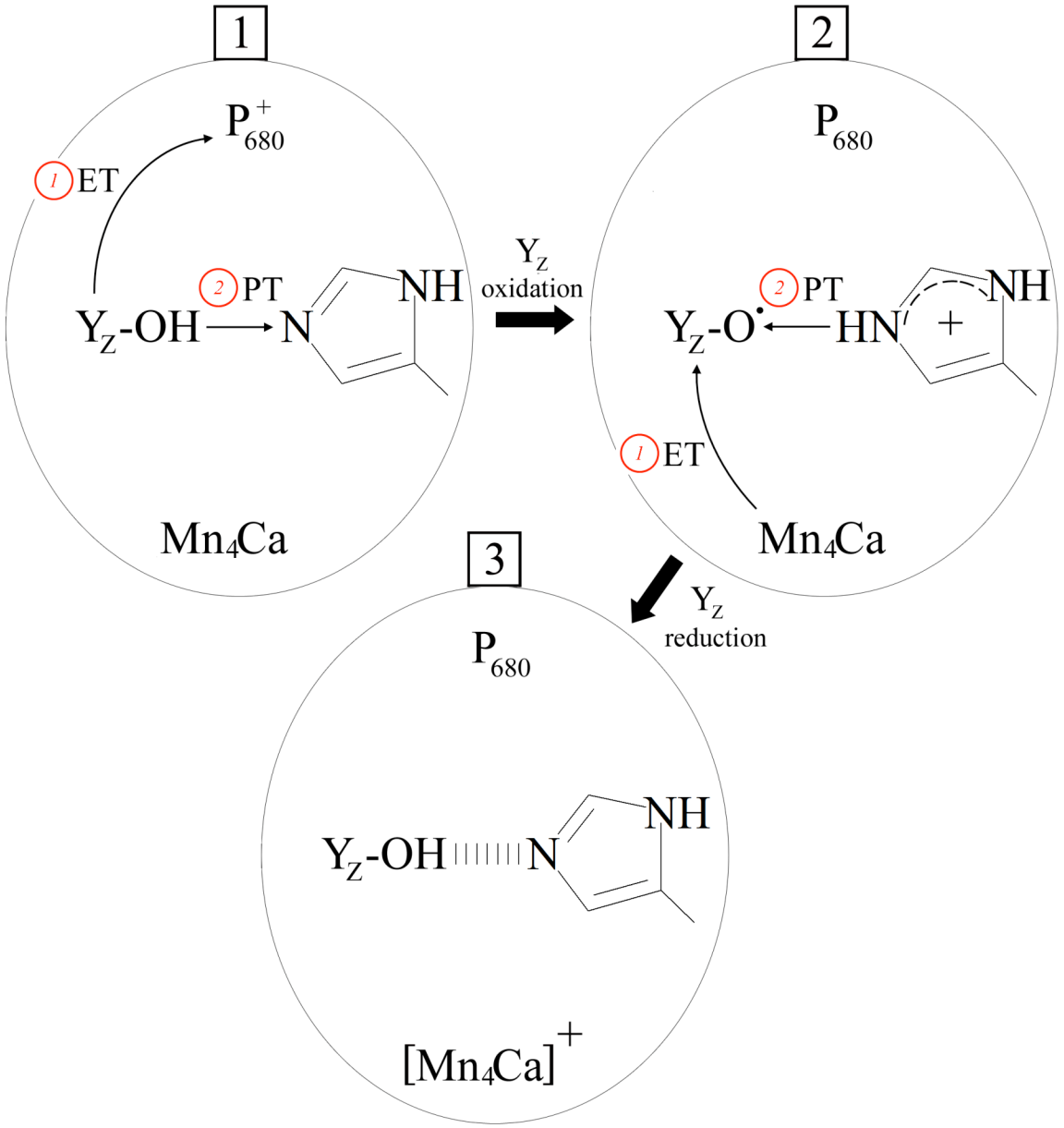

Figure 7. Examples of PCET proposed to occur in the OEC of PSII. These examples are proposed to occur during each S state transition. In circle 1, Y_Z reduces P_{680}^+ (1) which is proposed to result in proton transfer from Y_Z^+ to D1-H190 (2) ([88-90], but see [91]). In circle 2, Mn_4Ca reduces $Y_Z^{\bullet}$ (1), and upon reduction Y_Z^- is then proposed to reaccept a proton from D1-H190 (2) ([88-90], but see [91]). The final result is shown in circle 3 in which a hydrogen bond is shown between Y_Z and D1-H190 and Mn_4Ca has lost an electron. Using the nomenclature of figure 6, these examples involve an ETPT mechanism.

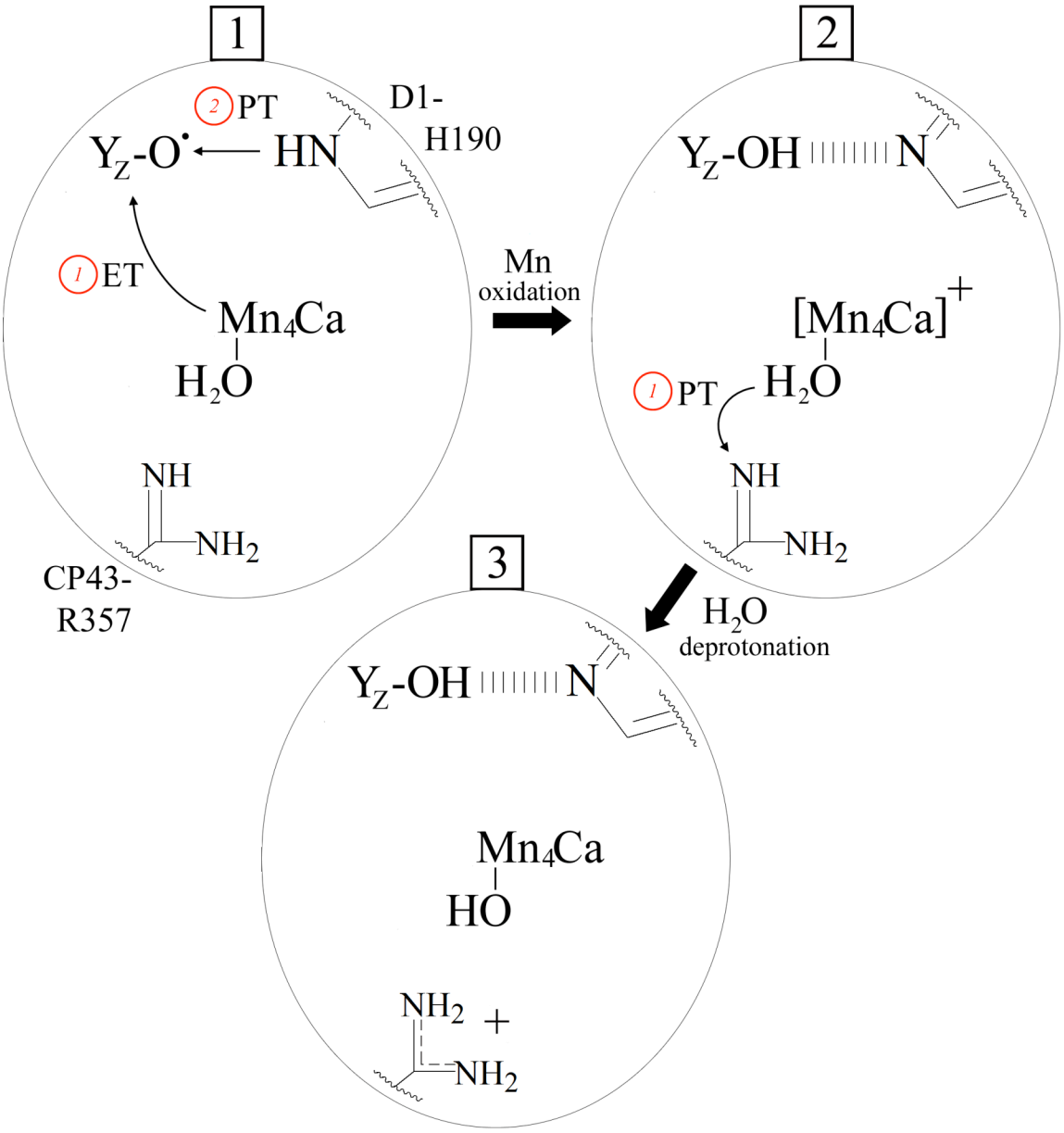

Figure 8. Example of PCET proposed to occur in the OEC of PSII. This example is proposed to occur during the S_2 to S_3 transition. Prior to the events of circle 1, CP43-R357 is proposed to become deprotonated. In circle 1, $Y_Z^{\bullet}$ is reduced by Mn_4Ca (1) which is proposed to result in proton transfer from D1-H190 to Y_Z^- (2) [52, 92-94]. In circle 2, a hydrogen bond in shown between Y_Z and D1-H190 and water bound to $[Mn_4Ca]^+$ transfers a proton to nearby CP43-R357 (1) [52, 92-94]. The final result is shown in circle 3 in which CP43-R357 has gained a positive charge after receiving a proton from water bound to Mn_4Ca.

as absorption bands. One may calculate the normal modes of vibration for a molecule through the use of isotopic substitution in experiment to compare shifts of vibrational motion caused by mass changes of component nuclei. One may also calculate the normal modes of vibration for a molecule using hybrid density functional theory computational methods.

Fourier Transform Infrared (FT-IR) Spectroscopy

Unlike dispersive infrared spectrometers, which measure the intensity of individual frequencies one at a time, FT-IR spectrometers employ an interferometer that allows the detection of all accessible infrared frequencies concomitantly and with greater time resolution. An interferometer is composed of a moving mirror, fixed mirror, and beamsplitter. As infrared light enters the interferometer, half of the light passes through the beamsplitter to the fixed mirror and the other half is reflected to the moving mirror. The separated light will recombine both constructively and destructively as a result of the differing distances the moving and fixed mirrors are from the beamsplitter. After leaving the interferometer, and passing through a sample, the light incident upon a detector surface is separated into the various component frequencies by Fourier transformation.

FT-IR spectroscopy can provide structural information including covalent bond strength, protonation, hydrogen-bonding, and electrostatic interactions. Particularly in biological samples, FT-IR spectroscopy can be performed under physiologically relevant conditions, which can supplement information from other structural techniques such as X-ray crystallography. In order to isolate specific reactions of an enzyme system, a technique known as reaction-induced FT-IR difference spectroscopy has been used [98-

103]. In this technique, infrared spectra taken before and after a reaction are compared in order to ascertain structural changes that occur as a result of the reaction.

PSII has been studied extensively using reaction-induced FT-IR difference spectroscopy. The oxygen-evolving cycle has been documented using reaction-induced methods and has revealed the individual infrared fingerprints of each S state transition on the seconds timescale [101, 104-106]. Infrared band assignments have been made based on shifts in normal mode vibrations caused by isotope labeling of specific amino acids [107-110] and solvent isotope exchange [101, 111]. Site-specific mutation of residues in and around the OEC has provided insight into the necessity of particular amino acids in water oxidation and Mn cluster assembly [112-114]. In addition to the detection of peptide and amino acid sidechain vibrational modes, metal-ligand interactions are accessible at low frequencies [115]. Also, cofactor depletion and replacement has aided in the identification of potential binding sites within the OEC [43, 101, 106, 116].

Time-Resolved Infrared Spectroscopy

In addition to the high-resolution structural advantage associated with the use of infrared spectroscopy, kinetic information may also be gathered. Fast events in catalysis including electron transfer, proton transfer, and peptide conformational changes can be monitored via infrared absorption [117-119]. In FT-IR spectroscopy, time resolution is exchanged for broad spectral resolution. However, greater time resolution can be achieved by focusing on a particular infrared frequency. With potentially sub-microsecond resolution, kinetics associated with changes in absorptivity or secondary structure can be examined and attributed to particular reaction events and/or participants [120].

PSII has been studied by time-resolved techniques in the past. Using visible absorption, the kinetics of P_{680}^{+} reduction have been observed in both intact and Mn-depleted preparations [16, 90, 121-124]. Reaction intermediates of S state oxidation changes in the OEC have been observed using transient UV [21, 125, 126], transient EPR [22, 127-129], and time-resolved X-ray [23, 130] experiments. Also, chl fluorescence has been used to study electron transfer events [131, 132]. To our knowledge, no one has employed time-resolved infrared spectroscopy to investigate intermediates in photosynthetic water oxidation.

Electron Paramagnetic Resonance (EPR) Spectroscopy

Electrons and nuclei making up atoms possess inherent magnetic-dipole moments arising from spin angular momenta. In atoms and molecules, electrons usually exist in pairs, causing a net spin moment of zero. However, in organic and inorganic radical species, and transition metals, electrons can exist unpaired and thus exhibit magnetic-dipole moments. The magnetic-dipole moment of a particle will interact with the magnetic component of electromagnetic radiation [133].

If placed in an induced magnetic field, a population of electrons will orient magnetic-dipole moments with and against the direction of the field. As the magnitude of the field increases, the difference in energy of the electron magnetic-dipole moments will also increase. If incident electromagnetic radiation is applied, resonance will occur where the difference in energy of the electron magnetic-dipole moments is equivalent to the energy of the light. Thus, electron paramagnetic resonance (EPR) spectroscopy is concerned with the observation of interactions between an induced magnet (paramagnet)

and light. The resonance condition by which the frequency of light is related to the magnetic field strength is denoted mathematically by:

$$h\nu = g\mu_B B_0$$

where h is Planck's constant, ν is the frequency of light, μ_B is the Bohr magneton, B_0 is the magnetic field strength, and g is a proportionality constant characterizing the magnetic moment of an electron.

EPR spectroscopy has been indispensible in the study of PSII. In the OEC, four Mn ions give rise to EPR signals in all of the S states ([134, 135] and references therein). The two redox-active tyrosines, Y_Z and Y_D, become neutral tyrosyl radicals that are observable via EPR spectroscopy [77, 78, 136]. The difference in environment, as well as proximity to the OEC and other electron transfer cofactors, make Y_Z and Y_D resolvable in spite of their common identity. The chl dimer P_{680} becomes a cation radical upon light-induced charge separation and is located at g = 2.0025 [137]. Concomitant with production of P_{680}^+ cation radical, Q_A becomes a semiquinone anion radical upon light-induced charge separation. The semiquinone radical interacts with nearby Fe^{+2} with g values of 1.67 and 1.82 [138]. Also, certain chl [139] and carotenoid [140] radicals have been observed.

The most common microwave frequency used to study PSII has been X-band (9-10 GHz). However, S-band (3.9 GHz) [141], P-band (15 GHz) [142], Q-band (34 GHz) [143, 144], W-band (94 GHz) [145, 146], D-band (130 GHz) [147], and J-band (245-285 GHz) [148, 149] frequencies have also been employed. The use of high-field (J-band) EPR techniques has resolved overlapping signals of tyrosyl radicals unobservable with low frequency EPR [150]. In addition to continuous-wave studies, pulsed EPR studies of

PSII have been performed including electron spin-echo envelope modulation (ESEEM) and electron-nuclear double resonance (ENDOR) spectroscopies. The use of pulsed EPR methods has allowed for detection of nuclear spin transitions of magnetic nuclei near the OEC. Such measurements directly probe water binding and protonation state of OEC ligands ([59] and references therein).

Thesis Overview

In this body of work, investigations into the chemistry involved in photosynthetic water oxidation have been performed, with a focus on proton-coupled electron transfer (PCET) reactions. In chapter 2, time-resolved infrared spectroscopy is used to probe reactions at the OEC on the timescale of water oxidation. Using this technique, we observed period-four oscillations in derived rate constants, which are attributable to S state changes and O_2 release at the OEC. The signals observed in the S state advancement experiments are assigned to perturbation of histidine residues near the OEC. The results indicate that proton transfer or structural changes at the OEC may precede Mn oxidation.

In chapter 3, time-resolved infrared spectroscopy is used to investigate the mechanism of PCET associated with Y_Z redox reactions. There are significant solvent isotope effects on microsecond rate constants, derived from a transient infrared signal at 1483 cm^{-1}. Isotopic labeling suggests that the $Y_Z^{\bullet}$ radical contributes to the infrared transient on this time scale. Comparing these results with previous model compound studies, a CPET mechanism is suggested, based on the significant kinetic isotope effect (KIE) ≥ 2.5.

In chapter 4, perturbations at the Cl^- binding site of the OEC are studied by reaction-induced difference FT-IR spectroscopy. Using a preparation of PSII in which Cl^- is depleted from the OEC, Br^- is reconstituted. Br^- reconstitution supports O_2 evolution activity, and difference FT-IR spectroscopy reveals structural perturbations due to the presence of Br^- versus Cl^-. These results suggest that an arginine residue may contribute to the Cl^- binding site in the OEC.

In chapter 5, azide (N_3^-) is used as a vibrational probe of proton transfer reactions in the OEC. Azide is an inhibitor of O_2 evolution and competes for binding at the Cl^- site in the OEC as a mixed inhibitor. In addition to binding at the Cl^- site, bound azide is perturbed by light-induced charge separation in PSII as indicated by shifts in its asymmetric stretching mode. Comparison of azide perturbation in different PSII preparations gives evidence for the transient protonation and deprotonation of azide in the OEC. This suggests that azide is involved in proton transfer reactions in the OEC prior to Mn oxidation.

References

1. Nelson, N. and C.F. Yocum, *Structure and function of photosystems I and II.* Annu Rev Plant Biol, 2006. **57**: p. 521-565.

2. Zouni, A., et al., *Crystal structure of photosystem II from Synechococcus elongatus at 3.8 Å resolution.* Nature, 2001. **409**: p. 739-743.

3. Kamiya, N. and J.-R. Shen, *Crystal structure of oxygen-evolving photosystem II from Thermosynechococcus vulcanus at 3.7 Å resolution.* Proc Natl Acad Sci USA, 2003. **100**: p. 98-103.

4. Biesiadka, J., et al., *Crystal structure of cyanobacterial photosystem II at 3.2 Å resolution: a closer look at the Mn-cluster.* Phys Chem Chem Phys, 2004. **6**: p. 4733-4736.

5. Ferreira, K.N., et al., *Architecture of the photosynthetic oxygen-evolving center.* Science, 2004. **303**: p. 1831-1837.

6. Loll, B., et al., *Towards complete cofactor arrangement in the 3.0 Å resolution structure of photosystem II.* Nature, 2005. **438**: p. 1040-1044.

7. Popelkova, H. and C.F. Yocum, *Current status of the role of Cl^- in the oxygen-evolving complex.* Photosynth Res, 2007. **93**: p. 111-121.

8. Diner, B.A. and F. Rappaport, *Structure, dynamics, and energetics of the primary photochemistry of photosystem II of oxygenic photosynthesis.* Annu Rev Plant Biol, 2002. **53**: p. 551-580.

9. Holzwarth, A.R., et al., *Kinetics and mechanism of electron transfer in intact photosystem II and in the isolated reaction center: pheophytin is the primary electron acceptor.* Proc Natl Acad Sci USA, 2006. **103**: p. 6895-6900.

10. Groot, M.L., et al., *Initial electron donor and acceptor in isolated photosystem II reaction centers identified with femtosecond mid-IR spectroscopy.* Proc Natl Acad Sci USA, 2005. **102**: p. 13087-13092.

11. Diner, B.A., et al., *Site-directed mutations at D1-His198 and D2-His197 of photosystem II in Synechocystis PCC 6803: sites of primary charge separation and cation and triplet stabilization.* Biochemistry, 2001. **40**: p. 9265-9281.

12. Nuijs, A.M., et al., *Primary-charge separation and excitation of chlorophyll a in photosystem II particles from spinach as studied by picosecond absorbance-difference spectroscopy.* Biochim Biophys Acta, 1986. **848**: p. 167-175.

13. Trissl, H.W. and W. Leibl, *Primary charge separation in photosystem II involves two electrogenic steps.* FEBS Lett, 1989. **244**: p. 85-88.

14. Schlodder, E. and B. Meyer, *pH dependence of oxygen evolution and reduction kinetics of photooxidized chlorophyll a_{II} (P-680) in photosystem II particles from Synechocystis sp.* Biochim Biophys Acta, 1987. **890**: p. 23-31.

15. Gerken, S., et al., *Optical characterization of the immediate donor to chlorophyll a_{II}^+ in O_2-evolving photosystem II complexes.* FEBS Lett, 1988. **237**: p. 69-75.

16. Conjeaud, H. and P. Mathis, *The effect of pH on the reduction kinetics of P-680 in Tris-treated chloroplasts.* Biochim Biophys Acta, 1980. **590**: p. 353-359.

17. Boska, M., et al., *Similarity of EPR Signal IIf rise and $P\text{-}680^+$ decay kinetics in Tris-washed chloroplast photosystem II preparations as a function of pH.* Biochim Biophys Acta, 1983. **722**: p. 327-330.

18. Haveman, J. and P. Mathis, *Flash-induced absorption changes of the primary donor of photosystem II at 820 nm in chloroplasts inhibitied by low pH or tris-treament.* Biochim Biophys Acta, 1976. **440**: p. 346-355.

19. Dekker, J.P., et al., *Kinetics of manganese redox transitions in the oxygen-evolving apparatus of photosynthesis.* Biochim Biophys Acta, 1984. **767**: p. 176-179.

20. de Wijn, R. and H.J. van Gorkom, *Kinetics of electron transfer from Q_A to Q_B in photosystem II.* Biochemistry, 2001. **40**: p. 11912-11922.

21. Clausen, J. and W. Junge, *Detection of an intermediate of photosynthetic water oxidation.* Nature, 2004. **430**: p. 480-483.

22. Razeghifard, M.R. and R.J. Pace, *EPR kinetic studies of oxygen release in thylakoids and PSII membranes: a kinetic intermediate in S_3 to S_0 transition.* Biochemistry, 1999. **38**: p. 1252-1257.

23. Haumann, M., et al., *Photosynthetic O_2 formation tracked by time-resolved X-ray experiments.* Science, 2005. **310**: p. 1019-1021.

24. Barry, B.A., et al., *Time-resolved vibrational spectroscopy detects protein-based intermediates in the photosynthetic oxygen-evolving cycle.* Proc Natl Acad Sci USA, 2006. **103**: p. 7288-7291.

25. Ghanotakis, D.F., G.T. Babcock, and C.F. Yocum, *Calcium reconstitutes high rates of oxygen evolution in polypeptide depleted photosystem II preparations.* FEBS Lett, 1984. **167**: p. 127-130.

26. Beauregard, M., L. Morin, and R. Popovic, *Sulfate inhibition of photosystem II oxygen evolving complex.* Appl Biochem Biotech, 1987. **16**: p. 109-117.

27. Wincencjusz, H., H.J. van Gorkom, and C.F. Yocum, *The photosynthetic oxygen evolving complex requires chloride for its redox state $S_2 \rightarrow S_3$ and $S_3 \rightarrow S_0$ transitions but not for $S_0 \rightarrow S_1$ or $S_1 \rightarrow S_2$ transitions.* Biochemistry, 1997. **36**: p. 3663-3670.

28. Boussac, A. and A.W. Rutherford, *Nature of the inhibition of the oxygen-evolving enzyme of photosystem II induced by NaCl washing and reversed by the addition of Ca^{2+} or Sr^{2+}.* Biochemistry, 1988. **27**: p. 3476-3483.

29. Westphal, K.L., et al., *Effects of Sr^{+2} substitution on the reduction rates of $Y_Z^{\bullet}$ in PSII membranes-Evidence for concerted hydrogen-atom transfer in oxygen evolution.* Biochemistry, 2000. **39**: p. 16220-16229.

30. Boussac, A., et al., *Biosynthetic Ca^{+2}/Sr^{+2} exchange in photosystem II oxygen-evolving enzyme of Thermosynechococcus elongatus.* J Biol Chem, 2004. **279**: p. 22809-22819.

31. Matysik, J., et al., *Exploring the calcium-binding site in photosystem II membranes by solid-state ^{113}Cd NMR.* Biochemistry, 2000. **39**: p. 6751-6755.

32. Vrettos, J.S., D.A. Stone, and G.W. Brudvig, *Quantifying the ion selectivity of the calcium site in photosystem II: Evidence for direct involvement of Ca^{+2} in O_2 formation.* Biochemistry, 2001. **40**: p. 7937-7945.

33. Faller, P., K. Kienzler, and A. Krieger-Liszkay, *Mechanism of Cd^{2+} toxicity: Cd^{2+} inhibits photoactivation of photosystem II by competitive binding to the essential Ca^{2+} site.* Biochim Biophys Acta, 2005. **1706**: p. 158-164.

34. Bartlett, J.E., et al., *Calcium controls the assembly of the photosynthetic water-oxidizing complex: a cadmium(II) inorganic mutant of the Mn_4Ca core.* Phil Trans R Soc Lond B, 2008. **363**: p. 1253-1261.

35. Yocum, C.F., *The calcium and chloride requirements of the O_2 evolving complex.* Coord Chem Rev, 2008. **252**: p. 296-305.

36. Riggs-Gelasco, P.J., et al., *Reduced derivatives of the Mn cluster in the oxygen-evolving complex of photosystem II: An EXAFS study.* J Am Chem Soc, 1996. **118**: p. 2387-2399.

37. Haumann, M. and W. Junge, *Photosynthetic water oxidation: a simplex-scheme of its partial reactions.* Biochim Biophys Acta, 1999. **1411**: p. 86-91.

38. Barry, B.A., et al., *Calcium ligation in photosystem II under inhibiting conditions.* Biophys J, 2005. **89**: p. 393-401.

39. Hendry, G. and T. Wydrzynski, *^{18}O isotope exchange measurements reveal that calcium is involved in the binding of one substrate-water molecule to the oxygen-evolving complex in photosystem II.* Biochemistry, 2003. **42**: p. 6209-6217.

40. Lindberg, K., T. Vanngard, and L.-E. Andreasson, *Studies of the slowly exchanging chloride in photosystem II of higher plants.* Photosynth Res, 1993. **38**: p. 401-408.

41. Clemens, K.L., D.A. Force, and R.D. Britt, *Acetate binding at the photosystem II oxygen evolving complex: an S_2-state multiline signal ESEEM study.* J Am Chem Soc, 2002. **124**: p. 10921-10933.

42. Wincencjusz, H., C.F. Yocum, and H.J. van Gorkom, *Activating anions that replace Cl^- in the O_2-evolving complex of photosystem II slow the kinetics of the*

terminal step in water oxidation and destabilize the S_2 and S_3 states. Biochemistry, 1999. **38**: p. 3719-3725.

43. Hasegawa, K., Y. Kimura, and T.-a. Ono, *Chloride cofactor in the photosynthetic oxygen-evolving complex studied by Fourier transform infrared spectroscopy.* Biochemistry, 2002. **41**: p. 13839-13850.

44. Baumgarten, M., J.S. Philo, and G.C. Dismukes, *Mechanism of photoinhibition of photosynthetic water oxidation by Cl^- depletion and F^- substitution: oxidation of a protein residue.* Biochemistry, 1990. **29**: p. 10814-10822.

45. DeRose, V.J., et al., *Fluoride substitution in the Mn cluster from photosystem II: EPR and X-ray absorption spectroscopy studies.* Chem Phys, 1995. **194**: p. 443-459.

46. Ono, T.-a., et al., *Modification of the properties of S_2 state in photosynthetic O_2-evolving center by replacement of chloride with other anions.* Arch Biochem Biophys, 1987. **256**: p. 618-624.

47. Katoh, S., *Inhibitors of electron transport associated with photosystem II in chloroplasts.* Plant Cell Physiol, 1972. **13**: p. 273-286.

48. Haddy, A., et al., *Azide as a competitor of chloride in oxygen evolution by photosystem II.* Biochemistry, 1999. **38**: p. 6104-6110.

49. Sandusky, P.O. and C.F. Yocum, *The chloride requirement for photosynthetic oxygen evolution. Analysis of the effects of chloride and other anions on amine inhibition of the oxygen evolving complex.* Biochim Biophys Acta, 1984. **766**: p. 603-611.

50. Olesen, K. and L.-E. Andreasson, *The function of the chloride ion in photosynthetic oxygen evolution.* Biochemistry, 2003. **42**: p. 2025-2035.

51. Boussac, A. and A.W. Rutherford, *Electron transfer events in chloride-depleted photosystem II.* J Biol Chem, 1994. **269**: p. 12462-12467.

52. McEvoy, J.P. and G.W. Brudvig, *Structure-based mechanism of photosynthetic water oxidation.* Phys Chem Chem Phys, 2004. **6**: p. 4754-4763.

53. Hasegawa, K., Y. Kimura, and T.-a. Ono, *Oxidation of the Mn cluster induces structural changes of NO_3^- functionally bound to the Cl^- site in the oxygen-evolving complex of photosystem II.* Biophys J, 2004. **86**: p. 1042-1050.

54. Haumann, M., et al., *Bromide does not bind to the Mn_4Ca complex in its S_1 state in Cl^--depleted and Br^--reconstituted oxygen-evolving photosystem II: Evidence*

from X-ray absorption spectroscopy at the Br K-edge. Biochemistry, 2006. **45**: p. 13101-13107.

55. Sauer, K., *A role for manganese in oxygen evolution in photosynthesis.* Acc Chem Res, 1980. **13**: p. 249-256.

56. Yano, J., et al., *X-ray damage to the Mn_4Ca complex in single crystals of photosystem II: A case study for metalloprotein crystallography.* Proc Natl Acad Sci USA, 2005. **102**: p. 12047-12052.

57. Yachandra, V.K., *Structure of the manganese complex in photosystem II: Insights from X-ray spectroscopy.* Phil Trans R Soc Lond B, 2002. **357**: p. 1347-1358.

58. Sauer, K., J. Yano, and V.K. Yachandra, *X-ray spectroscopy of the photosynthetic oxygen-evolving complex.* Coord Chem Rev, 2008. **252**: p. 318-335.

59. Britt, R.D., et al., *Recent pulsed EPR studies of the photosystem II oxygen-evolving complex: implications as to water oxidation mechanisms.* Biochim Biophys Acta, 2004. **1655**: p. 158-171.

60. Kulik, L.V., et al., *Electronic structure of the Mn_4O_XCa cluster in the S_0 and S_2 states of the oxygen-evolving complex of photosystem II based on pulse ^{55}Mn-ENDOR and EPR spectroscopy.* J Am Chem Soc, 2007. **129**: p. 13421-13435.

61. Kim, S.H., et al., *Investigation of the calcium-binding site of the oxygen evolving complex of photosystem II using ^{87}Sr ESEEM spectroscopy.* J Am Chem Soc, 2004. **126**: p. 7228-7237.

62. Sproviero, E.M., et al., *QM/MM models of the O_2-evolving complex of photosystem II.* J Chem Theor Comput, 2006. **2**: p. 1119-1134.

63. Sproviero, E.M., et al., *Quantum mechanics/molecular mechanics study of the catalytic cycle of water splitting in photosystem II.* J Am Chem Soc, 2008. **130**: p. 3428-3442.

64. Sproviero, E.M., et al., *Computational insights into the O_2-evolving complex of photosystem II.* Photosynth Res, 2008. **97**: p. 91-114.

65. McEvoy, J.P. and G.W. Brudvig, *Water-splitting chemistry of photosystem II.* Chem Rev, 2006. **106**: p. 4455-4478.

66. Yamamoto, Y., et al., *Release of polypeptides from highly active O_2-evolving photosystem-2 preparation by tris treatment.* FEBS Lett, 1981. **133**: p. 265-268.

67. Chen, G.-X., J. Kazimir, and G.M. Cheniae, *Photoinhibition of hydroxlamine-extracted photosystem II membranes: studies of the mechanism.* Biochemistry, 1992. **31**: p. 11072-11083.

68. Ghanotakis, D.F., J.N. Topper, and C.F. Yocum, *Structural organization of the oxidizing side of photosystem II. Exogenous reductants reduce and destroy the Mn-complex in photosystem II membranes depleted of the 17 and 23 kDa polypeptides.* Biochim Biophys Acta, 1984. **767**: p. 524-531.

69. Kuwabara, T. and N. Murata, *Quantitative analysis of the inactivation of photosynthetic oxygen evolution and the release of polypeptides and manganese in the photosystem II particles of spinach chloroplasts.* Plant Cell Physiol, 1984. **24**: p. 741-747.

70. Tsai, A., K.J. Richard, and P. Graham, *Spectroscopic evidence for reaction of prostaglandin H synthase-1 tyrosyl radical with arachidonic acid.* J Biol Chem, 1995. **270**: p. 10503-10508.

71. Tsai, A.-L. and R.J. Kulmacz, *Tyrosyl radicals in prostaglandin H synthase-1 and -2.* Prostag Oth Lipid M, 2000. **62**: p. 231-254.

72. Stubbe, J., *Di-iron-tyrosyl radical ribonucleotide reductases.* Curr Opin Chem Biol, 2003. **7**: p. 183-188.

73. Reece, S.Y., et al., *Proton-coupled electron transfer: the mechanistic underpinning for radical transport and catalysis in biology.* Phil Trans R Soc Lond B, 2006. **361**: p. 1351-1364.

74. Ostermeier, C., et al., *Structure at 2.7 Å resolution of the Paracoccus denitrificans two-subunit cytochrome c oxidase complexed with an antibody FV fragment.* Proc Natl Acad Sci USA, 1997. **94**: p. 10547-10553.

75. Proshlyakov, D.A., et al., *Oxygen activation and reduction in respiration: involvement of redox-active tyrosine 244.* Science, 2000. **290**: p. 1588-1591.

76. Rogers, M.S. and D.M. Dooley, *Copper-tyrosyl radical enzymes.* Curr Opin Chem Biol, 2003. **7**: p. 189-196.

77. Barry, B.A. and G.T. Babcock, *Tyrosine radicals are involved in the photosynthetic oxygen-evolving system.* Proc Natl Acad Sci USA, 1987. **84**: p. 7099-7103.

78. Debus, R.J., et al., *Site-specific mutagenesis identifies a tyrosine radical involved in the photosynthetic oxygen-evolving complex.* Proc Natl Acad Sci USA, 1988. **85**: p. 427-430.

79. Vermaas, W.F.J., A.W. Rutherford, and Ö. Hansson, *Site-directed mutagenesis in photosystem II of the cyanobacterium Synechocystis sp. PCC 6803: Donor D is a tyrosine residue in the D2 protein.* Proc Natl Acad Sci USA, 1988. **85**: p. 8477-8481.

80. Ananyev, G.M., et al., *A functional role for tyrosine-D in assembly of the inorganic core of the water complex of photosystem II and the kinetics of water oxidation.* Biochemistry, 2002. **41**: p. 974-980.

81. Rova, E.M., et al., *Coupled activation of the donor and the acceptor side of photosystem II during photoactivation of the oxygen evolving cluster.* Biochemistry, 1998. **37**: p. 11039-11045.

82. Sjödin, M., et al., *Proton-coupled electron transfer from tyrosine in a tyrosine-ruthenium-tris-bipyridine complex: comparison with tyrosine$_Z$ oxidation in photosystem II.* J Am Chem Soc, 2000. **122**: p. 3932-3936.

83. Sjödin, M., et al., *The mechanism for proton-coupled electron transfer from tyrosine in a model complex and comparisons with Y_Z oxidation in photosystem II.* Phil Trans R Soc Lond B, 2002. **357**: p. 1471-1478.

84. Sjödin, M., et al., *Tuning proton coupled electron transfer from tyrosine: a competition between concerted and step-wise mechanisms.* Phys Chem Chem Phys, 2004. **6**: p. 4851-4858.

85. Reece, S.Y. and D.G. Nocera, *Direct tyrosine oxidation using the MLCT excited states of rhenium polypyridyl complexes.* J Am Chem Soc, 2005. **127**: p. 9448-9458.

86. Rhile, I.J., et al., *Concerted proton-electron transfer in the oxidation of hydrogen bonded phenols.* J Am Chem Soc, 2006. **128**: p. 6075-6088.

87. Meyer, T.J., M.H.V. Huynh, and H.H. Thorp, *The possible role of proton-coupled electron transfer (PCET) in water oxidation by photosystem II.* Angew Chem Int Edit, 2007. **46**: p. 5284-5304.

88. Hays, A.-M.A., et al., *Role of D1-His190 in proton-coupled electron transfer reactions in photosystem II: a chemical complementation study.* Biochemistry, 1998. **37**: p. 11352-11365.

89. Mamedov, F., R.T. Sayre, and S. Styring, *Involvement of histidine 190 on the D1 protein in electron/proton transfer reactions on the donor side of photosystem II.* Biochemistry, 1998. **37**: p. 14245-14256.

90. Hays, A.M.A., et al., *Role of D1-His190 in the proton-coupled oxidation of tyrosine Y-Z in manganese-depleted photosystem II.* Biochemistry, 1999. **38**: p. 11851-11865.

91. Pujols-Ayala, I. and B.A. Barry, *His 190-D1 and Glu 189-D1 provide structural stabilization in photosystem II.* Biochemistry, 2002. **41**: p. 11456-11465.

92. Knoepfle, N., T.M. Bricker, and C. Putnam-Evans, *Site-directed mutagenesis of basic arginine residues 305 and 342 in the CP43 protein of photosystem II affects oxygen-evolving activity in Synechocystis 6803.* Biochemistry, 1999. **38**: p. 1582-1588.

93. Ishikita, H., et al., *Energetics of a possible proton exit pathway for water oxidation in photosystem II.* Biochemistry, 2006. **45**: p. 2063-2071.

94. Hwang, H.J., et al., *Mutation of Arginine 357 of the CP43 Protein of Photosystem II Severely Impairs the Catalytic S-State Cycle of the H_2O Oxidation Complex.* Biochemistry, 2007. **46**: p. 11987-11997.

95. Hundelt, M., et al., *Oxygenic photosystem II: the mutation D1-D61N in Synechocystis sp. PCC 6803 retards S-state transitions without affecting electron transfer from Y_Z to P_{680}^+.* Biochemistry, 1998. **37**: p. 14450-14456.

96. Liu, F., et al., *Mechanism of water oxidation from the blue dimer to photosystem II.* Inorg Chem, 2008. **47**: p. 1727-1752.

97. Berry, R.S., S.A. Rice, and J. Ross, *Physical Chemistry*. 2nd ed. 2000, New York: Oxford University Press. p. 247-255.

98. Rothschild, K.J., *FTIR difference spectroscopy of bacteriorhodopsin: toward a molecular model.* J Bioenerg Biomembr, 1992. **24**: p. 147-167.

99. Breton, J., *Fourier transform infrared spectroscopy of primary electron donors in type I photosynthetic reaction centers.* Biochim Biophys Acta, 2001. **1507**: p. 180-193.

100. McMahon, B.H., et al., *FTIR studies of internal proton transfer reactions linked to inter-heme electron transfer in bovine cytochrome c oxidase.* Biochim Biophys Acta, 2004. **1655**: p. 321-331.

101. Cooper, I.B. and B.A. Barry, *Perturbations at the chloride site during the photosynthetic oxygen-evolving cycle.* Photosynth Res, 2007. **92**: p. 345-354.

102. Bender, S.L., et al., *The vibrational spectrum of the secondary electron acceptor, A1, in photosystem I.* J Phys Chem B, 2008. **112**: p. 3844-3852.

103. Noguchi, T., *Fourier transform infrared analysis of the photosynthetic oxygen-evolving center.* Coord Chem Rev, 2008. **252**: p. 336-346.

104. Noguchi, T. and M. Sugiura, *Flash-induced Fourier transform infrared detection of the structural changes during the S-state cycle of the oxygen-evolving complex in photosystem II.* Biochemistry, 2001. **40**: p. 1497-1502.

105. Hillier, W. and G.T. Babcock, *S-state dependent Fourier transform infrared difference spectra for the photosystem II oxygen evolving complex.* Biochemistry, 2001. **40**: p. 1503-1509.

106. DeRiso, A., D.L. Jenson, and B.A. Barry, *Calcium exchange and structural changes during the photosynthetic oxygen evolving cycle.* Biophys J, 2006. **91**: p. 1999-2008.

107. Kim, S. and B.A. Barry, *The protein environment surrounding tyrosyl radicals $D^{\bullet}$ and $Z^{\bullet}$ in photosystem II: a difference Fourier-transform infrared spectroscopic study.* Biophys J, 1998. **74**: p. 2588-2600.

108. Ayala, I., S. Kim, and B.A. Barry, *A difference Fourier transform infrared study of tyrosyl radical $Z^{\bullet}$ decay in photosystem II.* Biophys J, 1999. **77**: p. 2137-2144.

109. Chu, H.-A., W. Hillier, and R.J. Debus, *Evidence that the C-terminus of the D1 polypeptide of photosystem II is ligated to the manganese ion that undergoes oxidation during the S_1 to S_2 transition: an isotope-edited FTIR study.* Biochemistry, 2004. **43**: p. 3152-3166.

110. Kimura, Y., et al., *FTIR detection of structural changes in a histidine ligand during S-state cycling of photosynthetic oxygen-evolving complex.* Biochemistry, 2005. **44**: p. 16072 -16078.

111. Noguchi, T. and M. Sugiura, *Structure of an active water molecule in the water-oxidizing complex of photosystem II as studied by FTIR spectroscopy.* Biochemistry, 2000. **39**: p. 10943-10949.

112. Kim, S., J. Liang, and B.A. Barry, *Chemical complementation identifies a proton acceptor for redox-active tyrosine D in photosystem II.* Proc Natl Acad Sci USA, 1997. **94**: p. 14406-14412.

113. Debus, R.J., et al., *Histidine 332 of the D1 polypeptide modulates the magnetic and redox properties of the manganese cluster and tyrosine Y_Z in photosystem II.* Biochemistry, 2000. **39**: p. 470-478.

114. Mizusawa, N., et al., *Impact of replacement of D1 C-terminal alanine with glycine on structure and function of photosynthetic oxygen-evolving complex.* J Biol Chem, 2004. **279**: p. 29622-29627.

115. Chu, H.-A., et al., *Vibrational spectroscopy of the oxygen-evolving complex and of manganese model compounds.* Biochim Biophys Acta, 2001. **1503**: p. 69-82.

116. Noguchi, T., T.-a. Ono, and Y. Inoue, *Direct detection of a carboxylate bridge between Mn and Ca^{+2} in the photosynthetic oxygen-evolving center by means of Fourier transform infrared spectroscopy.* Biochim Biophys Acta, 1995. **1228**: p. 189-200.

117. Anfinrud, P.A., C. Han, and R.M. Hochstrasser, *Direct observation of ligand dynamics in hemoglobin by subpicosecond infrared spectroscopy.* Proc Natl Acad Sci USA, 1989. **86**: p. 8387-8391.

118. Heberle, J., et al., *Bacteriorhodopsin: the functional details of a molecular machine are being resolved.* Biophys Chem, 2000. **85**: p. 229-248.

119. Callender, R.H. and R.B. Dyer, *Advances in time-resolved approaches to characterize the dynamical nature of enzyme catalysis.* Chem Rev, 2006. **106**: p. 3031-3042.

120. Williams, S., et al., *Fast events in protein folding: helix melting and formation in a small peptide.* Biochemistry, 1996. **35**: p. 691-697.

121. Reinman, S., et al., *Kinetics of reduction of the primary donor of photosystem II: influence of pH in various preparations.* Biochim Biophys Acta, 1981. **635**: p. 429-433.

122. Brettel, K., E. Schlodder, and H.T. Witt, *Nanosecond reduction kinetics of photooxidized chlorophyll-a_{II} (P-680) in single flashes as a probe for the electron pathway, H^+ release and charge accumulation on the O_2-evolving complex.* Biochim Biophys Acta, 1984. **766**: p. 403-415.

123. Ahlbrink, R., et al., *Function of tyrosine Z in water oxidation by photosystem II: Electrostatical potential instead of hydrogen abstractor.* Biochemistry, 1998. **37**: p. 1131-1142.

124. Diner, B.A., et al., *Hydrogen bonding, solvent exchange, and coupled proton and electron transfer in the oxidation and reduction of redox-active tyrosine Y_Z in Mn-depleted core complexes of photosystem II.* Biochemistry, 1998. **37**: p. 17931-17943.

125. Weiss, W. and G. Renger, *UV-spectral characterization in tris-washed chloroplasts of the redox component D_1 which functionally connects the reaction center with the water-oxidizing enzyme system Y in photosynthesis.* FEBS Lett, 1984. **169**: p. 219-223.

126. Weiss, W. and G. Renger, *Studies on the nature of the water-oxidizing enzyme. II. On the functional connection between the reaction-center complex and the water-oxidizing enzyme system Y in photosystem II.* Biochim Biophys Acta, 1986. **850**: p. 173-183.

127. Shigemori, K., H. Mino, and A. Kawamori, *pH and temperature dependence of tyrosine $Z^{\bullet}$ decay kinetics in tris-treated PSII particles studied by time-resolved EPR.* Plant Cell Physiol, 1997. **38**: p. 1007-1011.

128. Jajoo, A., S. Bharti, and A. Kawamori, *Decay kinetics of tyrosine radical ($Y_Z^{\bullet}$) in chloride anion-depleted photosystem 2 studied by time-resolved EPR.* Photosynthetica, 2004. **42**: p. 59-64.

129. Ioannidis, N., G. Zahariou, and V. Petrouleas, *The EPR spectrum of tyrosine $Z^{\bullet}$ and its decay kinetics in O_2-evolving photosystem II preparations.* Biochemistry, 2008. **47**: p. 6292-6300.

130. Haumann, M., et al., *The first room-temperature X-ray absorption spectra of higher oxidation states of the tetra-manganese complex of photosystem II.* FEBS Lett, 2002. **512**: p. 116-120.

131. Zhu, X.-G., et al., *Chlorophyll a fluorescence induction kinetics in leaves predicted from a model describing each discrete step of excitation energy and electron transfer associated with photosystem II.* Planta, 2005. **223**: p. 114-133.

132. Papageorgiou, G.C., M. Tsimilli-Michael, and K. Stamatakis, *The fast and slow kinetics of chlorophyll a fluorescence induction in plants, algae, and cyanobacteria.* Photosynth Res, 2007. **94**: p. 275-290.

133. Weil, J.A., J.R. Bolton, and J.E. Wertz, *Electron Paramagnetic Resonance: Elementary Theory and Practical Applications*. 1994, New York: John Wiley & Sons, Inc. p. 568.

134. Miller, A.-F. and G.W. Brudvig, *A guide to electron paramagnetic resonance spectroscopy of photosystem II membranes.* Biochim Biophys Acta, 1991. **1056**: p. 1-18.

135. Haddy, A., *EPR spectroscopy of the manganese cluster of photosystem II.* Photosynth Res, 2007. **92**: p. 357-368.

136. Metz, J.G., et al., *Directed alteration of the D1 polypeptide of photosystem II: evidence that tyrosine-161 is the redox component, Z, connecting the oxygen-evolving complex to the primary electron donor, P680.* Biochemistry, 1989. **28**: p. 6960-6969.

137. Hoganson, C.W. and G.T. Babcock, *Redox cofactor interactions in photosystem II: electron spin resonance spectrum of P_{680}^{+} is broadened in the presence of Y_Z^{+}.* Biochemistry, 1989. **28**: p. 1448-1454.

138. Nugent, J.H.A., B.A. Diner, and M.C.W. Evans, *Direct detection of the electron acceptor of Photosystem II: evidence that Q is an iron-quinone complex.* FEBS Lett, 1981. **124**: p. 241-244.

139. Visser, J.W.M., C.P. Rijgersberg, and P. Gast, *Photooxidation of chlorophyll in spinach chloroplasts between 10 and 180 K.* Biochim Biophys Acta, 1977. **460**: p. 36-46.

140. Hanley, J., et al., *Carotenoid oxidation in photosystem II.* Biochemistry, 1999. **38**: p. 8189-8195.

141. Haddy, A., R. Aasa, and L.-E. Andreasson, *S-Band EPR studies of the S_2-state multiline signal from the photosynthetic oxygen-evolving complex.* Biochemistry, 1989. **28**: p. 6954-6959.

142. Haddy, A., et al., *Multifrequency EPR investigations into the origin of the S_2-state signal at g = 4 of the O_2-evolving complex.* Biochim Biophys Acta, 1992. **1099**: p. 25-34.

143. Smith, P.J., K.A. Åhrling, and R.J. Pace, *Nature of the S_2 state electron paramagnetic resonance signals from the oxygen-evolving complex of photosystem II: Q-band and oriented X-band studies.* J Chem Soc Faraday T, 1993. **89**: p. 2863-2868.

144. Haddy, A., et al., *Q-band EPR of the S_2 state of photosystem II confirms an S = 5/2 origin of the X-band g = 4.1 signal.* Biophys J, 2004. **87**: p. 2885-2896.

145. Koulougliotis, D., et al., *The $S_1Y_Z^{\bullet}$ metalloradical intermediate of photosystem II: an X- and W-band EPR study.* Phys Chem Chem Phys, 2004. **6**: p. 4859-4863.

146. Matsuoka, H., et al., *g-Anisotropy of the S_2-state manganese cluster in single crystals of cyanobacterial photosystem II studied by W-band electron paramagnetic resonance spectroscopy.* J Phys Chem B, 2006. **110**: p. 13242-13247.

147. Pashenko, S.V., et al., *Triplet state of photosystem II reaction centers as studied by 130 GHz EPR.* Chem Phys, 2003. **394**: p. 439-449.

148. Un, S., X.-S. Tang, and B.A. Diner, *245 GHz high-field EPR study of tyrosine-$D^{\bullet}$ and tyrosine-$Z^{\bullet}$ in mutants of photosystem II.* Biochemistry, 1996. **35**: p. 679-684.

149. Ivancich, A., T.A. Mattioli, and S. Un, *Effect of the protein microenvironment on tyrosyl radicals. A high-field (285 GHz) EPR, resonance raman, and hybrid density functional study.* J Am Chem Soc, 1999. **121**: p. 5743-5753.

150. Faller, P., et al., *Resolving intermediates in biological proton-coupled electron transfer: a tyrosyl radical prior to proton movement.* Proc Natl Acad Sci USA, 2003. **100**: p. 8732-8735.

151. Rappaport, F. and B.A. Diner, *Primary photochemistry and energetics leading to the oxidation of the $(Mn)_4Ca$ cluster and to the evolution of molecular oxygen in photosystem II.* Coord Chem Rev, 2008. **252**: p. 259-272.

152. Yano, J., et al., *Where water is oxidized to dioxygen: structure of the photosynthetic Mn_4Ca cluster.* Science, 2006. **314**: p. 821-825.

CHAPTER 2

TIME-RESOLVED VIBRATIONAL SPECTROSCOPY DETECTS PROTEIN-BASED INTERMEDIATES IN THE PHOTOSYNTHETIC OXYGEN-EVOLVING CYCLE

by

Bridgette A. Barry*, Ian B. Cooper*, Antonio De Riso*, Scott H. Brewer†, Dung M. Vu†, and R. Brian Dyer†

* - School of Chemistry and Biochemistry and the Petit Institute for Bioengineering and Bioscience, Georgia Institute of Technology, Atlanta, GA 30332

† - Integrated Spectroscopy Laboratory, Chemistry Division, Los Alamos National Laboratory, Group C-PCS, Mail Stop J567, Los Alamos, NM 87545

Reprinted with permission from Proc Natl Acad Sci USA
(Barry, B. A. et al. Proc Natl Acad Sci USA, 2006. **103**: p. 7288-7291.)

Abstract

Photosynthetic oxygen production by photosystem II (PSII) is responsible for the maintenance of aerobic life on earth. The production of oxygen occurs at the PSII oxygen-evolving complex (OEC), which contains a tetranuclear manganese (Mn) cluster. Photo-induced electron transfer events in the reaction center lead to the accumulation of oxidizing equivalents on the OEC. Four sequential photooxidation reactions are required for oxygen production. The oxidizing complex cycles among five oxidation states, called the S_n states, where n refers to the number of oxidizing equivalents stored. Oxygen release occurs during the S_3-to-S_0 transition from an unstable intermediate, known as the

S_4 state. In this report, we present data providing evidence for the production of an intermediate during each S state transition. These protein-derived intermediates are produced on the microsecond to millisecond time scale and are detected by time-resolved vibrational spectroscopy on the microsecond time scale. Our results suggest that a protein-derived conformational change or proton transfer reaction precedes Mn redox reactions during the S_2-to-S_3 and S_3-to-S_0 transitions.

Introduction

Time-resolved vibrational spectroscopy can detect chemical intermediates formed during enzymatic catalysis. Advantages include the technique's exquisite structural sensitivity and its high temporal resolution. Recent advances in methodology and interpretation have produced insights into the catalytic mechanism in several biological systems (for examples, see [1-4]).

In this paper, we report the use of time-resolved IR spectroscopy to investigate the mechanism of photosynthetic water oxidation. Photosystem II (PSII) catalyzes the oxidation of water and the reduction of bound plastoquinone. Photoexcitation of PSII leads to the oxidation of the chlorophyll donor, P_{680}, and the sequential reduction of a pheophytin (figure 1A, reaction 1) and a plastoquinone, Q_A (figure 1A, reaction 2), in picoseconds. Q_A reduces Q_B to generate a semiquinone radical, Q_B^-, on the microsecond time scale (figure 1A, reaction 3) (reviewed in [5]). A second photoexcitation leads to the reduction and protonation of Q_B^- to form the quinol Q_BH_2. The rate of reduction of Q_B is faster than the rate of reduction of Q_B^- (see [6] and references therein), which gives

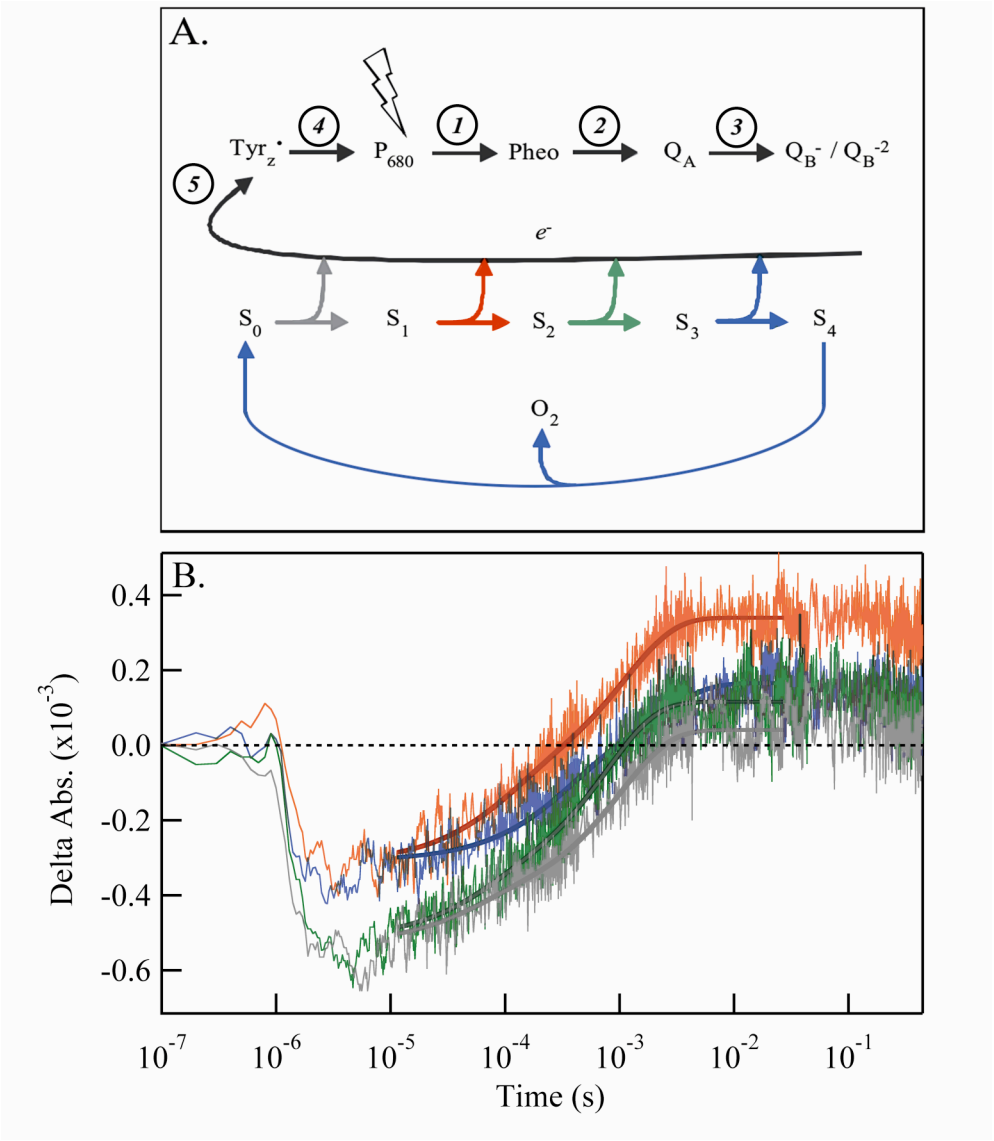

Figure 1. PSII electron transfer and representative IR results. (A) Diagram of electron transfer steps in PSII and the S state cycle of photosynthetic oxygen evolution. From the S_1 state, three saturating flashes (shown in red, green, and blue, respectively) are required to produce oxygen. (B) Flash dependence of transients recorded at 1483-cm^{-1} and 10°C from PSII, which contained 0.6 mM DCBQ and 7.2 mM potassium ferricyanide. Flash 1, generating the S_2 state, is shown in the red trace; flash 2, generating the S_3 state, is shown in the green trace; flash 3, generating the S_0 state, is shown in the blue trace; and flash 4, generating the S_1 state, is shown in the gray trace. The transients are displayed with vertical offsets, which serve to superimpose the traces at the first data point. Multiexponential fits to the data (table 1) are shown superimposed.

rise to a characteristic period-2 oscillation in kinetics originating on the PSII acceptor side [7].

The primary chlorophyll donor, P_{680}, oxidizes a tyrosine, Y_Z (Y161 in the D1 subunit), on the nanosecond to microsecond time scale (figure 1A, reaction 4). In turn, tyrosine $Y_Z^{\bullet}$ oxidizes the oxygen-evolving complex (OEC) on every flash (figure 1A, reaction 5) [8]. Four sequential photooxidation reactions are required for oxygen production, and the oxidizing complex cycles among five oxidation states, called the S_n states, where *n* refers to the number of oxidizing equivalents stored [9]. The rate of OEC oxidation slows as oxidizing equivalents are stored on the OEC [10, 11]. This slowing gives rise to a characteristic period-4 oscillation in OEC kinetics (figure 1A). Recently, UV spectroscopy was used to detect an intermediate that could not proceed to the S_4 state at high oxygen pressure [12]. X-ray spectroscopy was used to detect a lag in the reduction of Mn during the S_3-to-S_0 transition; this lag phase was attributed to a proton transfer event that precedes the Mn redox reaction [11]. Structural models of PSII have been derived from X-ray diffraction at $\geq$ 3.0-Å resolution [13-17].

There are many proposed mechanisms for water oxidation (for recent reviews, see [18, 19]). IR spectroscopy provides a method of distinguishing among proposed water oxidation mechanisms and probing new intermediate states formed during each of the S state transitions. To our knowledge, this report is the first study of the OEC with kinetic IR spectroscopy on the microsecond time scale. These studies show that a protein-derived intermediate state is formed on each S state transition.

Materials and Methods

Spinach PSII preparations [20] with steady-state rates of oxygen evolution (>600 μmol O_2 (mg Chl-h)$^{-1}$ [21]) were exchanged into a ^2H_2O buffer (^2H_2O, 99%; Cambridge Isotope Laboratories, Andover, MA) containing 0.4 M sucrose, 50 mM MES-NaO^{2}H (p^{2}H 6.0), and 15 mM NaCl. In some control experiments, Mn was removed by treatment with 1.8 M alkaline Tris [22] under illumination for 30 min. Mn-depleted samples were exchanged into a buffer containing 50 mM MES-NaO^{2}H (p^{2}H 6.0). ^2H_2O buffers were necessary to minimize the background absorbance and to eliminate a rapid thermal response of solvent absorbance to a saturating photolysis pulse.

For the transient IR measurements [23], the PSII sample was pelleted by centrifugation and was transferred to a calcium fluoride window. The IR cell was assembled by using another calcium fluoride window and a 25-μm spacer. The 25-μm path length spacer was greased, and the sample was sealed with vacuum grease and parafilm to prevent dehydration during the experiment [24, 25]. A continuous-wave diode laser (Ekips Technology, Norman, OK) emitting at 1483 cm^{-1} was used as the probe, a Q-switched Nd:YAG (neodymium:yttrium aluminum garnet) laser (Spectra-Physics) was used to produce a 532-nm photolysis pulse, and the transient absorbance of the probe was detected with a liquid nitrogen-cooled mercury-cadmium-telluride detector. The instrument response time was 1 μs. The IR sample was maintained at 10°C during the measurement by using a refrigerated water bath. The 532-nm photolysis

pulses had a 10-ns pulse width and a 0.2-cm spot radius (38 mJ/cm^2)[‡]. Samples were aligned with one or more 532-nm flashes before the beginning of data acquisition and then translated to a new spot.

For the S state experiments, the sample was preflashed and dark-adapted for 15 min to achieve synchronization in the S_1 state [26]. After dark adaptation, 12 (532 nm) photolysis flashes were given at an ≈ 1-Hz repetition rate, and an IR transient was recorded after each flash. For other PSII control experiments, kinetics transients were averaged. The transients were fit with a multiexponential function to extract amplitudes and rate constants using Igor Pro software (Wavemetrics, Lake Oswego, OR). Derived time constants depended on the choice of initial and final fit points. For consistency, transients from the same experiment were fit with identical beginning and ending points.

Results

In figure 1B, the effects of multiple, saturating laser flashes on PSII samples containing 2,6-dichlorobenzoquinone (DCBQ) and potassium ferricyanide as electron acceptors are shown. The data exhibit an initial 1483-cm^{-1} bleach on the microsecond time scale on each flash. This initial bleach, which is limited by the instrument response time, is followed by a delayed increase in amplitude over baseline (figure 1B). Alterations in the kinetics as a function of flash number are observed in figure 1B and will be discussed below.

[‡] We wish to clarify that the data presented in this work was collected using a 532 nm spot size of 0.1 cm diameter.

Control experiments in figure 2 address the origin of these IR transients. The green trace was acquired from oxygen-evolving PSII containing DCBQ and ferricyanide (repeated from figure 1B). As a negative control, the red trace in figure 2 was acquired on PSII, which contained an OEC, 3-(3,4-dichlorophenyl)-1,1-dimethylurea (DCMU), and no exogenous acceptors. DCMU is an inhibitor that will block electron transfer to Q_B [27] (figure 1A, reaction 3) and cause transfer of any electrons on Q_B back to Q_A [28]. This reequilibration, coupled with multiple flash illuminations, will result in a majority of closed centers containing Q_A^- in the dark, which cannot undergo a stable $P_{680}^+Q_A^-$ charge separation. As observed by comparison of the red and green traces, an IR transient, which is the average of multiple flashes in a DCMU-treated sample (figure 2, red trace), does not show the bleach that is observed in the presence of the electron acceptors (figure 2, green trace). This result demonstrates that the bleach is caused by PSII electron transfer events in open PSII centers.

Experiments were conducted on PSII from which the OEC had been removed with 1.8 M alkaline Tris and which contained hydroxylamine and DCMU (figure 2, brown trace). In this hydroxylamine- and DCMU-treated sample, the $P_{680}^+Q_A^-$ charge separated state will be produced because reactions 3 and 4 in figure 1A are blocked [29, 30]. The production of this state has been shown to be reversible after an extended incubation with hydroxylamine [29, 30]. In agreement with these previous studies, we found that extended incubation reproducibly gave a photo-induced negative 1483-cm^{-1} signal, the production of which was reversible. A multiexponential fit to the transient gave three time constants equal to 5 ms (46%), 470 μs (19%), and 20 μs (35%).

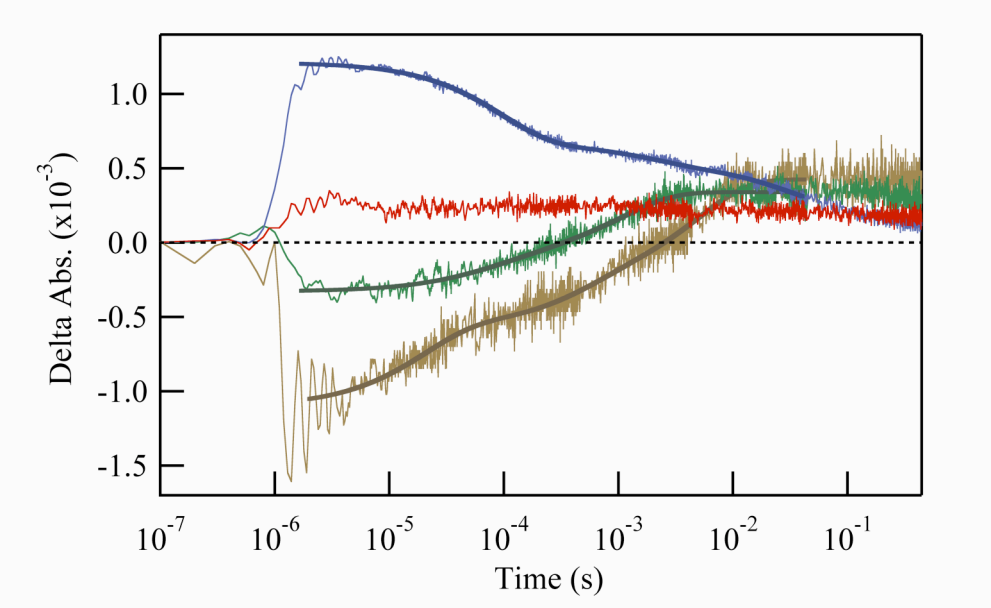

Figure 2. Control transients recorded at 1483-cm^{-1} and 10°C from PSII. In the green trace, OEC-containing samples contained 0.6 mM DCBQ and 7.2 mM potassium ferricyanide (repeated from figure 1B, flash 1). In the red trace, OEC-containing samples contained 5 mM DCMU alone. In the beige trace, OEC-inactivated samples contained 7.5 mM hydroxylamine and 100 μM DCMU. In the blue trace, OEC-inactivated samples contained 0.6 mM DCBQ and 7.2 mM potassium ferricyanide. For the red, blue, and beige traces, transients (5, 24, and 2, respectively) were averaged. Multiexponential fits to the data (table 1) are shown superimposed.

Previously, time constants of ≤ 20 and ≈ 200-300 μs have been reported under these conditions and assigned to rates of $P_{680}^{+}Q_A^{-}$ decay [29, 30]. The observation of a 5-ms component in our experiments may be due to a difference in sample preparation. In some hydroxylamine- and DCMU-treated samples, we observed a small positive signal, which we attribute to an incomplete block of Y_Z-to-P_{680}^{+} electron transfer, as previously proposed [29, 30]. When this signal was observed, longer incubation of the sample with hydroxylamine and DCMU gave the reproducible negative signal (figure 2, brown trace). The data acquired on hydroxylamine- and DCMU-treated samples (figure 2, brown trace)

suggest that the initial bleach in the OEC sample (figure 2, green trace) is due to the generation of Q_A^-.

As an additional control, DCBQ and ferricyanide were added to a Mn-depleted sample (figure 2, blue trace). In this sample, the OEC is inactivated with 1.8 M alkaline Tris [22], Y_Z is the terminal electron donor [31, 32], and reaction 5 in figure 1A is blocked. In this sample, Y_Z reduces P_{680}^+ with a lifetime in the microsecond time domain [31, 32]. The blue trace in figure 2 shows an immediate increase in amplitude, as opposed to the decrease in amplitude observed in oxygen-evolving preparations (green trace). We attribute the 1483-cm^{-1} amplitude increase to a contribution from $Y_Z^\bullet$ in these OEC-inactivated samples. This $Y_Z^\bullet$ assignment is in agreement with the previous assignments of MacDonald et al. [33], which were derived from analysis of the photoaccumulated $Y_Z^\bullet$ spectrum and have been supported by additional studies (reviewed in [34] and [35]).

This $Y_Z^\bullet$ assignment is also supported by fits to the 1483-cm^{-1} transient (figure 2, blue trace), which gave three time constants equal to 34 ms (32%), 1.8 ms (14%), and 95 μs (54%). Time constants of 50 ms (40% amplitude) and 3 s (60%) have previously been reported for the decay of the $Y_Z^\bullet$ UV signal [36]. The 3-s time constant would not be observable with our data acquisition conditions. In Mn-depleted PSII, the relatively intense, positive 1483-cm^{-1} absorption from $Y_Z^\bullet$ masks the less intense bleach, which is expected from the formation of the $P_{680}^+Q_A^-$ charge-separated state. In OEC-containing PSII, the spectrum of $Y_Z^\bullet$ must be shifted away from the 1483-cm^{-1} observation frequency.

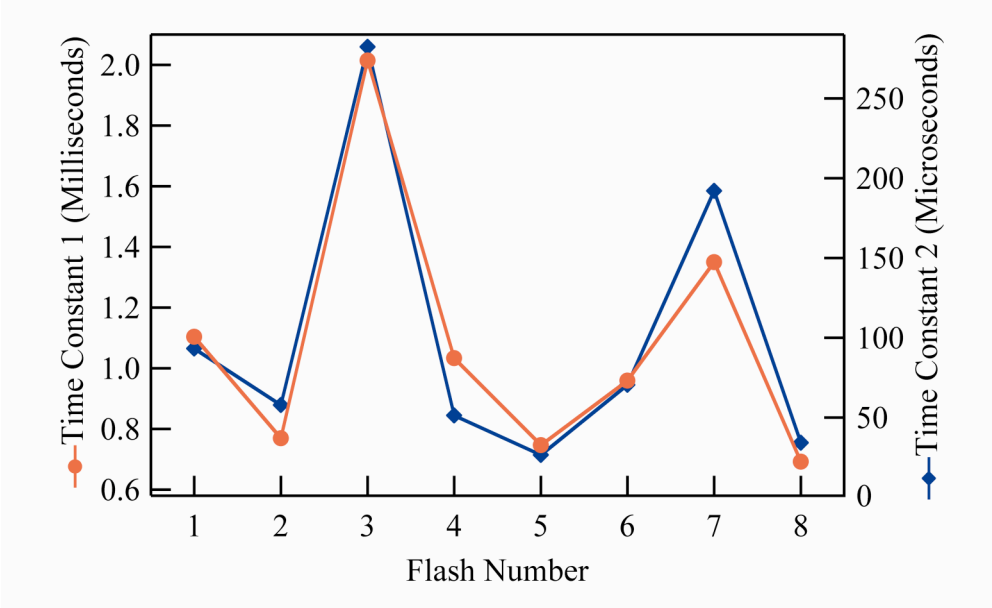

Figure 3. Plot of extracted time constants versus flash number derived from biexponential fits to the IR transients recorded at 1483-cm^{-1}. Two time constants were derived, and these time constants are plotted on different scales on the two *y* axes. Data acquired on the first four flashes are shown in figure 1B.

Comparison of these controls suggests that the initial bleach in the OEC-containing sample is due to the generation of the Q_A^- state (figure 1A, reactions 1 and 2). Interestingly, the initial amplitude shows period-2 dependence (figure 1B). If Q_A^- and Q_B^- have a similar contribution at this wavelength, then on this time scale, the acceptor side contribution will remain relatively stable. Therefore, we hypothesized that the slower processes after the initial bleach are due to an amino acid side chain that is close to or ligating the Mn cluster in the OEC. To test this hypothesis, transients were fit with a double exponential function between 12 μs and 26 ms (figure 1B). As observed in figure 3 and table 1, the derived time constants show a four-flash dependence, with the rate slowing by a factor of three to five on the third and seventh flash. This period-4 dependence is characteristic of reactions in the OEC (for examples, see [9-11]).

Table 1. Rate constants derived from multiexponential fits to 1483-cm^{-1} infrared transients.

Flash no.	Phase 1		Phase 2	
	Percentage	Rate, s^{-1}	Percentage	Rate, s^{-1}
1	32	10700	68	906
2	22	17300	78	1300
3	45	3540	55	496
4	21	19500	79	968
5	20	37700	80	1340
6	33	14200	67	1040
7	29	5200	71	741
8	21	29200	79	1440

Discussion

In this paper, we present a time-resolved IR study of the photosynthetic water-oxidizing complex. The observed immediate decrease in 1483-cm^{-1} absorption in the OEC-containing samples (figure 1B) is attributed to an amino acid side chain in the vicinity of Q_A that is perturbed in frequency when Q_A is reduced (figure 1A, reaction 2). We propose that this effect cancels the expected positive absorption from Q_A^- and Q_B^- [37-39] on this time scale and at this frequency. From the frequency, one possible assignment is to an imidazole ring stretching vibration. Imidazole ring stretching vibrations have been reported in the range of 1490-1460 cm^{-1} in ^2H_2O and ^1H_2O [40-42]. Histidine side chains are known to be ligands to an acceptor side, nonheme iron in PSII [15, 16]. This ferrous iron is 9 Å from Q_A and is magnetically coupled to Q_A^-, and its histidine ligands are close to Q_A and Q_B [13-17].

The overlapping 1483-cm^{-1} negative signal from the OEC, which shows period-4 dependence, is also assigned to an amino acid side chain. A reasonable assignment is to a

histidine (see discussion above) that is bound to manganese or near the OEC [13-17, 43]. To explain our results, a histidine frequency change must occur on each S state transition (figure 1B). The transients show an initial bleach, which is followed by an increase over the baseline and by an eventual decay to baseline (figure 1B). Therefore, these measurements suggest that an intermediate state in which an OEC histidine is perturbed is formed on each S state transition.

Our extracted rate constants for the OEC reactions (table 1) can be compared with previous measurements. Through UV spectroscopy, half-times of 110, 350, 1300, and 30 μs were derived for the S_1-to-S_2, S_2-to-S_3, S_3-to-S_0, and S_0-to-S_1 transitions, respectively [10]. Through X-ray measurements, similar half-times were reported and assigned to Mn redox reactions [11], except that a lag time of 200 μs was detected before Mn reduction during the S_4-to-S_0 transition. The ^2H_2O isotope effects on the S state transitions have been reported in the range of 1.3- to 1.4-fold [44].

In contrast, our measured rates exhibit both microsecond and millisecond phases on each S state transition, all of which show period-4 oscillation. This result suggests that IR spectroscopy can detect a kinetic heterogeneity that is not detectable by UV spectroscopy or X-ray fluorescence. For the S_1-to-S_2 and S_0-to-S_1 transitions, the microsecond time constants derived from our data (≈ 90 and 50 μs, respectively) are in agreement with the previously reported rates of Mn oxidation [11]. Therefore, on these two transitions, we attribute the perturbative mechanism to the Mn oxidation reaction. However, for the S_2-to-S_3 and S_3-to-S_0 transitions, the microsecond time constants derived from our data (≈ 60 and 300 μs, respectively) are significantly faster than the reported rates of Mn redox reactions [11]. Although we have not accounted for S state

misses, these results suggest that the perturbative mechanism on these two transitions is not a Mn redox change but a conformational change or a proton transfer reaction. This conformational change or proton transfer reaction may be linked to Y_Z oxidation either through electrostatics [11] or allosterics. The idea that proton transfer reactions may precede electron transfer has important implications for the overall water oxidation reaction. Such behavior has recently been observed for the proton-coupled electron transfer reactions in cytochrome *c* oxidase [45] and has been suggested to occur during the S_3-to-S_0 transition, based on the lag phase observed by X-ray spectroscopy [11].

Our measurements are unique when compared with previous studies of the OEC with vibrational spectroscopy. For example, our measurements are on a much faster time scale compared with rapid-scan Fourier-transform IR (FT-IR) studies of the OEC (for examples see [24, 46, 47]). Note that it has recently been suggested that a histidine perturbation may occur with S state cycling on the 10-s time scale [48]. Although cryogenic, rapid-scan FT-IR spectroscopy has been used to study the S_1-to-S_2 transition, this technique cannot be applied to the other S state transitions, which do not occur at cryogenic temperature [49]. Raman spectroscopy has been used to study the S_1 and S_2 states, but these experiments were designed to probe structure on a relatively long time scale under cryogenic conditions [50]. Thus, to our knowledge, our measurements are the first to detect these short-lived intermediates with vibrational spectroscopy.

References

1. Rubtsov, I.V., J. Wang, and R.M. Hochstrasser, *Dual-frequency 2D-IR spectroscopy heterodyned photon echo of the peptide bond.* Proc Natl Acad Sci USA, 2003. **100**: p. 5601-5606.

2. McCamant, D.W., P. Kukura, and R.A. Mathies, *Femtosecond broadband stimulated Raman: a new approach for high-performance vibrational spectroscopy.* Appl Spectrosc, 2003. **57**: p. 1317-1323.

3. Ataka, K., et al., *Oriented attachment and membrane reconstitution of His-tagged cytochrome c oxidase to a gold electrode: in situ monitoring by surface-enhanced infrared absorption spectroscopy.* J Am Chem Soc, 2004. **126**: p. 16199-16206.

4. Kotting, C. and K. Gerwert, *Monitoring protein-ligand interactions by time-resolved FTIR difference spectroscopy.* Methods Mol Biol, 2005. **305**: p. 261-286.

5. Britt, R.D., *Oxygen evolution*, in *Oxygenic Photosynthesis: The Light Reactions*, D.R. Ort and C.F. Yocum, Editors. 1996, Kluwer Academic Publisher: Dordrecht. p. 137-164.

6. de Wijn, R. and H.J. van Gorkom, *Kinetics of electron transfer from Q_A to Q_B in photosystem II.* Biochemistry, 2001. **40**: p. 11912-11922.

7. Velthuys, B.R. and J. Amesz, *Charge accumulation at the reducing side of system 2 of photosynthesis.* Biochim Biophys Acta, 1974. **333**: p. 85-94.

8. Gerken, S., et al., *Optical characterization of the immediate donor to chlorophyll a_{II}^+ in O_2-evolving photosystem II complexes.* FEBS Lett, 1988. **237**: p. 69-75.

9. Joliot, P. and B. Kok, *Oxygen evolution in photosynthesis*, in *Bioenergetics of Photosynthesis*, Govindjee, Editor. 1975, Academic Press: New York. p. 388-412.

10. Dekker, J.P., et al., *Kinetics of manganese redox transitions in the oxygen-evolving apparatus of photosynthesis.* Biochim Biophys Acta, 1984. **767**: p. 176-179.

11. Haumann, M., et al., *Photosynthetic O_2 formation tracked by time-resolved X-ray experiments.* Science, 2005. **310**: p. 1019-1021.

12. Clausen, J. and W. Junge, *Detection of an intermediate of photosynthetic water oxidation.* Nature, 2004. **430**: p. 480-483.

13. Zouni, A., et al., *Crystal structure of photosystem II from Synechococcus elongatus at 3.8 Å resolution.* Nature, 2001. **409**: p. 739-743.

14. Kamiya, N. and J.-R. Shen, *Crystal structure of oxygen-evolving photosystem II from Thermosynechococcus vulcanus at 3.7 Å resolution.* Proc Natl Acad Sci USA, 2003. **100**: p. 98-103.

15. Ferreira, K.N., et al., *Architecture of the photosynthetic oxygen-evolving center.* Science, 2004. **303**: p. 1831-1837.

16. Biesiadka, J., et al., *Crystal structure of cyanobacterial photosystem II at 3.2 Å resolution: a closer look at the Mn-cluster.* Phys Chem Chem Phys, 2004. **6**: p. 4733-4736.

17. Loll, B., et al., *Towards complete cofactor arrangement in the 3.0 Å resolution structure of photosystem II.* Nature, 2005. **438**: p. 1040-1044.

18. Messinger, J., *Evaluation of different mechanistic proposals for water oxidation in photosynthesis on the basis of Mn_4O_xCa structures for the catalytic site and spectroscopic data.* Phys Chem Chem Phys, 2004. **6**: p. 4764-4771.

19. McEvoy, J.P. and G.W. Brudvig, *Structure-based mechanism of photosynthetic water oxidation.* Phys Chem Chem Phys, 2004. **6**: p. 4754-4763.

20. Berthold, D.A., G.T. Babcock, and C.F. Yocum, *A highly resolved, oxygen-evolving photosystem II preparation from spinach thylakoid membranes.* FEBS Lett, 1981. **134**: p. 231-234.

21. Barry, B.A., *Tyrosyl radicals in photosystem II.* Methods Enzymol, 1995. **258**: p. 303-319.

22. Yamamoto, Y., et al., *Release of polypeptides from highly active O_2-evolving photosystem-2 preparation by tris treatment.* FEBS Lett, 1981. **133**: p. 265-268.

23. Vu, D.M., et al., *Probing the folding and unfolding dynamics of secondary and tertiary structures in a three-helix bundle protein.* Biochemistry, 2004. **43**: p. 3582-3589.

24. Barry, B.A., et al., *Calcium ligation in photosystem II under inhibiting conditions.* Biophys J, 2005. **89**: p. 393-401.

25. Noguchi, T. and M. Sugiura, *Flash-induced FTIR difference spectra of the water oxidizing complex in moderately hydrated photosystem II core films: effect of hydration extent on S-state transitions.* Biochemistry, 2002. **41**: p. 2322-2330.

26. Roelofs, T.A., et al., *Oxidation states of the manganese cluster during the flash-induced S-state cycle of the photosynthetic oxygen-evolving complex.* Proc Natl Acad Sci USA, 1996. **93**: p. 3335-3340.

27. Metz, J.G., et al., *Evidence for a dual function of the herbicide-binding D1 protein in photosytem II.* FEBS Lett, 1986. **205**: p. 269-274.

28. Boerner, R.J., et al., *Evidence from directed mutagenesis that aspartate 170 of the D1 polypeptide influences the assembly and/or stability of the manganese cluster*

in the photosynthetic water-splitting complex. Biochemistry, 1992. **31**: p. 6660-6672.

29. Ghanotakis, D.F. and G.T. Babcock, *Hydroxylamine as an inhibitor between Z and P_{680} in photosystem II.* FEBS Lett, 1983. **153**: p. 231-234.

30. Hoganson, C.W. and G.T. Babcock, *Redox cofactor interactions in photosystem II: electron spin resonance spectrum of P_{680}^{+} is broadened in the presence of Y_Z^{+}.* Biochemistry, 1989. **28**: p. 1448-1454.

31. Conjeaud, H. and P. Mathis, *The effect of pH on the reduction kinetics of P-680 in tris-treated chloroplasts.* Biochim Biophys Acta, 1980. **590**: p. 353-359.

32. Boska, M., et al., *Similarity of EPR signal IIf rise and P-680^{+} decay kinetics in tris-washed chloroplast photosystem II preparations as a function of pH.* Biochim Biophys Acta, 1983. **722**: p. 327-330.

33. MacDonald, G.M., K.A. Bixby, and B.A. Barry, *A difference Fourier-transform infrared study of two redox-active tyrosine residues in photosystem II.* Proc Natl Acad Sci USA, 1993. **90**: p. 11024-11028.

34. Kim, S., et al., *Infrared spectroscopic identification of the C-O stretching vibration associated with the tyrosyl $Z^{\bullet}$ and $D^{\bullet}$ radicals in photosystem II.* Biochim Biophys Acta, 1998. **1366**: p. 330-354.

35. Pujols-Ayala, I. and B.A. Barry, *Tyrosyl radicals in photosystem II.* Biochim Biophys Acta, 2004. **1655**: p. 205-216.

36. Dekker, J.P., et al., *Optical characterization of photosystem II electron donors.* Biochim Biophys Acta, 1984. **764**: p. 301-309.

37. Razeghifard, M.R., et al., *The in vivo, in vitro, and calculated vibrational spectra of plastoquinone and the plastosemiquinone anion radical.* J Phys Chem B, 1999. **103**: p. 9790-9800.

38. Zhang, H., et al., *A time-resolved FTIR difference study of the plastoquinone Q_A and redox-active tyrosine Y_Z interactions in photosystem II.* Biochemistry, 1997. **36**: p. 11762-11768.

39. Zhang, H., G. Fischer, and T. Wydrzynski, *Room-temperature vibrational difference spectrum for $S_2Q_B^{-}/S_1Q_B$ of photosystem II determined by time-resolved Fourier transform infrared spectroscopy.* Biochemistry, 1998. **37**: p. 5511-5517.

40. Caswell, D.S. and T.G. Spiro, *Ultraviolet resonance Raman spectroscopy of imidazole, histidine, and Cu(imidazole)$_4^{2+}$: Implications for protein studies.* J Am Chem Soc, 1986. **108**: p. 6470-6477.

41. Yoshida, C.M., T.B. Freedman, and T.M. Loehr, *Resonance Raman study of cobalt(II)-imidazole complexes as models for metalloproteins.* J Am Chem Soc, 1975. **97**: p. 1028-1030.

42. Garfinkel, D. and J.T. Edsall, *Raman spectra of amino acids and related compounds. VIII. Raman and infrared spectra of imidazole, 4-methylimidazole, and histidine.* J Am Chem Soc, 1958. **80**: p. 3807-3812.

43. Tang, X.-S., et al., *Identification of histidine at the catalytic site of the photosynthetic oxygen evolving complex.* Proc Natl Acad Sci USA, 1994. **91**: p. 704-708.

44. Karge, M., K.-D. Irrgang, and G. Renger, *Analysis of the reaction coordinate of photosynthetic water oxidation by kinetic measurements of 355 nm absorption changes at different temperatures in photosystem II preparations suspended in either H_2O or D_2O.* Biochemistry, 1997. **36**: p. 8904-8913.

45. Faxén, K., et al., *A mechanistic principle for proton pumping by cytochrome c oxidase.* Nature, 2005. **437**: p. 286-289.

46. Hillier, W. and G.T. Babcock, *S-state dependent Fourier transform infrared difference spectra for the photosystem II oxygen evolving complex.* Biochemistry, 2001. **40**: p. 1503-1509.

47. Noguchi, T. and M. Sugiura, *Flash-induced Fourier transform infrared detection of the structural changes during the S-state cycle of the oxygen-evolving complex in photosystem II.* Biochemistry, 2001. **40**: p. 1497-1502.

48. Kimura, Y., et al., *FTIR detection of structural changes in a histidine ligand during S-state cycling of photosynthetic oxygen-evolving complex.* Biochemistry, 2005. **44**: p. 16072 -16078.

49. Steenhuis, J.J. and B.A. Barry, *The protein and ligand environment of the S_2 state in photosynthetic oxygen evolution: a difference FT-IR study.* J Phys Chem, 1997. **101**: p. 6652-6660.

50. Cua, A., et al., *Low-frequency resonance Raman characterization of the oxygen-evolving complex of photosystem II.* J Am Chem Soc, 2000. **122**: p. 2069-2077.

CHAPTER 3

PROTON COUPLED ELECTRON TRANSFER REACTIONS AND TYROSINE Z OF THE PHOTOSYNTHETIC WATER OXIDIZING COMPLEX

by

Ian B. Cooper*, David L. Jenson*, Shana L. Bender*, Scott H. Brewer†, Dung M. Vu†, R. Brian Dyer†, and Bridgette A. Barry*

* - School of Chemistry and Biochemistry and the Petit Institute for Bioengineering and Bioscience, Georgia Institute of Technology, Atlanta, GA 30332

† - Integrated Spectroscopy Laboratory, Chemistry Division, Los Alamos National Laboratory, Group C-PCS, Mail Stop J567, Los Alamos, NM 87545

Abstract

In oxygenic photosynthesis, Photosystem II (PSII) is the photosynthetic reaction center that oxidizes water and reduces bound plastoquinone. Electron transfer in PSII is mediated by two redox-active tyrosine residues. One of these residues, tyrosine Z (Y_Z), has been assigned as Tyr161 of the D1 polypeptide by site-directed mutagenesis and isotopic labeling. Y_Z reduces a chlorophyll cation radical, P_{680}^+, and oxidizes the PSII catalytic site, which is the manganese-containing, oxygen evolving complex (OEC). Oxidation and reduction of Y_Z are expected to change the pK_A of the phenolic oxygen, resulting in coupled electron and proton transfer reactions. However, the mechanisms of these reactions have not yet been elucidated. In this report, transient infrared spectroscopy was used to investigate the pH dependence of $Y_Z^\bullet$ reduction reactions. PSII samples were treated with alkaline Tris, which removes the OEC and slows both the Y_Z

oxidation and $Y_Z^{\bullet}$ radical reduction rate. The kinetic isotope effect (KIE), induced by solvent deuterium exchange, was also measured. Transient measurements at 1483 cm^{-1} revealed a positive band, with a microsecond kinetic component. Isotopic labeling of tyrosine suggested that a fast kinetic component is assignable to $Y_Z^{\bullet}$. Slower millisecond kinetic components at 1483 cm^{-1} may be assignable to Q_A^{-}. The microsecond rate increased by a factor of ten, when the pH was increased from 5.0 to 8.0. In addition, this reaction exhibited a significant solvent isotope effect (> 2.5), which was pH independent. Transient measurements at 1483 cm^{-1} revealed that the millisecond rate decreased by a factor of seven, when the pH was increased from 5.0 to 8.0. However, the reduction reaction exhibited an insignificant solvent isotope effect.

Introduction

PSII carries out the light-catalyzed oxidation of water in oxygenic photosynthesis. Water oxidation occurs at a Mn_4-Ca^{+2} containing, oxygen-evolving complex (OEC) [1-4]. Electron transfer is initiated when the primary chlorophyll (chl) donor absorbs light. Subsequent electron transfer reactions lead to the production of a chl cation radical, P_{680}^{+}, and the sequential reduction of a pheophytin (pheo), of a single electron-accepting quinone, Q_A, and of Q_B, a two electron acceptor (reviewed in [5]). P_{680}^{+} is very unstable and readily generates other oxidized species [6]. One of these oxidized species, $Y_Z^{\bullet}$ [7, 8], is an intermediary in electron transfer reactions involving P_{680} and the OEC. Another redox-active tyrosine, Y_D, is also oxidized by P_{680}^{+} [7, 9-11]. However, $Y_D^{\bullet}$ forms a stable radical and is not required for oxygen evolution [7, 9, 10]. Y_D may be involved in the

assembly of the Mn_4-Ca^{+2} cluster [12]. Site directed mutagenesis has been used to assign Y_Z to Tyr 161 in the D1 polypeptide and Y_D to Tyr 160 in the D2 polypeptide [13-16].

Because the pK_a of the phenolic proton is dramatically altered by tyrosyl radical formation [17], redox-active tyrosines function in proton-coupled electron transfer reactions in enzymes (reviewed in [18]). Differences in the mechanism of these reactions may contribute to observed alterations in midpoint potential and electron transfer rate. For Y_Z and Y_D, three distinct mechanisms are possible [19-22]. The first is rate-limiting electron transfer to $Y^{\bullet}$ to yield an anionic Y^{-}, followed by fast proton transfer to give the product, Y (ETPT). A second is a pre-equilibrium proton transfer to give a tyrosyl cation radical, $YH^{+\bullet}$, followed by electron transfer to give the product, Y (PTET). A third is the concerted transfer of an electron and a proton to $Y^{\bullet}$ in one kinetic step (CPET), which is expected to give a kinetic isotope effect [19-22]. Other mechanisms involve sequential electron and proton transfer reactions in which proton transfer is the slow, rate-limiting step. However, proton transfer reactions occur over short distances and are usual facile in biological systems (see [21-24] and references therein).

In the 3.0 Å PSII structure [4], both redox-active tyrosines are within hydrogen bonding distance of a histidine. His189 in the D2 polypeptide is 2.6 Å from Y_D, and His190 in the D1 polypeptide is 2.8 Å from Y_Z. The placement of other amino acid side chains, the location of metal ions, and the orientation of the histidines distinguishes the protein environment of Y_D and Y_Z. Spectroscopic evidence suggests that proton transfer occurs from Y_D to D2-His189 [25] and that $Y_D^{\bullet}$ is hydrogen bonded to this histidine [26]. D1-His190 has also been implicated as the proton transfer reaction partner of Y_Z ([27, 28]

but see [29]). Magnetic resonance studies of $Y_Z^{\bullet}$ in manganese depleted PSII have been interpreted to be consistent with a disordered hydrogen bond to this radical [30, 31].

To obtain more information concerning the mechanism of the Y_D proton-coupled electron transfer reaction, we recently performed solvent isotope exchange and measured the solvent isotope effect on $Y_D^{\bullet}$ reduction [22]. $Y_D^{\bullet}$ was detected independently of $Y_Z^{\bullet}$ and other PSII electron donors by EPR spectroscopy. Under the conditions employed, the reduction of $Y_D^{\bullet}$ was attributed to recombination with the PSII Q_A^- plastoquinone acceptor. The majority amplitude kinetic phase exhibited a pL-dependent rate constant, with a minimum at pL 7.0. Between pL 7.5 and 8.0, solvent exchange gave significant (> 2.1) kinetic isotope effects. These results were consistent with a coupled electron and proton transfer reaction (CPET), which occurs with a single kinetic step at pL values $\geq$ 7.5. At pL values below 7.0, smaller KIE values and a significant rate acceleration were consistent with a change of mechanism, in which the protonation of $Y_D^{\bullet}$ occurs first, followed by rate-limiting electron transfer (PTET).

For Y_Z, a discussion of previous, proposed proton-coupled electron transfer mechanisms can be found in [32] and references therein. Reported experiments have focused mainly on Y_Z oxidation kinetics using 820 nm optical spectroscopy to monitor P_{680}^+ decay. The mechanism of Y_Z oxidation has been attributed by different authors to a CPET reaction [32], to a gated reaction in which the reaction rate is governed by histidine deprotonation [31], or to consecutive PTET [33].

In this study, we have used microsecond, time-resolved infrared spectroscopy to monitor Y_Z redox reactions. In previous work, we have used this transient infrared approach to monitor the PSII oxygen evolving reactions at the OEC [34]. Here, we have

treated PSII with alkaline Tris to remove the OEC [34, 35]. This treatment has the effect of slowing both the oxidation and reduction of $Y_Z/Y_Z^{\bullet}$ [36-38].

Materials and Methods

PSII membranes were isolated from market spinach [39]. Manganese was removed by treatment with alkaline Tris at elevated pH [35]. Manganese-depleted PSII was pooled and exchanged into ^1H_2O or ^2H_2O buffers at pL 5.0, 6.0, 7.0, and 8.0 by dialysis, as previously described [22]. The samples contained 0.4 M sucrose and 15 mM NaCl. Succinate (50 mM) was used as the buffer at pL 5, MES (2-(*N*-morpholino)ethanesulfonic acid) (50 mM) was used as the buffer at pL 6 and 7, and HEPES (4-(2-hydroxyethyl)-1-piperazineethanesulfonic acid) (50 mM) was used as the buffer at pL 8. ^2H_2O was purchased from Cambridge Isotope Laboratories, Inc. (99% ^2H enrichment, Andover, CA).

As a control, PSII was also isolated from cyanobacterium *Synechocystis* PCC 6803 which was grown in the presence of either control tyrosine (L-tyrosine) or labeled tyrosine (L-tyrosine-ring-d_4). Cultivation of this cyanobacterium in the presence of the control or labeled tyrosine leads to the global incorporation of the supplied amino acid into PSII [7]. In L-tyrosine-ring-d_4, the protons of the phenol ring are replaced with deuterons. Deuteration of tyrosine has the effect of shifting vibrational bands of tyrosine and tyrosyl radical [40]. Cyanobacterial PSII was isolated as previously described [41], and manganese was removed by treatment with NH_2OH [42]. The samples were stored in 5 mM MES, p^{2}H 6.0, and 0.03% n-dodecyl-β-D-maltopyranoside at –70°C.

Spinach PSII samples for transient IR measurements were prepared as previously described [34]. Briefly, a manganese-depleted PSII suspension was mixed with reagents and centrifuged, after which the supernatant was removed. The pellet was placed between two CaF_2 windows with a 25 micron Teflon spacer. The sample cell was sealed with parafilm to control hydration and maintained at 10°C by circulating water bath. Cyanobacterial PSII samples for transient IR measurement were concentrated to a volume of 10 microliters and mixed with reagents. The mixture was injected between two CaF_2 windows pre-sealed sealed with parafilm and maintained at 10°C by circulating water bath. Flash-induced excitation was provided by a Nd:YAG pulse laser (Spectra Physics, Mountain View, CA), which was frequency-doubled to 532 nm. The sample was probed by a continuous-wave infrared diode laser (Ekips Technologies, Norman, OK) at 1483 cm^{-1}. Infrared absorbance changes were monitored with a liquid nitrogen cooled MCT detector (Kolmar Technologies, Newburyport, MA) with a time resolution of 1 microsecond.

Signal alignment was performed on one spot of the sample followed by translation to a new spot for data collection. After translation, a single 532 nm laser pulse was given, and the transient IR signal was recorded. The data were fit and analyzed using Igor Pro software (Wavemetrics, Lake Oswego, OR).

Results and Discussion

Figure 1 shows the kinetic transients acquired at 1483 cm^{-1} from OEC-depleted PSII. Y_Z and Q_B are the terminal electron donor and acceptor in this type of PSII

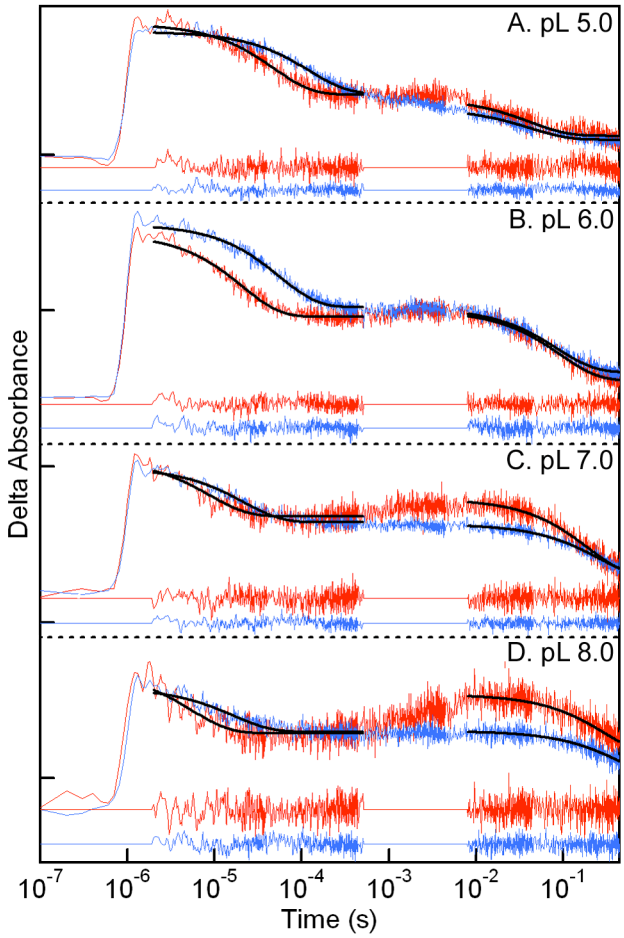

Figure 1. Flash-induced kinetic transients acquired at 1483 cm^{-1} from OEC-depleted PSII. In (A-D), data were recorded at pL 5.0 (A), 6.0 (B), 7.0 (C), or 8.0 (D). The red and blue traces were obtained either in ^1H_2O or ^2H_2O buffer, respectively. Samples contained 3 mM ferricyanide and 3 mM ferrocyanide, and the 532 nm laser energy was 1 mJ $(cm)^{-2}$. Each kinetic trace was an average of 48 experiments, except for (C, red trace), which was an average of 68; (D, red trace), which was an average of 66; and (D, blue trace), which was average of 52. The temperature was 10°C. Exponential fits are shown superimposed over each trace, with residuals color-coded at the bottom of each panel. The tick marks on the y axis represent 1 x 10^{-3} absorbance units.

preparation [38]. The 1483 cm^{-1} transients in red were acquired in ^1H_2O at pH 5.0 (figure 1A), 6.0 (figure 1B), 7.0 (figure 1C) and 8.0 (figure 1D), respectively. Immediately (2 microseconds) after the 532 nm flash, the sign of the transient is positive,

Table 1. Rate constants and kinetic isotope effects derived from the kinetic transient at 1483 cm^{-1}: pL and solvent isotope effects[a]

Sample	^1H_2O rate constant (s^{-1})	^2H_2O rate constant (s^{-1})	KIE[b]
Fast Phase[c]			
pL 5.0[d]	20,600 ± 2,600	8,100 ± 200	2.5 ± 0.3
pL 6.0[d]	47,500 ± 3,000	18,100 ± 2,500	2.6 ± 0.4
pL 7.0[d]	114,000 ± 36,800	45,600 ± 1,900	2.5 ± 0.8
pL 8.0[d]	292,000 ± 145,000	61,700 ± 2,000	4.7 ± 2.8
DCMU[e]	ND[f]	10,600 ± 620	ND
No DCMU[e]	ND	11,400 ± 157	ND
Control[j]	ND	150,000 ± 65,000	ND
Y-ring-d_4[j]	ND	33,000 ± 8,000	ND
Slow Phase[c]			
pL 5.0[d]	23.4 ± 0.7	23.4 ± 3.0	1.0 ± 0.1
pL 6.0[d]	10.5 ± 1.3	11.6 ± 1.0	0.9 ± 0.1
pL 7.0[d]	5.3 ± 0.9	3.9 ± 0.2	1.3 ± 0.2
pL 8.0[d]	3.3 ± 0.9	2.4 ± 0.4	1.4 ± 0.4
DCMU[e]	ND	16.2 ± 2.5	ND
No DCMU[e]	ND	14.4 ± 0.6	ND

[a] Derived from exponential fits, $A_0 + A_1\exp(-k_1 t)$, to transient infrared data recorded at 1483 cm^{-1}. Values are reported plus or minus one standard deviation. Mean chi-squared values for the fits were (3.1 ± 1.3) $x10^{-6}$.

[b] Calculated as the ratio of the rate constant measured in ^1H_2O to the rate constant measured in ^2H_2O.

[c] Fast phase derived from a single exponential fit to the data between 2 and 500 microseconds, and slow phase derived from a single exponential fit to the data between 8 and 444 ms.

[d] Data acquired with 3 mM ferricyanide, 3 mM ferrocyanide, and energy density 1 mJ $(cm)^{-2}$.

[e] Data acquired at p^2H 6.0 with 2.5 mM ferricyanide, 2.5 mM ferrocyanide, 0 or 100 μM DCMU, and energy density 38 mJ $(cm)^{-2}$.

[f] Data acquired at p^2H 6.0 with 3 mM ferricyanide, 3 mM ferrocyanide, and energy density 63 mJ $(cm)^{-2}$.

[g] ND, not determined.

and there are two decaying components on the microsecond and millisecond time scales. Table 1 presents rate constants derived from single exponential fits (figure 1, solid superimposed lines) in these two time regimes. At pH 6.0, the derived time constants are 20 microseconds (fast phase) and 95 milliseconds (slow phase; table 1). Figure 2A and B, red traces, show that increases in pH accelerate the decay rate of the fast phase and decrease the decay rate of the slow phase. The differential pH dependence of the two rate

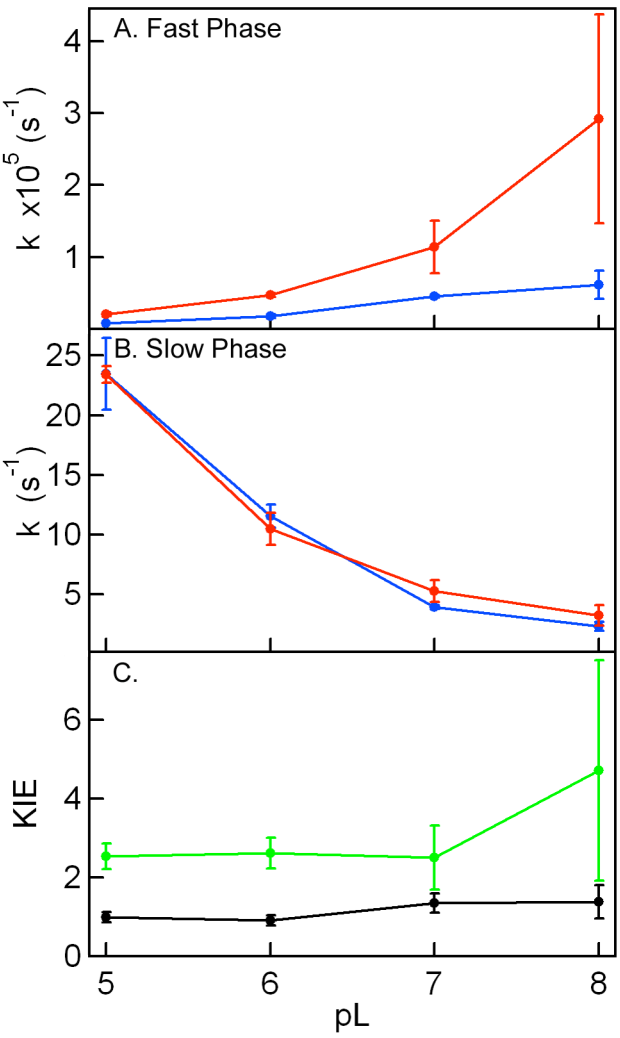

Figure 2. Rate constants and kinetic isotope effects as a function of pL. The rate constants were derived from exponential fits to the 1483 cm^{-1} kinetic transients in Figure 1A-D. Samples contained either ^1H_2O (red) or ^2H_2O (blue). In (A), rate constants were derived from a single exponential fit to the data between 2 and 500 microseconds (fast phase). In (B), rate constants were derived from a single exponential fit to the data between 8 and 444 ms (slow phase). In (C), the solvent, kinetic isotope effects for the fast (green) and slow (black) phases are shown; the solvent isotope effect was calculated as the ratio of the rate constant in ^1H_2O to the rate constant in ^2H_2O. Error bars represent one standard deviation. Rate constants and kinetic isotope effects are also presented in table 1.

constants (figure 2A and B) suggests that two different species, with different infrared molar absorptivities, are monitored at this frequency.

In previous work, we found that the positive sign of the transient at 1483 cm^{-1} is dependent on OEC removal, because OEC-containing PSII preparations showed an immediate bleach at this frequency [34]. In addition, a DCMU-containing, negative control, in which the PSII reaction center was closed to charge separation [34], exhibited no kinetic transient (figure 3A, black trace). A control, in which hydroxylamine and DCMU were used to generate the $P_{680}^{+}Q_A^{-}$ state [43, 44], also generated an immediate bleach [34] at this frequency (figure 3A, brown trace). Triple exponential fits to the transient gave rate constants of 36,000 ± 6,000 (32%), 2900 ± 600 (24%), and 214 ± 24 (44%) s^{-1}.

Compared to our earlier work, which was performed in ^2H_2O buffer at p^{2}H 6.0, the data in figure 1A-D were acquired at much lower 532 nm energy density [34]. Comparison of data in figures 1 and 3 demonstrates that this change in 532 nm energy, from 1 (figure 1B, blue trace) to 38 mJ $(cm)^{-2}$ (figure 3B, blue trace), had little or no effect on the 1483 cm^{-1} decay kinetics (also see table 1). Furthermore, figure 4 and table 2 also demonstrate that laser energy densities ranging from 6.4 to 63 mJ $(cm)^{-2}$ produced similar 1483 cm^{-1} decay kinetics. Previously, we indicated a 532 nm spot size of 0.2 cm radius used in data collection [34]. We wish to clarify here that the data presented in [34] as well as in figure 3B, blue trace, was collected at a 532 nm spot size of 0.1 cm diameter.

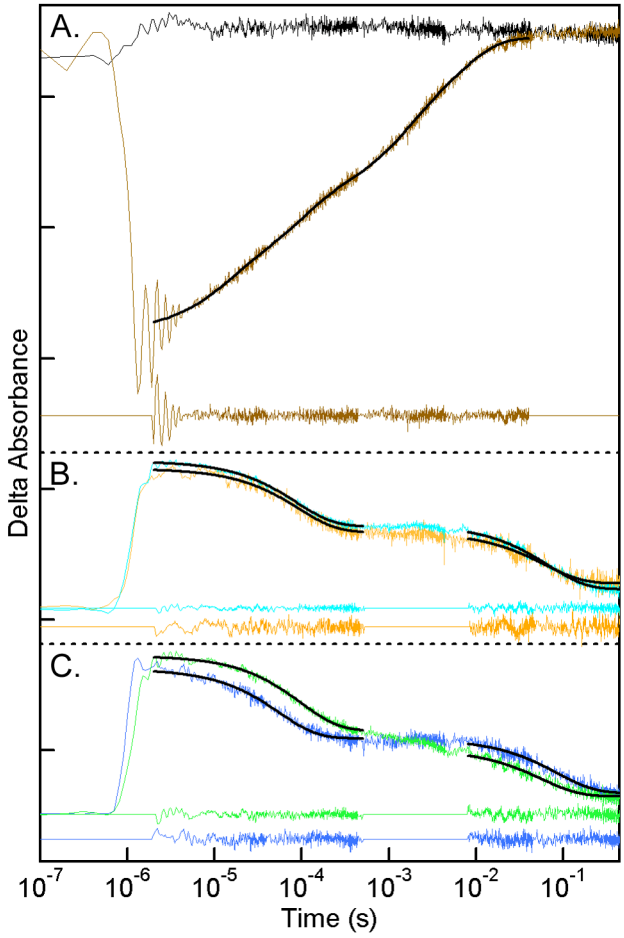

Figure 3. Flash-induced kinetic transients acquired at 1483 cm^{-1} from PSII. In (A), data were acquired from OEC-depleted PSII treated with 7.5 mM NH_2OH and 100 micromolar DCMU (brown trace, avg. of 36, energy density 33 mJ $(cm)^{-2}$) or OEC-containing PSII treated with 5 mM DCMU (black trace, avg. of 5, energy density 38 mJ $(cm)^{-2}$). In (B), data were recorded from OEC-depleted PSII treated with 2.5 mM potassium ferricyanide, 2.5 mM potassium ferrocyanide, and either 0 (light blue trace, avg. of 21) or 100 micromolar (orange trace, avg. of 4) DCMU, energy density 38 mJ $(cm)^{-2}$. In (C), data were acquired from OEC-depleted PSII treated with 0.6 mM DCBQ and 7.2 mM ferricyanide (green trace, avg. of 24, energy density 38 mJ $(cm)^{-2}$) or with 3 mM ferricyanide and 3 mM ferrocyanide (blue trace, repeated from figure 1B, energy density 1 mJ $(cm)^{-2}$). The samples were suspended in ^2H_2O buffer (0.4 M sucrose, 50 mM MES-NaO^2H, 15 mM NaCl) at p^{2}H 6.0. The temperature was 10^{o}C. Exponential fits are shown superimposed over each trace, with residuals for each fit color-coded below the data. The space between tick marks of the y-axis represents $1x10^{-3}$ absorbance units.

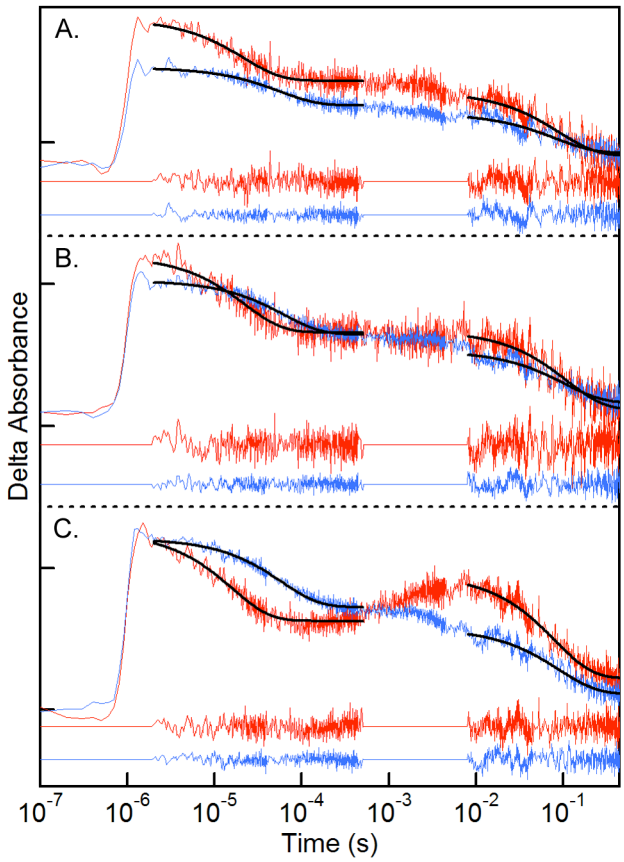

Figure 4. Flash-induced kinetic transients acquired at 1483 cm^{-1} from PSII. In (A), data were acquired from OEC-depleted PSII in $^{1}H_2O$ (red trace, avg. of 40) or $^{2}H_2O$ (blue trace, avg. of 40) at energy density 6.4 mJ $(cm)^{-2}$. In (B), data were acquired from OEC-depleted PSII in $^{1}H_2O$ (red trace, avg. of 40) or $^{2}H_2O$ (blue trace, avg. of 40) at energy density 20 mJ $(cm)^{-2}$. In (C), data were acquired from OEC-depleted PSII in $^{1}H_2O$ (red trace, avg. of 40) or $^{2}H_2O$ (blue trace, avg. of 40) at energy density 63 mJ $(cm)^{-2}$. Samples were suspended in either $^{1}H_2O$ buffer (0.4 M sucrose, 50 mM MES-NaOH, p^{1}H 6.0, 15 mM NaCl) or $^{2}H_2O$ buffer (0.4 M sucrose, 50 mM MES-NaO^{2}H, p^{2}H 6.0, 15 mM NaCl). The temperature was 10°C. Exponential fits are shown superimposed over each trace, with residuals for each fit color-coded below the data. The space between tick marks of the y-axis represents $1x10^{-3}$ absorbance units.

Table 2. Rate constants and kinetic isotope effects derived from the kinetic transient at 1483 cm^{-1}: laser energy density effects[a]

Laser energy density (mJ/cm^2)	^1H_2O rate constant (s^{-1})	^2H_2O rate constant (s^{-1})	KIE[b]
Fast Phase[c]			
6.4[d]	45,600 ± 6,000	17,800 ± 3,200	2.6 ± 0.6
20[d]	44,400 ± 8,300	15,900 ± 2,100	2.8 ± 0.6
63[d]	62,200 ± 7,000	16,800 ± 1,000	3.7 ± 0.5
Slow Phase[c]			
6.4[d]	11.2 ± 1.4	12.2 ± 1.9	0.9 ± 0.2
20[d]	9.1 ± 0.8	9.9 ± 3.1	0.9 ± 0.3
63[d]	12.4 ± 0.7	11.1 ± 2.2	1.1 ± 0.2

[a] Derived from exponential fits, $A_0 + A_1\exp(-k_1 t)$, to transient infrared data recorded at 1483 cm^{-1}. Values are reported plus or minus one standard deviation. Mean chi-squared values for the fits were (6.4 ± 5.1) $x10^{-6}$.

[b] Calculated as the ratio of the rate constant measured in ^1H_2O to the rate constant measured in ^2H_2O.

[c] Fast phase derived from a single exponential fit to the data between 2 and 500 microseconds, and slow phase derived from a single exponential fit to the data between 8 and 444 ms.

[d] Data acquired at p^1H 6.0 and p^2H 6.0 with 3 mM ferricyanide and 3 mM ferrocyanide.

The effect on the rate constants of changes in exogenous electron donor and acceptor was investigated. There was no significant change in the rate of the slow or fast phase when 0.6 mM DCBQ/7.2 mM ferricyanide (figure 3C, green trace) was substituted for 3 mM ferrocyanide/3 mM ferricyanide (figure 3C, blue trace). Indeed, treatment of the sample with 4.5 mM ferrocyanide/0.5 mM ferricyanide (figure 5A), 6 mM ferricyanide (figure 5B), or 6 mM ferrocyanide (figure 5C) did not change the derived rate constants for the fast and slow phases (see table 3). These results demonstrate that the 1483 cm^{-1} transient is monitoring internal recombination events, which are independent of the concentration of exogenous electron donors/acceptors.

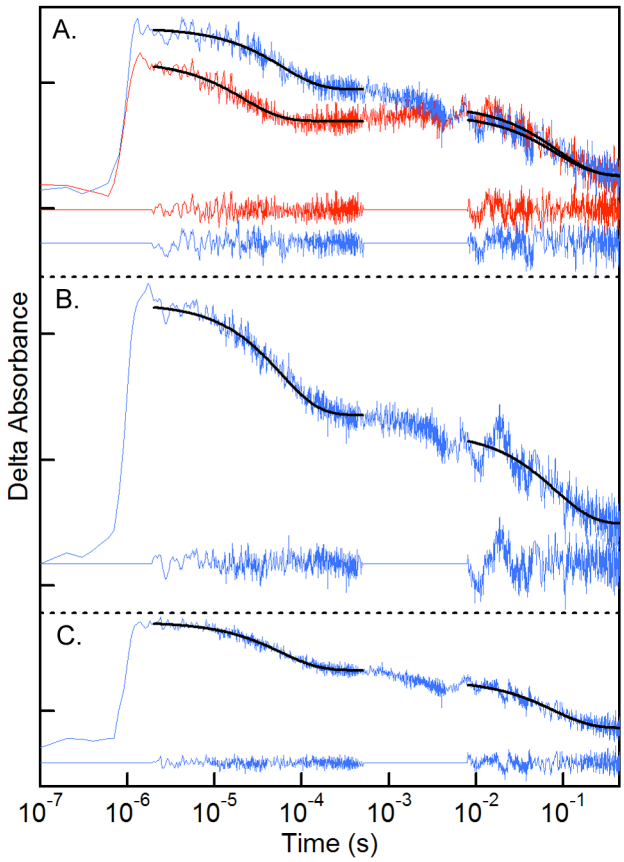

Figure 5. Flash-induced kinetic transients acquired at 1483 cm^{-1} from PSII. In (A), data were acquired from OEC-depleted PSII with 0.5 mM ferricyanide and 4.5 mM ferrocyanide in $^{1}H_2O$ (red trace, avg. of 50) or $^{2}H_2O$ (blue trace, avg. of 50). In (B), data were acquired from OEC-depleted PSII with 6 mM ferricyanide in $^{2}H_2O$ (avg. of 50). In (C), data were acquired from OEC-depleted PSII with 6 mM ferrocyanide in $^{2}H_2O$ (avg. of 50). Samples were suspended in either $^{1}H_2O$ buffer (0.4 M sucrose, 50 mM MES-NaOH, p^{1}H 6.0, 15 mM NaCl) or $^{2}H_2O$ buffer (0.4 M sucrose, 50 mM MES-NaO^{2}H, p^{2}H 6.0, 15 mM NaCl). The energy density was 20 mJ $(cm)^{-2}$ and the temperature was 10°C. Exponential fits are shown superimposed over each trace, with residuals for each fit color-coded below the data. The space between tick marks of the y-axis represents $1x10^{-3}$ absorbance units.

Table 3. Rate constants and kinetic isotope effects derived from the kinetic transient at 1483 cm^{-1}: exogenous electron acceptor and donor effects[a]

ferricyanide (mM)	ferrocyanide (mM)	^1H_2O rate constant (s^{-1})	^2H_2O rate constant (s^{-1})	KIE[b]
		Fast Phase[c]		
3	3[d]	47,500 ± 3,000	18,100 ± 2,500	2.6 ± 0.4
7.2	0[e]	ND[h]	10,000 ± 250	ND
0.5	4.5[f]	45,500 ± 2,300	16,500 ± 2,000	2.8 ± 0.3
6	0[g]	ND	17,100 ± 1,500	ND
0	6[g]	ND	16,900 ± 900	ND
		Slow Phase		
3	3[d]	10.5 ± 1.3	11.6 ± 1.0	0.9 ± 0.1
7.2	0[e]	ND	17.3 ± 2.4	ND
0.5	4.5[f]	11.5 ± 0.5	11.9 ± 2.1	1.0 ± 0.2
6	0[g]	ND	11.9 ± 2.2	ND
0	6[g]	ND	13.1 ± 2.3	ND

[a] Derived from exponential fits, $A_0 + A_1\exp(-k_1 t)$, to transient infrared data recorded at 1483 cm^{-1}. Values are reported plus or minus one standard deviation. Mean chi-squared values for the fits were (8.7 ± 2.5) $x10^{-6}$.

[b] Calculated as the ratio of the rate constant measured in ^1H_2O to the rate constant measured in ^2H_2O.

[c] Fast phase derived from a single exponential fit to the data between 2 and 500 microseconds, and slow phase derived from a single exponential fit to the data between 8 and 444 ms.

[d] Data acquired at p^1H 6.0 and p^2H 6.0, and energy density 1 mJ $(cm)^{-2}$.

[e] Data acquired at p^2H 6.0 with 7.2 mM ferricyanide, 0.6 mM DCBQ, and energy density 38 mJ $(cm)^{-2}$.

[f] Data acquired at p^1H 6.0 and p^2H 6.0, and energy density 20 mJ $(cm)^{-2}$.

[g] Data acquired at p^2H 6.0 and energy density 20 mJ $(cm)^{-2}$.

[h] ND, not determined.

Based on previous FT-IR and Raman experiments, positive spectral contributions at this frequency could, in principle, be derived from a chl cation radical, Q_A^-, Q_B^-, $Y_Z^\bullet$, or $Y_D^\bullet$ [45-50]. However, $Y_D^\bullet$ reactions are too slow to be directly monitored on this time scale (for example, see [22]). A positive P_{680}^+ cation radical contribution is also unlikely, because the $P_{680}^+Q_A^-$ control, presented in our earlier work and in figure 3A (hydroxylamine/DCMU), exhibited a bleach at 1483 cm^{-1}. In this hydroxylamine-containing control, the Y_Z to P_{680}^+ reduction reaction is blocked [43, 44].

To evaluate a possible Q_B^- contribution, 1483 cm^{-1} kinetic transients were acquired in the presence (figure 3B, orange trace) or the absence (figure 3B, light blue trace) of the Q_B inhibitor, DCMU [51]. As shown in the derived rate constants in table 1, DCMU had no significant effect on the 1483 cm^{-1} decay kinetics. This result suggests that Q_B reduction reactions are not monitored directly under these conditions.

Possible contributions from Q_A^- and $Y_Z^{\bullet}$ can be evaluated by comparison to kinetic experiments in the literature. Previously, 820 nm optical spectroscopy was used to monitor the pH dependence of the P_{680}^+ reduction reaction in Tris-treated, OEC-depleted samples [36]. In that previous report, the kinetics of Y_Z oxidation accelerated with increasing pH and exhibited a lifetime of 20 microseconds at pH 5.0 and 3.5 microseconds at pH 8.0. In our experiments, the time constant of the fast phase of 1483 cm^{-1} decay (table 1) was 50 microseconds at pH 5.0 and was 4 microseconds at pH 8.0. This comparison suggests that the 1483 cm^{-1} fast phase is monitoring a donor side electron transfer reaction.

In a previous report, a two flash experiment was used to monitor the kinetics of charge recombination between P_{680}^+ and Q_A^- [36]. This reaction rate was slower than the Y_Z to P_{680}^+ reduction reaction, with a reported lifetime of 200 microseconds. The $P_{680}^+Q_A^-$ recombination was also found to be pH independent. In an EPR study of hydroxylamine-treated PSII, two half times were reported [44]. The fast phase decayed with the time constant of the apparatus, 20 microseconds. The other half time was 200 microseconds and was assigned to the $P_{680}^+Q_A^-$ recombination reaction. In that previous work, the 20 microsecond phase was assigned to reduction of P_{680}^+ by hydroxylamine or

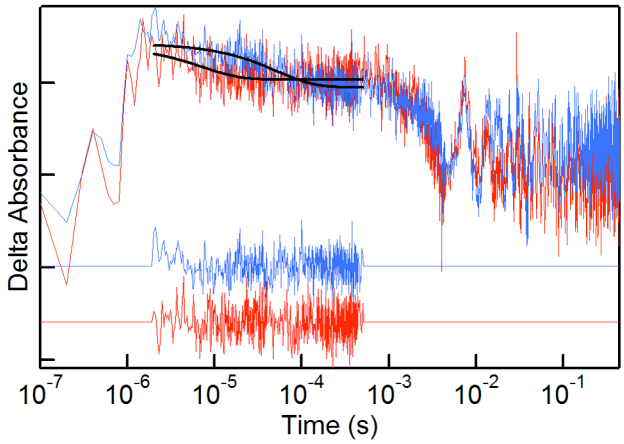

Figure 6. Flash-induced kinetic transients acquired at 1483 cm^{-1} from cyanobacterial PSII. Data were acquired from OEC-depleted PSII containing control tyrosine (red trace, avg. of 90) or labeled tyrosine-ring-d_4 (blue trace, avg. of 120) with 3 mM ferricyanide and 3 mM ferrocyanide. Samples were suspended in ^2H_2O buffer (5 mM MES-NaO^2H, p^{2}H 6.0, and 0.03% n-dodecyl-β-D-maltopyranoside). The energy density was 63 mJ $(cm)^{-2}$ and the temperature was 10°C. The traces have been normalized to a common initial microsecond amplitude. Exponential fits are shown superimposed over each trace, with residuals for each fit color-coded below the data. The space between tick marks of the y-axis represents $1x10^{-4}$ absorbance units.

another donor [44]. This faster reaction was reported to be inhibited with longer incubation times in hydroxylamine, perhaps due to a PSII modification reaction. Therefore, the time constants (20 microseconds and 95 milliseconds) and pH dependence of the 1483 cm^{-1} transients in our data are not consistent with an attribution to a $P_{680}^{+}Q_A^{-}$ recombination reaction.

In order to test the hypothesis that the traces collected at 1483 cm^{-1} contain contributions from $Y_Z^{\bullet}$ decay, we collected data using manganese-depleted PSII in which tyrosine had been replaced with labeled ($^2H_4$-deuterated) tyrosine. Figure 6 displays traces collected at 1483 cm^{-1} from control (red trace) and labeled (blue trace) PSII. Exponential fits between 2 and 500 microseconds revealed kinetic rate constants of

150,000 ± 65,000 and 33,000 ± 8,000 s^{-1} for the control and labeled samples, respectively. $^2H_4$ deuteration of the phenol ring of tyrosine is expected to shift vibrational bands of tyrosine and the tyrosyl radical [40]. If $Y_Z^{\bullet}$ is a contributor to the kinetic traces observed at 1483 cm^{-1}, labeling will lead to a change in the 1483 cm^{-1} kinetics and amplitude. Comparing the difference in rate constants derived from the transient IR experiments suggests that $Y_Z^{\bullet}$ may contribute to the absorption change at 1483 cm^{-1} on the microsecond timescale. Contributions on the millisecond time scale are difficult to evaluate due to low frequency noise in this data set. Previous isotopic labeling and site directed mutagenesis work have suggested that the CO vibrational band of $Y_Z^{\bullet}$ makes a spectral contribution at 1478 cm^{-1} (reviewed in [52]) on longer time scales.

Previous work has also measured the rate of $Y_Z^{\bullet}$ reduction by Q_A^- or ferrocyanide [38]. This experiment was performed by monitoring the absorbance change at 325 nm in Tris-treated, OEC-depleted samples at pH 6.0. A 20 millisecond half time was attributed to $Y_Z^{\bullet}$ reduction by Q_A^-, and an 80 millisecond half time was attributed to $Y_Z^{\bullet}$ reduction by ferrocyanide. In that previous report, addition of DCMU did not alter the kinetics of $Y_Z^{\bullet}$ reduction [38]. In our experiments, the time constant for the 1483 cm^{-1} slow phase was 95 milliseconds at pH 6.0 and was found to be DCMU and ferrocyanide independent (table 1 and 3). This comparison suggests that the 1483 cm^{-1} slow phase is monitoring $Y_Z^{\bullet}$ recombination with Q_A^-. A positive band from Q_A^- is expected to overlap in this spectral region and may be the major contributor on the millisecond time scale [46, 49, 50]. In addition to a contribution from $Y_Z^{\bullet}$ and Q_A^-, histidine and other amino residues near P_{680} may also be contributing to the infrared transients on the microsecond/millisecond timescale.

To examine the solvent isotope effect on $Y_Z^{\bullet}$ (microsecond) and Q_A^- (millisecond) reduction reactions, transient infrared data were acquired in ^2H_2O buffers as a function of p^2H (figure 1A-D, blue traces). The data were fit, and, as shown in figure 2A and B, blue, the derived rate constants for the microsecond and millisecond phases are p^2H dependent. The solvent isotope effect was then calculated as a function of pL (table 1) for the microsecond (figure 2C, green) and millisecond reactions (figure 2C, black). A significant KIE ($\geq 2.5 \pm 0.3$, Table 1) was observed for the microsecond rate; the KIE was pH independent (figure 2C, green). On the other hand, a smaller or insignificant KIE, in the range from 1.4 ± 0.4 to 0.9 ± 0.1 (table 1), was observed for the millisecond rate. Given the standard deviations, the KIE for the slow phase was also pL independent (figure 2C, black).

Based on models built to study inter- and intra-molecular PCET, three possible mechanisms exist [19-21, 32, 53, 54]. Proton transfer may precede electron transfer (PTET, 1), electron transfer may precede proton transfer (ETPT, 2), or proton transfer and electron transfer may occur through one step (CPET, 3). Each of these mechanisms can be distinguished based on the pL dependence and sensitivity to solvent isotope exchange of a particular reaction. In a study of the oxidation of hydrogen-bonded phenols, a CPET mechanism was proposed based on high KIE and thermodynamic arguments [21]. Also, using tyrosine covalently linked to a ruthenium tris-bipyridine complex, oxidation of tyrosine was concluded to follow a CPET mechanism based also on high KIE as well as a pH dependent rate [19, 32]. This conclusion was drawn in spite of lower reorganization energy predicted for sequential ETPT mechanism.

Oxidation/reduction of Y_Z has been argued to follow a CPET mechanism when comparing the kinetics of a model complex displaying the same mechanism [32, 55]. A concerted pathway avoids the high energy intermediates ($Y_ZO^{\bullet}H^+$ or Y_ZO^-) of the sequential pathways [53]. Multiple authors agree that formation of a tyrosine radical cation is highly unfavorable [21, 56, 57]. Indeed, when approximating the ΔG for formation of $Y_ZO^{\bullet}H^+$, Y_ZO^-, or $Y_ZO^{\bullet}$, the one step concerted mechanism involving $Y_ZO^{\bullet}$ is favored by more than 10 kcal/mol [54]. Based on the significant KIE observed here on the microsecond phase of 1483 cm^{-1} decay, a concerted proton-electron transfer mechanism is likely for the reduction of $Y_Z^{\bullet}$. Moreover, the pL dependence observed here distinguishes the $Y_Z^{\bullet}$ reduction mechanism from the previously studied $Y_D^{\bullet}$ reduction reaction [22].

References

1. Zouni, A., et al., *Crystal structure of photosystem II from Synechococcus elongatus at 3.8 Å resolution.* Nature, 2001. **409**: p. 739-743.

2. Kamiya, N. and J.-R. Shen, *Crystal structure of oxygen-evolving photosystem II from Thermosynechococcus vulcanus at 3.7 Å resolution.* Proc Natl Acad Sci USA, 2003. **100**: p. 98-103.

3. Ferreira, K.N., et al., *Architecture of the photosynthetic oxygen-evolving center.* Science, 2004. **303**: p. 1831-1837.

4. Loll, B., et al., *Towards complete cofactor arrangement in the 3.0 Å resolution structure of photosystem II.* Nature, 2005. **438**: p. 1040-1044.

5. Britt, R.D., *Oxygen evolution*, in *Oxygenic Photosynthesis: The Light Reactions*, D.R. Ort and C.F. Yocum, Editors. 1996, Kluwer Academic Publisher: Dordrecht. p. 137-164.

6. Barry, B.A., *Tyrosyl radicals in photosystem II.* Methods Enzymol, 1995. **258**: p. 303-319.

7. Barry, B.A. and G.T. Babcock, *Tyrosine radicals are involved in the photosynthetic oxygen-evolving system.* Proc Natl Acad Sci USA, 1987. **84**: p. 7099-7103.

8. Boerner, R.J. and B.A. Barry, *Isotopic labeling and EPR spectroscopy show that a tyrosine residue is the terminal electron donor, Z, in manganese-depleted photosystem II preparations.* J Biol Chem, 1993. **268**: p. 17151-17154.

9. Babcock, G.T. and K. Sauer, *Electron paramagnetic resonance signal II in spinach chloroplasts.* Biochim Biophys Acta, 1973. **325**: p. 483-503.

10. Babcock, G.T. and K. Sauer, *Electron paramagnetic resonance signal in spinach chloroplasts II. Alternative spectral forms and inhibitor effects on the kinetics of signal II in flashing light.* Biochim Biophys Acta, 1973. **325**: p. 504-519.

11. Faller, P., et al., *Rapid formation of the stable tyrosyl radical in photosystem II.* Proc Natl Acad Sci USA, 2001. **98**: p. 14368-14373.

12. Ananyev, G.M., et al., *A functional role for tyrosine-D in assembly of the inorganic core of the water complex of photosystem II and the kinetics of water oxidation.* Biochemistry, 2002. **41**: p. 974-980.

13. Debus, R.J., et al., *Site-specific mutagenesis identifies a tyrosine radical involved in the photosynthetic oxygen-evolving complex.* Proc Natl Acad Sci USA, 1988. **85**: p. 427-430.

14. Debus, R.J., et al., *Directed mutagenesis indicates that the donor to P680+ in photosystem II is Tyr-161 of the D1 polypeptide.* Biochemistry, 1988. **27**: p. 9071-9074.

15. Vermaas, W.F.J., A.W. Rutherford, and Ö. Hansson, *Site-directed mutagenesis in photosystem II of the cyanobacterium Synechocystis sp. PCC 6803: Donor D is a tyrosine residue in the D2 protein.* Proc Natl Acad Sci USA, 1988. **85**: p. 8477-8481.

16. Metz, J.G., et al., *Directed alteration of the D1 polypeptide of photosystem II: evidence that tyrosine-161 is the redox component, Z, connecting the oxygen-evolving complex to the primary electron donor, P680.* Biochemistry, 1989. **28**: p. 6960-6969.

17. Dixon, W.T. and D. Murphy, *Determination of the acidity constants of some phenol radical cations by means of electron spin resonance.* J Chem Soc London, Faraday Trans II, 1976. **72**: p. 1221-1229.

18. Reece, S.Y., et al., *Proton-coupled electron transfer: the mechanistic underpinning for radical transport and catalysis in biology.* Phil Trans R Soc Lond B, 2006. **361**: p. 1351-1364.

19. Sjödin, M., et al., *Proton-coupled electron transfer from tyrosine in a tyrosine-ruthenium-tris-bipyridine complex: comparison with tyrosine$_Z$ oxidation in photosystem II.* J Am Chem Soc, 2000. **122**: p. 3932-3936.

20. Reece, S.Y. and D.G. Nocera, *Direct tyrosine oxidation using the MLCT excited states of rhenium polypyridyl complexes.* J Am Chem Soc, 2005. **127**: p. 9448-9458.

21. Rhile, I.J., et al., *Concerted proton-electron transfer in the oxidation of hydrogen bonded phenols.* J Am Chem Soc, 2006. **128**: p. 6075-6088.

22. Jenson, D.L., A. Evans, and B.A. Barry, *Proton-coupled electron transfer and tyrosine D of photosystem II.* J Phys Chem B, 2007. **111**: p. 12599-12604.

23. Graige, M.S., et al., *Mechanism of proton-coupled electron transfer for quinone (Q_B) reduction in reaction centers of Rhodopseudomonas sphaeroides.* J Am Chem Soc, 1996. **118**: p. 9005-9016.

24. Graige, M.S., et al., *Observation of the protonated semiquinone intermediate in isolated reaction centers from Rhodobacter sphaeroides: implications for the mechanism of electron and proton transfer in proteins.* Biochemistry, 1999. **38**: p. 11465-11473.

25. Kim, S., J. Liang, and B.A. Barry, *Chemical complementation identifies a proton acceptor for redox-active tyrosine D in photosystem II.* Proc Natl Acad Sci USA, 1997. **94**: p. 14406-14412.

26. Campbell, K.A., et al., *The τ-Nitrogen of D2 histidine 189 is the hydrogen bond donor to the tyrosine radical $Y_D^{\bullet}$ of photosystem II.* J Am Chem Soc, 1997. **119**: p. 4787-4788.

27. Hays, A.-M.A., et al., *Role of D1-His190 in proton-coupled electron transfer reactions in photosystem II: a chemical complementation study.* Biochemistry, 1998. **37**: p. 11352-11365.

28. Hays, A.M.A., et al., *Role of D1-His190 in the proton-coupled oxidation of tyrosine Y-Z in manganese-depleted photosystem II.* Biochemistry, 1999. **38**: p. 11851-11865.

29. Pujols-Ayala, I. and B.A. Barry, *His 190-D1 and Glu 189-D1 provide structural stabilization in photosystem II.* Biochemistry, 2002. **41**: p. 11456-11465.

30. Force, D.A., et al., *^{2}H ESE-ENDOR study of hydrogen bonding to the tyrosine radicals $Y_D^{\bullet}$ and $Y_Z^{\bullet}$ of photosystem II.* J Am Chem Soc, 1995. **117**: p. 12643-12644.

31. Diner, B.A., et al., *Hydrogen bonding, solvent exchange, and coupled proton and electron transfer in the oxidation and reduction of redox-active tyrosine Y_Z in Mn-depleted core complexes of photosystem II.* Biochemistry, 1998. **37**: p. 17931-17943.

32. Sjödin, M., et al., *The mechanism for proton-coupled electron transfer from tyrosine in a model complex and comparisons with Y_Z oxidation in photosystem II.* Phil Trans R Soc Lond B, 2002. **357**: p. 1471-1478.

33. Ahlbrink, R., et al., *Function of tyrosine Z in water oxidation by photosystem II: Electrostatical potential instead of hydrogen abstractor.* Biochemistry, 1998. **37**: p. 1131-1142.

34. Barry, B.A., et al., *Time-resolved vibrational spectroscopy detects protein-based intermediates in the photosynthetic oxygen-evolving cycle.* Proc Natl Acad Sci USA, 2006. **103**: p. 7288-7291.

35. Yamamoto, Y., et al., *Release of polypeptides from highly active O_2-evolving photosystem-2 preparation by tris treatment.* FEBS Lett, 1981. **133**: p. 265-268.

36. Conjeaud, H. and P. Mathis, *The effect of pH on the reduction kinetics of P-680 in Tris-treated chloroplasts.* Biochim Biophys Acta, 1980. **590**: p. 353-359.

37. Boska, M., et al., *Similarity of EPR signal IIf rise and $P\text{-}680^{+}$ decay kinetics in Tris-washed chloroplast photosystem II preparations as a function of pH.* Biochim Biophys Acta, 1983. **722**: p. 327-330.

38. Dekker, J.P., et al., *Optical characterization of photosystem II electron donors.* Biochim Biophys Acta, 1984. **764**: p. 301-309.

39. Berthold, D.A., G.T. Babcock, and C.F. Yocum, *A highly resolved, oxygen-evolving photosystem II preparation from spinach thylakoid membranes.* FEBS Lett, 1981. **134**: p. 231-234.

40. MacDonald, G.M., K.A. Bixby, and B.A. Barry, *A difference Fourier-transform infrared study of two redox-active tyrosine residues in photosystem II.* Proc Natl Acad Sci USA, 1993. **90**: p. 11024-11028.

41. Noren, G.H., R.J. Boerner, and B.A. Barry, *EPR characterization of an oxygen-evolving photosystem II preparation from the cyanobacterium, Synechocystis 6803.* Biochemistry, 1991. **30**: p. 3943-3950.

42. MacDonald, G.M. and B.A. Barry, *Difference FT-IR study of a novel biochemical preparation of photosystem II.* Biochemistry, 1992. **31**: p. 9848-9856.

43. Ghanotakis, D.F. and G.T. Babcock, *Hydroxylamine as an inhibitor between Z and P_{680} in photosystem II.* FEBS Lett, 1983. **153**: p. 231-234.

44. Hoganson, C.W. and G.T. Babcock, *Redox cofactor interactions in photosystem II: electron spin resonance spectrum of P_{680}^{+} is broadened in the presence of Y_Z^{+}.* Biochemistry, 1989. **28**: p. 1448-1454.

45. MacDonald, G.M., J.J. Steenhuis, and B.A. Barry, *A difference infrared spectroscopic study of chlorophyll oxidation in hydroxylamine treated photosystem II.* J Biol Chem, 1995. **270**: p. 8420-8428.

46. Zhang, H., et al., *A time-resolved FTIR difference study of the plastoquinone Q_A and redox-active tyrosine Y_Z interactions in photosystem II.* Biochemistry, 1997. **36**: p. 11762-11768.

47. Kim, S., et al., *Infrared spectroscopic identification of the C-O stretching vibration associated with the tyrosyl $Z^{\bullet}$ and $D^{\bullet}$ radicals in photosystem II.* Biochim Biophys Acta, 1998. **1366**: p. 330-354.

48. Cua, A., et al., *Selective resonance Raman scattering from chlorophyll Z in photosystem II via excitation into the near-infrared absorption band of the cation.* J Am Chem Soc, 1998. **120**: p. 4532-4533.

49. Razeghifard, M.R., et al., *The in vivo, in vitro, and calculated vibrational spectra of plastoquinone and the plastosemiquinone anion radical.* J Phys Chem B, 1999. **103**: p. 9790-9800.

50. Kim, S., et al., *Isotope-based discrimination between the infrared modes of plastosemiquinone anion radicals and neutral tyrosyl radicals in photosystem II.* J Phys Chem B, 2000. **104**: p. 9720-9727.

51. Metz, J.G., et al., *Evidence for a dual function of the herbicide-binding D1 protein in photosytem II.* FEBS Lett, 1986. **205**: p. 269-274.

52. Pujols-Ayala, I. and B.A. Barry, *Tyrosyl radicals in photosystem II.* Biochim Biophys Acta, 2004. **1655**: p. 205-216.

53. Sjödin, M., et al., *Tuning proton coupled electron transfer from tyrosine: a competition between concerted and step-wise mechanisms.* Phys Chem Chem Phys, 2004. **6**: p. 4851-4858.

54. Meyer, T.J., M.H.V. Huynh, and H.H. Thorp, *The possible role of proton-coupled electron transfer (PCET) in water oxidation by photosystem II.* Angew Chem Int Edit, 2007. **46**: p. 5284-5304.

55. Ioannidis, N., G. Zahariou, and V. Petrouleas, *The EPR spectrum of tyrosine $Z^{\bullet}$ and its decay kinetics in O_2-evolving photosystem II preparations.* Biochemistry, 2008. **47**: p. 6292-6300.

56. Tommos, C. and G.T. Babcock, *Proton and hydrogen currents in photosynthetic water oxidation.* Biochim Biophys Acta, 2000. **1458**: p. 199-219.

57. Rappaport, F. and J. Lavergne, *Coupling of electron and proton transfer in the photosynthetic water oxidase.* Biochim Biophys Acta, 2001. **1503**: p. 246-259.

CHAPTER 4

PERTURBATIONS AT THE CHLORIDE SITE DURING THE PHOTOSYNTHETIC OXYGEN-EVOLVING CYCLE

by

Ian B. Cooper and Bridgette A. Barry

School of Chemistry and Biochemistry and the Petit Institute for Bioengineering and Bioscience, Georgia Institute of Technology, Atlanta, GA 30332

Reprinted with permission from Photosynth Res
(Cooper, I. B. and B. A. Barry. Photosynth Res, 2007. **92**: p. 345-356)

Abstract

Photosystem II (PSII) catalyzes the oxidation of water to O_2 at the manganese-containing, oxygen-evolving complex (OEC). Photoexcitation of PSII results in the oxidation of the OEC; four sequential oxidation reactions are required for the generation and release of molecular oxygen. Therefore, with flash illumination, the OEC cycles among five S_n states. Chloride depletion inhibits O_2 evolution. However, the binding site of chloride in the OEC is not known, and the role of chloride in oxygen evolution has not yet been elucidated. We have employed reaction-induced FT-IR spectroscopy and selective flash excitation, which cycles PSII samples through the S state transitions. On the time scale employed, these FT-IR difference spectra reflect long-lived structural changes in the OEC. Bromide substitution supports oxygen evolution and was used to identify vibrational bands arising from structural changes at the chloride-binding site. Contributions to the vibrational spectrum from bromide-sensitive bands were observed on

each flash. Sulfate treatment led to an elimination of oxygen evolution activity and of the FT-IR spectra assigned to the S_3 to S_0 (third flash) and S_0 to S_1 transitions (fourth flash). However, sulfate treatment changed, but did not eliminate, the FT-IR spectra obtained with the first and second flashes. Solvent isotope exchange in chloride-exchanged samples suggests flash-dependent structural changes, which alter protein dynamics during the S state cycle.

Introduction

Photosystem II (PSII) carries out the light-driven oxidation of water and reduction of plastoquinone. A heterodimeric core of subunits, called D1 and D2, binds most of the electron transfer cofactors. Other subunits include the chlorophyll (chl) binding subunits, CP47 and CP43, and the extrinsic subunits, the manganese stabilizing subunit (MSP), 18, and 24 kDa subunits. Electron transfer is initiated when the primary chlorophyll (chl) donor, P_{680}, absorbs light. Subsequent electron transfer reactions lead to the production of a chl cation radical, P_{680}^{+}, and the sequential reduction of a pheophytin, of a single electron-accepting quinone, Q_A, and of Q_B, a two electron acceptor (reviewed in [1]). P_{680}^{+} is very unstable and readily generates other oxidized species [2]. One of these oxidized species, tyrosine radical $Y_Z^{\bullet}$ [3, 4], is an intermediary in electron transfer reactions involving P_{680} and the catalytic site for water oxidation. Another redox-active tyrosine, Y_D, is also oxidized via P_{680}^{+} and is in redox equilibrium with the manganese (Mn) cluster [3, 5-7]. However, $Y_D^{\bullet}$ forms a stable radical and is not required for oxygen evolution [3, 5, 6]. Y_D may be involved in assembly of the Mn cluster [8].

The catalytic site of water oxidation cycles among five oxidation states, called the S_n states, where *n* refers to the number of oxidizing equivalents stored at the active site [9]. Each S state advancement is driven by one light-driven charge separation in the reaction center, and Y_Z is oxidized and reduced on every S state transition [10]. The S state transitions occur in the microsecond to millisecond time regime, with a rate that slows as oxidizing equivalents are stored in the oxygen-evolving complex (OEC) [11, 12].

Oxygen release occurs during the S_3 to S_0 transition from an unstable intermediate, known as the S_4 state. Evidence that an intermediate state is produced during the S_3 to S_0 transition has been obtained with EPR [13], XANES [14], UV [15], and transient infrared [16] spectroscopies. Four flashes are required to produce molecular oxygen from water, and the S_1 state is the dark-adapted state [9]. Therefore, in a dark-adapted sample, oxygen is produced on the third flash and then on every fourth flash. PSII structural models, derived from X-ray diffraction on three-dimensional crystals, have been presented at 3.8-3.0 Å resolution [17-21]. The issue of X-ray-induced Mn reduction has been raised as a potential concern in the interpretation of PSII electron density [19, 22, 23].

Chloride plays an intriguing and important role in photosynthetic oxygen evolution (reviewed in [24, 25]). Although chloride has not as yet been identified in PSII X-ray structures [20, 21], biochemical evidence for a single chloride ion has been presented [26]. Electron spin echo envelope modulation (ESEEM) measurements suggest that the chloride site is close to the Mn cluster [27, 28]. The OEC chloride can be depleted by long dialysis [25], by removal of PSII extrinsic subunits with sodium

chloride [26], or by removal of PSII extrinsic subunits with sodium sulfate at high pH [29-31]. After these treatments, steady state oxygen-evolving activity is either completely suppressed (sodium sulfate and sodium chloride treatment) [26, 31] or suppressed to 30-40% of the control rate (dialysis) [26]. With sulfate treatment, optical studies demonstrate that chloride depletion leads to a block of the S_2 to S_3 and S_3 to S_0 transitions [31, 32]. Mn oxidation does not occur on these transitions. Changes in the S_2 EPR signals are associated with reconstitution of other anions, such as fluoride and azide, at the chloride site [28, 33, 34]. Bromide can support oxygen evolution if this anion is reconstituted at the chloride site [25, 26, 31, 32]. A few other anions, such as nitrate, give lower levels of activity [25, 26, 31, 32]. However, replacement of chloride either with fluoride, acetate, or azide inhibits activity [25, 32, 35-38].

Site directed mutagenesis has shown that modification of positive amino acid side chains in CP47 [39-41], CP43 [42], and MSP [43], influence the K_m for chloride. Chloride has been proposed to have a role as a ligand to Mn [29, 44], in maintaining a hydrogen-bonded network, which facilitates proton transfer [25], in maintaining the potential of the Mn cluster [45], or in activation of substrate water in coordination with chloride [46]. These proposed roles for chloride are not mutually exclusive. In addition to a possible role as a Mn ligand [29, 44], it has also been proposed that chloride may associate with amino acid residues in the Mn coordination shell [47, 48].

Reaction-induced, rapid scan FT-IR spectroscopy has been used previously to study structural changes occurring on each of the S state transitions in PSII (for examples, see [49-52]). These spectral changes are measured on time scales, which are long (seconds) compared with oxygen production (microsecond-millisecond), but these

spectral changes are tightly coupled with the water splitting reactions (see review in [53]). It has been proposed that long-lived thermodynamic intermediates, called S_n', are detected in this type of experiment [53]. We have used this rapid scan method to study persistent structural changes at the OEC calcium site [53, 54]. In addition, microsecond time resolved infrared spectroscopy has been used to identify kinetically accessible intermediate states formed on each S state transition [16].

In this paper, we use rapid scan FT-IR spectroscopy to identify long-lived structural changes at the chloride site during the photosynthetic oxygen-evolving cycle. Structural changes at the OEC halide-binding site are pinpointed by comparison of chloride-exchanged, bromide-exchanged, and chloride-depleted PSII samples.

Materials and Methods

PSII was isolated from market spinach as previously described [55] with an activity of > 600 μmol O_2 (mg Chl-h)$^{-1}$, as measured with a Clarktype electrode [2]. Chloride-depleted samples were prepared by sulfate treatment [31]. Briefly, PSII was exchanged from SMN buffer (400 mM sucrose, 50 mM MES-NaOH, pH 6.0, 15 mM NaCl) into buffer containing 400 mM sucrose and 50 mM HEPES-NaOH, pH 7.5 by centrifugation and resuspension. The samples were then incubated in a sulfate buffer (400 mM sucrose, 50 mM HEPES-NaOH, pH 7.5, 50 mM Na_2SO_4) in darkness on ice while shaking for 15 minutes. This preparation will be referred to as ‘‘chloride-depleted.’’ Halide reconstitution was performed by suspension of SO_4^{-2}-treated PSII in a SH (0.4 M sucrose, 50 mM HEPES-NaOH, pH 7.5) buffer containing either 15 mM NaCl (SHCl) or 15 mM NaBr (SHBr). These preparations will be referred to as ‘‘chloride-

exchanged'' and ''bromide-exchanged'' samples. Solvent isotope exchange was performed on chloride-exchanged PSII as described above, except that ^2H_2O (Cambridge Isotopes Laboratories, Andover, MA, 99% ^2H) replaced ^1H_2O as the solvent. The p^2H of the ^2H_2O buffer is reported as the uncorrected pH meter reading; the p^2H was adjusted with NaO^2H (Cambridge Isotopes laboratories, 99.5% ^2H). For some comparative experiments, salt-washed PSII was prepared according to a method previously described [53]. The final resuspension buffer contained SMN and 20 mM $CaCl_2$.

FT-IR measurements were conducted at p^1H or p^2H 7.5 as previously described [53, 54]. Briefly, samples for FT-IR analysis were mixed with 0.65 mM recrystallized 2,6-dichlorobenzoquinone (DCBQ) and 7.5 mM $K_3Fe(CN)_6$ as electron acceptors and centrifuged. The pellet was spread onto a CaF_2 window, and a second CaF_2 window was placed over the sample. The windows were sealed with vacuum grease and wrapped with parafilm to control sample hydration. A doubled Nd:YAG laser (Continuum, Santa Clara, CA) was used to provide a 532 nm, 35 mJ $(cm)^{-2}$ excitation pulse. Samples were maintained at 4°C (^1H_2O) or 6°C (^2H_2O) during data collection. A Bruker IFS/66vs spectrometer (Bruker Optics, Billerica, MA) equipped with a MCT detector (Infrared Associated Inc., Stuart, FL) was employed. Data acquisition parameters were: resolution, 8 cm^{-1}; zero filling, four levels; apodization function, Happ-Genzel; mirror velocity, 60 kHz; phase correction, Mertz. The sample was given one saturating laser pulse followed by a 20 min dark adaptation to synchronize all reaction centers in the S_1 state. The sample was then given a train of laser pulses separated by 15 s of rapid scan data collection. Difference spectra were generated by calculating the ratio of single beam spectra collected before and after each flash and then converting the ratio to absorbance.

To measure the intensity of the amide II band, data were ratioed to an open beam background and then converted to absorbance. To eliminate any small differences in concentration or pathlength, data were normalized to an amide II absorbance of 0.5 absorbance units [53, 54]. The hydration was adjusted to give a 3370 cm^{-1} (^1H_2O buffers) or a 2500 cm^{-1} (^2H_2O buffers) to amide II absorbance ratio of greater than 3. To construct double difference spectra, data were scaled to give equal intensity in the 2300-2200 cm^{-1} region, in which the vibrational bands of ferricyande and ferrocyanide contribute. This corrects for any differences in the amount of charge separation. The number of spectra averaged was 93 for chloride-exchanged PSII in ^1H_2O buffer, 89 for bromide-exchanged PSII in ^1H_2O buffer, 76 for chloride-depleted PSII in ^1H_2O buffer, and 80 for chloride-exchanged PSII in ^2H_2O buffer.

Results

Table 1 presents steady state oxygen evolution rates for chloride-depleted, sulfate-treated PSII and control, untreated PSII in various buffers. When assayed at pH 6.0 and pH 7.5, untreated PSII had oxygen rates of 750 ± 90 μmol O_2 (mg chl-h)$^{-1}$ and 440 ± 70 μmol O_2 (mg chl-h)$^{-1}$, respectively. As expected from previous work [31], sulfate treatment resulted in a complete suppression of oxygen evolution activity at pH 7.5 (≤ 10 μmol O_2 (mg chl-h)$^{-1}$). Under these conditions, hydroxide ion is believed to be bound to the OEC anion binding site, and sulfate is a non-interacting anion [29, 38, 44]. Table 1 shows that addition either of chloride or bromide resulted in the equivalent reconstitution of oxygen-evolving activity at pH 7.5, demonstrating that this procedure exchanges bromide into the OEC chloride site.

Table 1. Steady-state oxygen evolution rates for sulfate-treated and untreated PSII at pH 6.0 and 7.5.

pH	Assay buffer[a]	Untreated PSII	Sulfate-treated PSII
6.0	SMCl	750 ± 90	370 ± 60
7.5	SHCl	440 ± 70	200 ± 20
7.5	SHBr	490 ± 30	220 ± 20
7.5	SHU	20 ± 10	10 ± 6
7.5	SH	280 ± 40	30 ± 10

[a] Activity was measured in buffers containing 400 mM sucrose (S), 50 mM MES-NaOH, pH 6.0 (M), 50 mM HEPES-NaOH, pH 7.5 (H), 0.5 mM DCBQ, 1 mM $K_3Fe(CN)_6$, and either 15 mM sodium bromide (Br), 15 mM sodium chloride (Cl), 50 mM sodium sulfate (U), or no added anion. Oxygen evolution activities are reported in μmol O_2 (mg Chl-h)$^{-1}$. The reported values are the average of 12 measurements.

As expected [31], sulfate treatment was associated with loss of the 24 and 18 kDa extrinsic subunits (data not shown). Also, as previously described [31], the addition of calcium had little effect on the oxygen-evolving activity of sulfate-treated, chloride-depleted PSII (data not shown), indicating that sulfate treatment does not remove calcium from the OEC. Table 2 shows the effects of increasing concentrations of chloride on the oxygen-evolving activity of BBY membranes at pH 7.5. Increasing concentrations of chloride dramatically stimulate the oxygen-evolving activity of chloride-depleted PSII, but have a less significant effect on the activity of untreated PSII at pH 7.5. A concentration of 15 mM chloride, which was used in the FT-IR spectroscopic experiments described below, reconstitutes the majority (~ 80%) of oxygen-evolving activity at pH 7.5.

Comparative FT-IR experiments on chloride-depleted, chloride-exchanged, and bromide-exchanged samples were conducted at pH 7.5 to insure the maximum level of chloride exchange. For example, consistently higher levels of residual activity, attributed

Table 2. Chloride dependence of PSII oxygen evolution.

pH	$[Cl^-]$ (mM)	PSII	Sulfate treated PSII
6.0[a]	15	750 ± 90[b]	370 ± 60
7.5[c]	0	490 ± 10	60 ± 4
7.5	10	540 ± 10	240 ± 8
7.5	15	590 ± 10	260 ± 9
7.5	25	570 ± 20	310 ± 10
7.5	50	610 ± 2	330 ± 2
7.5	100	560 ± 20	330 ± 10

[a] Assays at pH 6.0 were performed in a buffer containing 400 mM sucrose, 50 mM MES-NaOH, pH 6.0, 15 mM NaCl, 0.5 mM DCBQ, and 1 mM $K_3Fe(CN)_6$.

[b] Oxygen evolution activities are reported in μmol O_2 (mg Chl-h)$^{-1}$. The reported values are the average of three measurements.

[c] Assays at pH 7.5 were performed in a buffer containing 400 mM sucrose, 50 mM HEPES-NaOH, pH 7.5, indicated concentrations of NaCl, 0.5 mM DCBQ, and 1 mM $K_3Fe(CN)_6$.

to higher levels of contaminating chloride, were observed when chloride-depleted samples were assayed at pH 6.0 in sulfate buffer (60 ± 30 μmol O_2 (mg chl-h)$^{-1}$), compared to assay at pH 7.5 in sulfate buffer (table 1, 10 ± 6 μmol O_2 (mg chl-h)$^{-1}$).

Figure 1 shows the 2200-1200 cm^{-1} region of difference FT-IR spectra acquired from untreated, control PSII samples at pH 6.0 with one (figure 1A, black line), two (figure 1B, black line), three (figure 1C, black line), and four (figure 1D, black line) saturating, 532 nm flashes. Samples were dark adapted before data acquisition to set the OEC in the S_1 state. The data in figure 1 resemble spectra previously assigned to the S_1' to S_2' (A), S_2' to S_3' (B), S_3' to S_0' (C), and S_0' to S_1' (D) transitions (for example, see [49-52]). Dark-dark spectra in figure 1E exhibit the level of noise before the measurement.

In figure 1, the difference FT-IR spectra acquired from chloride-exchanged PSII samples at pH 7.5 are shown superimposed as the green lines (figure 1A-E). pH 6.0 and pH 7.5 FT-IR spectra are similar except for changes in the amide I region [56] (1670-

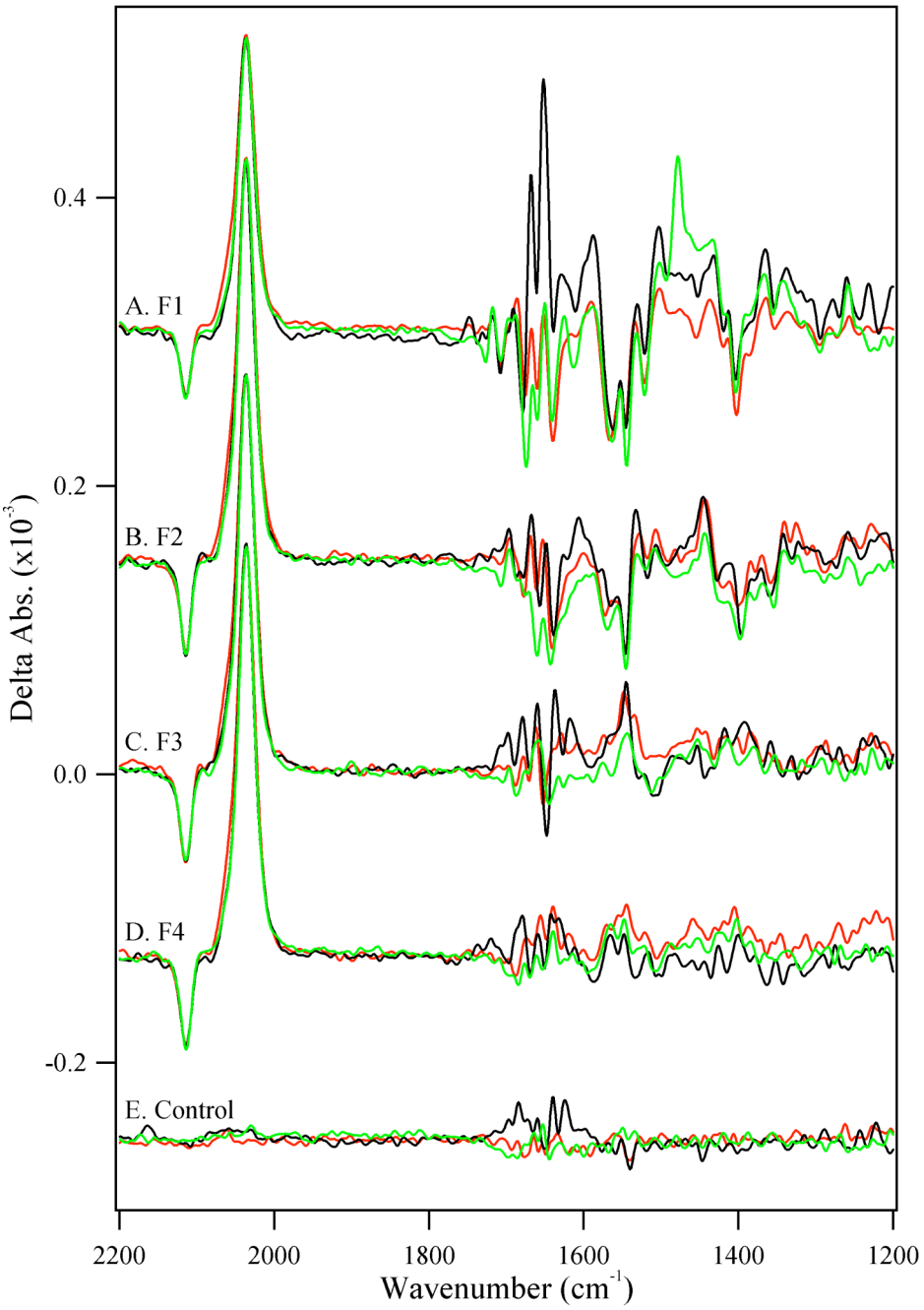

Figure 1. Difference FT-IR spectra of untreated PSII at pH 6.0 (black traces), salt-washed PSII at pH 6.0 (red traces), and chloride-exchanged PSII at pH 7.5 (green traces). The spectra are associated with the first (A), second (B), third (C), and fourth (D) flashes to a dark-adapted sample in the S_1 state. In (E), dark-minus-dark controls are presented.

1650 cm^{-1}) and increased intensity at 1478 cm^{-1} at pH 7.5. This difference at 1478 cm^{-1}, which is only observed after the long dark adaptation before the first flash, may be attributable to tyrosyl radical $D^{\bullet}$, which makes a contribution at this frequency [57, 58].

In figure 1, red line, data from salt-washed PSII at pH 6.0 are also superimposed [53]. Salt washing removes the 18 and 24 kDa subunits and increases accessibility to the OEC [59-61]. The miss parameter in salt-washed PSII is higher than chloride-depleted PSII [31], but the spectra, derived from salt-washed PSII, in figure 1, red line, show changes with flash number. This indicates that S state advancement occurs in this preparation under the conditions of FT-IR spectroscopy. We have recently used strontium editing in salt-washed PSII to identify the structural changes at the calcium site throughout the S state cycle. A subsequent study of citrate PSII has obtained similar results, given the respective signal to noise ratios [62].

Figure 2 shows the 2200-1200 cm^{-1} region of difference FT-IR spectra acquired from chloride-exchanged (green lines) and chloride-depleted samples (black lines) at pH 7.5. Chloride-depleted PSII samples are inhibited in oxygen evolution (tables 1 and 2). Chloride depletion is expected to block the S_2 to S_3 transition [31, 63-65]. As shown in figure 2A, after one flash, a S_2'-minus-S_1' FT-IR spectrum was obtained in chloride-depleted samples (black line). However, substantial frequency and amplitude shifts were observed in this spectrum compared to the control (figure 2A, black line).

Surprisingly, in chloride-depleted PSII, the second flash produced a difference FT-IR spectrum on the 15 s time scale. Evidence from multiple laboratories has shown that Mn is not oxidized on this transition; instead, a $Y_Z^{\bullet}S_2$ state is formed. The lifetime of

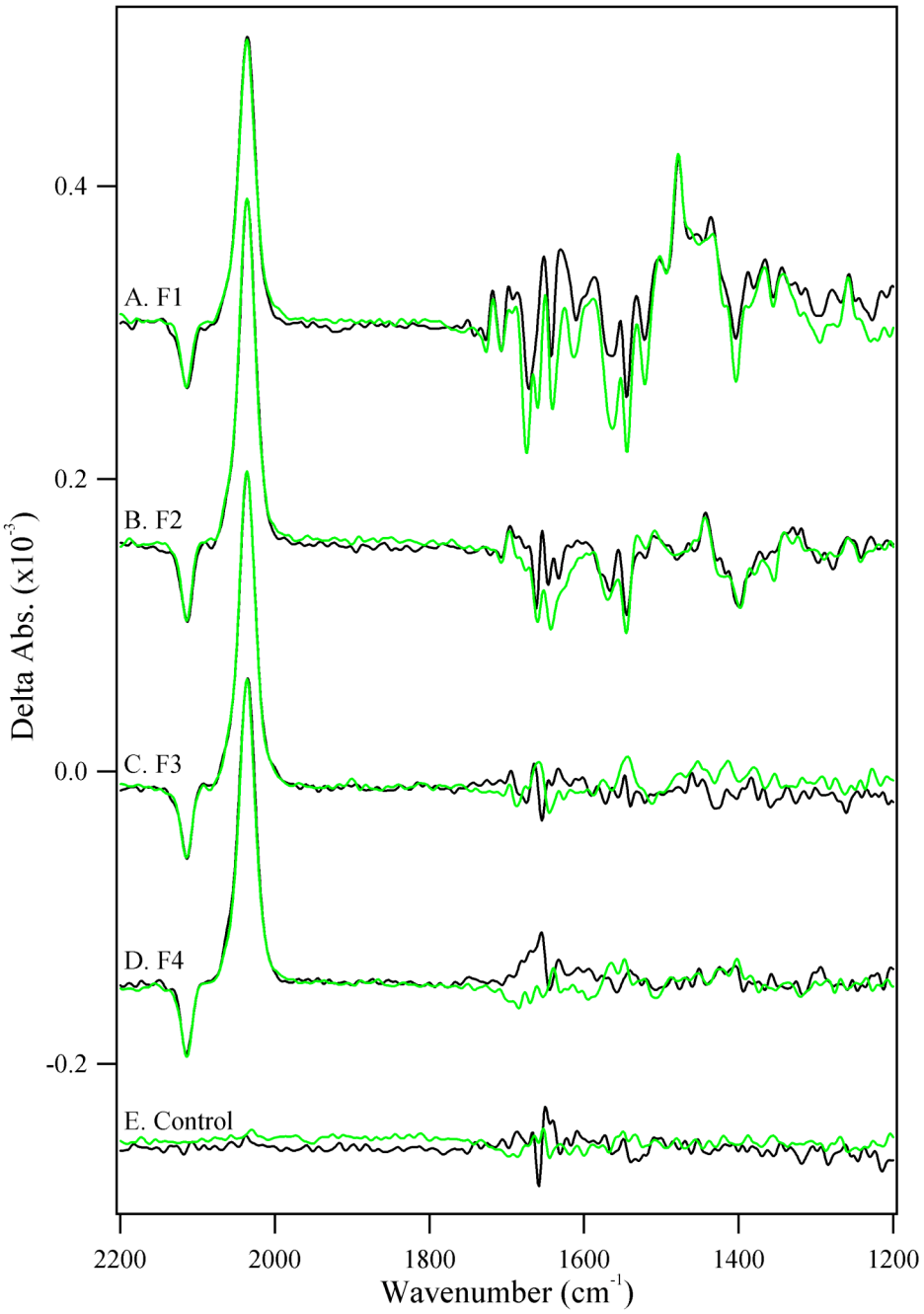

Figure 2. Difference FT-IR spectra of chloride-exchanged PSII at pH 7.5 (green traces) and sulfate-treated PSII, which have been depleted of chloride, at pH 7.5 (black traces). The spectra are associated with the first (A), second (B), third (C), and fourth (D) flashes to a dark-adapted sample in the S_1 state. In (E), dark-minus-dark controls are presented.

this state has been reported to be 500 ms [32]. Our FT-IR experiments are conducted with a 15 s data acquisition time and a ~ 100 ms gap before the beginning of data acquisition, so direct contributions from $Y_Z^{\bullet}$ decay will not be detected. For example, in Mn-depleted PSII (Tris washed), $Y_Z^{\bullet}$ has a similar lifetime [66], and reaction-induced FT-IR spectra on a similar time scale gave a flat line, with no defined spectral features relative to the baseline [67]. Therefore, we attribute the FT-IR spectrum, acquired on the second flash in chloride-depleted PSII, to a long-lived structural change in the OEC, which is driven by decay of $Y_Z^{\bullet}S_2$. This structural change may correspond to a relaxation of the Mn ligand environment. Spontaneous structural changes in the OEC have been detected with long dark adaptation [67].

In figure 2C and D, the third and fourth flashes did not result in a well-defined FT-IR spectrum in the chloride-depleted sample. This result is consistent with the expected block in S state advancement in the absence of chloride (see [32] and references therein).

The observed spectral differences on the first and second flash, when chloride-exchanged and chloride-depleted samples are compared, can be identified through construction of a double-difference spectrum. After correction for any small difference in concentration and pathlength, the spectra in figure 2A and B were subtracted (control-minus-chloride depleted) to generate double difference spectra (figure 3A and B). To appear in these double difference spectra, a vibrational band must be perturbed in frequency and/or amplitude by the S′ state transition *and also* perturbed by chloride removal. Figure 3C shows a control subtraction, which was generated by subtracting

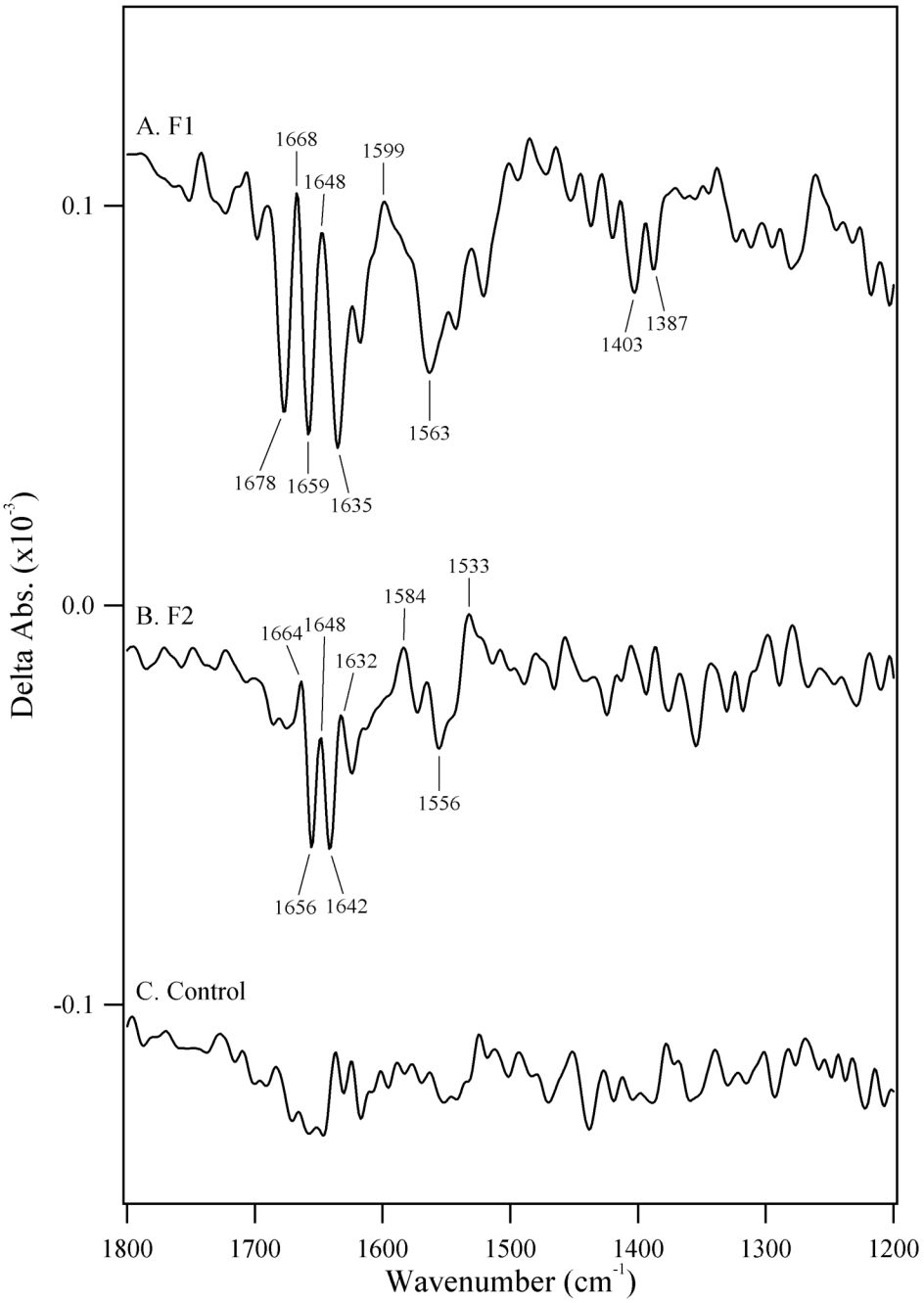

Figure 3. Double difference FT-IR spectra showing the effect of chloride depletion on the data from figure 2 acquired with one flash (A) and two flashes (B) to a dark-adapted sample. In (C), a representative double difference control is presented in which no vibrational bands are expected. This control was constructed from the dataset acquired with the first flash in the chloride-exchanged sample.

one-half of the chloride-exchanged data set (first flash) from the other half of the dataset. Figure 3C will contain no vibrational bands, allows an estimation of the noise in the measurement, and shows that the vibrational bands observed in figure 3A and B are significant.

As observed in figure 3A, the removal of chloride has a dramatic effect on the spectrum acquired with the first flash. Most of the spectral bands exhibit flash-induced changes in amplitude and frequency. In particular, changes in frequency and amplitude are observed between 1680 and 1635 cm^{-1}, between 1599 and 1563 cm^{-1}, and in the 1400 cm^{-1} region. The spectrum acquired on the first flash has been assigned as a S_2'-minus-S_1' spectrum; the S_1 to S_2 transition corresponds to a Mn oxidation reaction (reviewed in [68]). It has been suggested that the S_1 to S_2 oxidation reaction may be uncompensated by proton transfer and thus lead to the build up of charge on the OEC (reviewed in [46]). In such a case, a possible origin of the S_2'-minus-S_1' FT-IR spectrum is an electrostatic effect (or Stark effect) on the frequencies of Mn ligand vibrations. Stark effects are sensitive to small changes in the magnitude and direction of an electric field [69]. Therefore, the spectral changes observed in the absence of chloride may be due to an alteration in the arrangement of first and second shell ligands to the OEC. This result is consistent with a chloride-binding site in close proximity to the Mn cluster.

On the second flash, we have suggested the possibility (see above) that the difference FT-IR spectrum reflects a delayed structural change in the Mn cluster, which is caused by $Y_Z^{\bullet}$ recombination. When chloride is removed from PSII and replaced by hydroxide (figure 3B), the double difference spectrum exhibits spectral contributions that

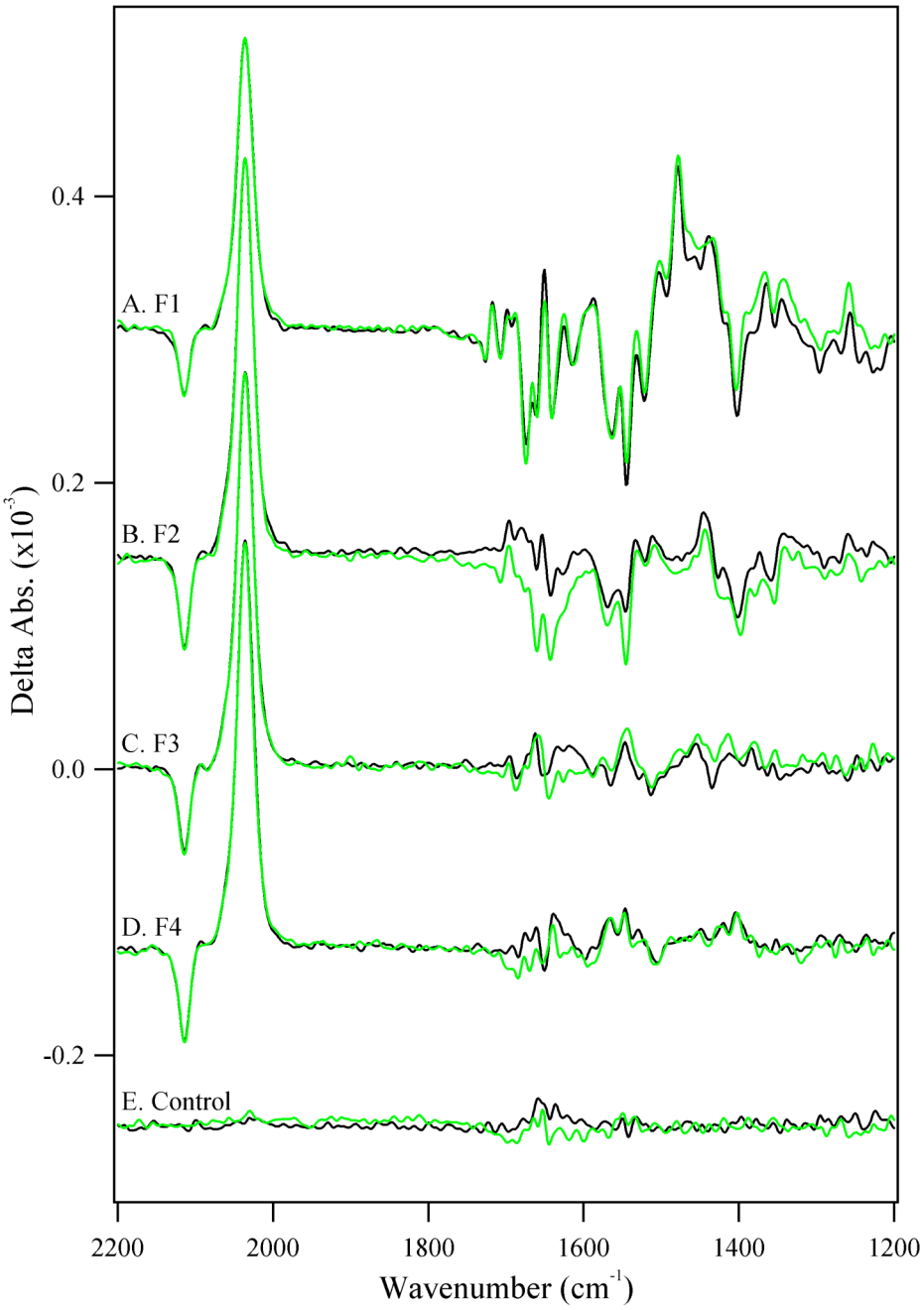

Figure 4. Difference FT-IR spectra of chloride-exchanged PSII (green traces) and bromide-exchanged PSII (black traces). The spectra are associated with the first (A), second (B), third (C), and fourth (D) flashes to a dark-adapted sample in the S_1 state. In (E), dark-minus-dark controls are presented.

are observed mainly in the 1660-1630 cm^{-1} (amide I) and 1580-1530 cm^{-1} (amide II) spectral regions [56]. Since the frequencies of these bands are known to be sensitive mainly to hydrogen bonding, this result suggests that there is a change in the position and hydrogen bonding of the peptide backbone when chloride is depleted. This change in protein structure may contribute to the block observed in S state advancement when PSII is depleted of chloride.

Figure 4 shows the 2200-1200 cm^{-1} region of difference FT-IR spectra acquired from chloride-exhanged PSII samples with one (figure 4A, green line), two (figure 4B, green line), three (figure 4C, green line), and four (figure 4D, green line) saturating, 532 nm flashes. The corresponding difference FT-IR spectra acquired from bromide-exchanged samples are shown superimposed as the black lines (figure 4A-D). Figure 4E is a control difference spectrum, which provides an estimate of the noise in the measurements. An optical study has shown no significant change in the oscillation pattern of oxygen production in bromide-reconstituted samples [38]. This previous result indicates that there is little difference in the miss parameter when chloride-exchanged and bromide-exchanged samples are compared. Consistent with this, the amplitudes of the CN vibrational bands of ferricyanide and ferrocyanide were similar in chloride-exchanged and bromide-exchanged samples. Bromide addition should have the effect of downshifting vibrational bands of amino acids, which interact with chloride through hydrogen bonding interactions [70, 71].

After correction for any small difference in concentration and pathlength, the spectra in figure 4 were subtracted (chloride-minus-bromide) to generate ‘‘bromide-

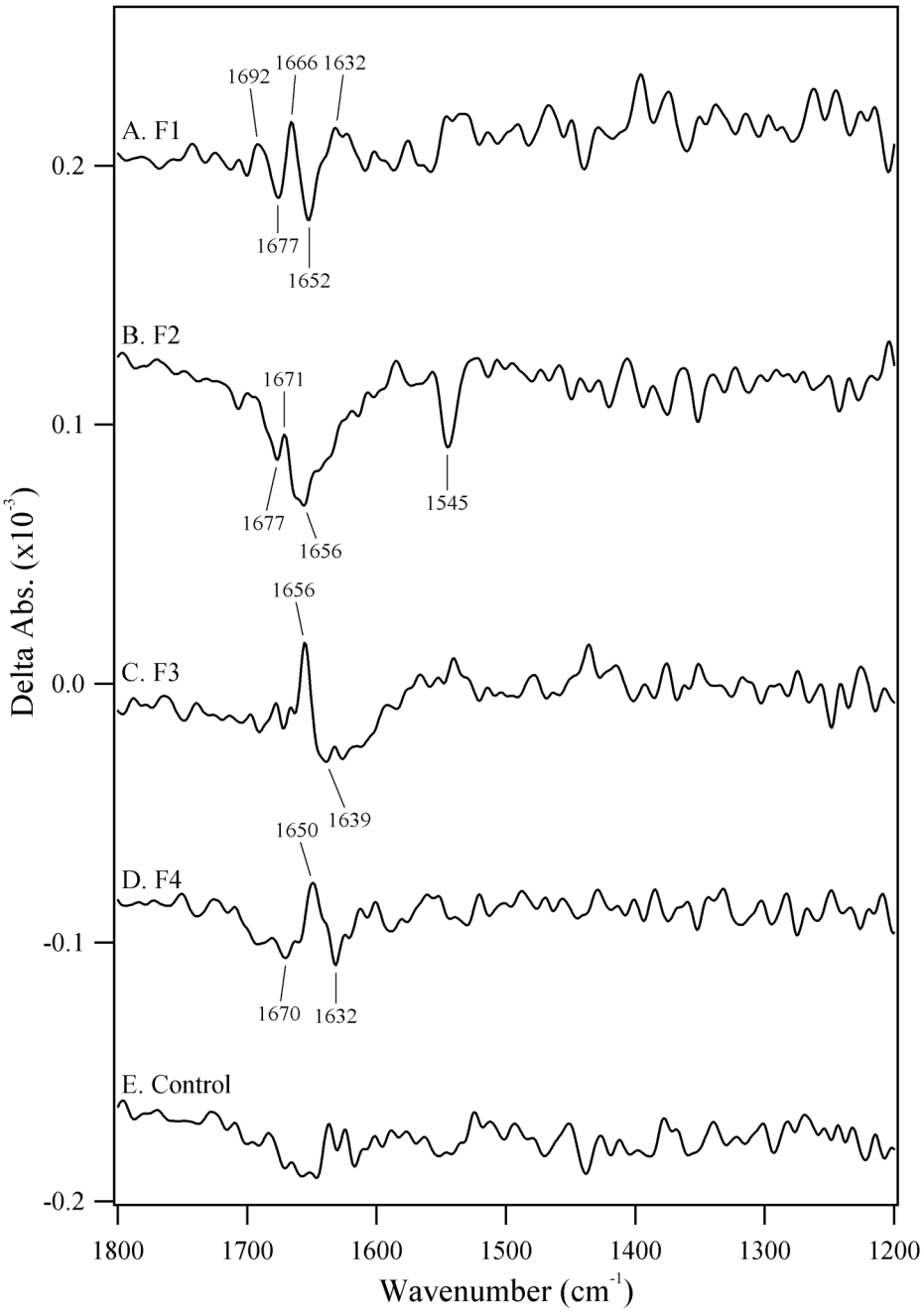

Figure 5. Bromide-edited double difference spectra constructed from the data in figure 4 (chloride-minus-bromide). The spectra are associated with the first (A), second (B), third (C), and fourth (D) flashes to a dark-adapted sample in the S_1 state. In (E), a representative double difference control is presented in which no vibrational bands are expected. This control was constructed from the dataset acquired with the first flash in the chloride-exchanged sample.

edited'' spectra (figure 5). This bromide-editing method picks out S_n' state dependent changes at the chloride site in the OEC. Figure 5E shows a control subtraction. The data in figure 5 suggest that each of the four flash-induced transitions is associated with a small, persistent perturbation of the OEC chloride site. In particular, each of the four spectra is distinct and exhibits bromide-sensitive spectral features in the 1690-1630 cm^{-1} region. Figure 5B also shows an additional negative band at 1545 cm^{-1}. Possible assignments for the observed bands in figure 5A, C, and D are to arginine or to the peptide bond [56, 72]. For arginine, two CN vibrational bands are expected at ~1670 and ~1630-40 cm^{-1} [70-72]. For the peptide bond vibrations, the amide I frequency is dependent on secondary structure content and hydrogen bonding [73], but for an alpha helical protein, the C=O vibration is expected at ~ 1660 cm^{-1}. In figure 5B, in which bands between 1680-1660 cm^{-1} and the band at 1545 cm^{-1} are both observed, we assign the observed spectral features to amide I and II vibrational modes or to the lysine side chain. For the lysine side chain, NH_3^+ bending modes are expected at ~ 1630 and ~ 1530 cm^{-1} [72]. Taken together, these data indicate that each S state transition structurally perturbs the OEC chloride-binding site.

The data above provide evidence for changes in protein structure during the S state cycle. Changes in structure can alter protein dynamics and thereby alter the extent of solvent isotope exchange. To address this question, reaction-induced FT-IR spectroscopy was performed on chloride-exchanged PSII either in the presence of ^1H_2O or ^2H_2O. The transmembrane regions of membrane proteins do not exchange readily (for

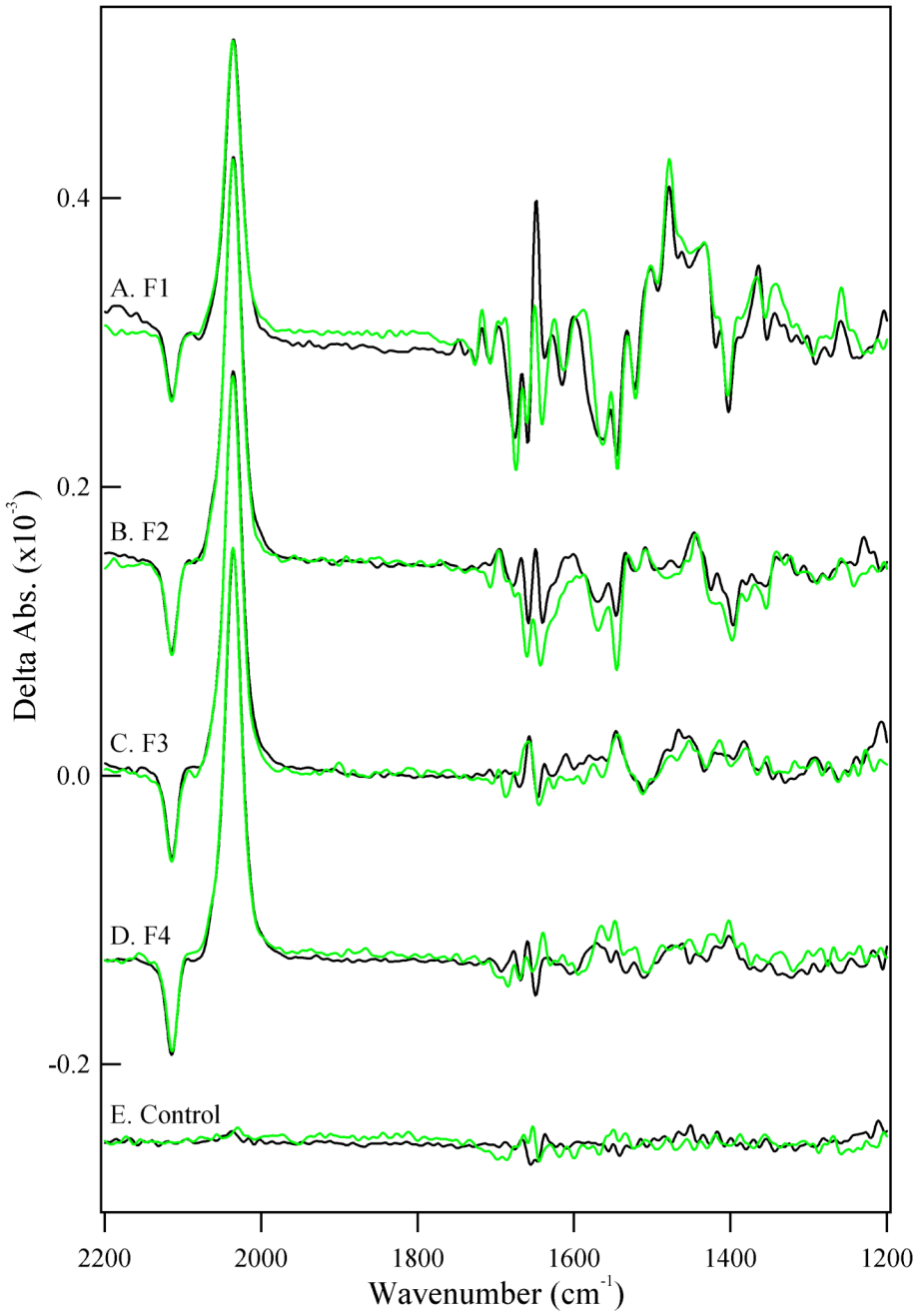

Figure 6. Difference FT-IR spectra of chloride-exchanged PSII in $^{1}H_2O$ SHCl buffer at p^{1}H 7.5 (green traces) and chloride-exchanged PSII in $^{2}H_2O$ SHCl buffer at p^{2}H 7.5 (black traces). The spectra are associated with the first (A), second (B), third (C), and fourth (D) flashes to a dark-adapted sample in the S_1 state. In (E), dark-minus-dark controls are presented.

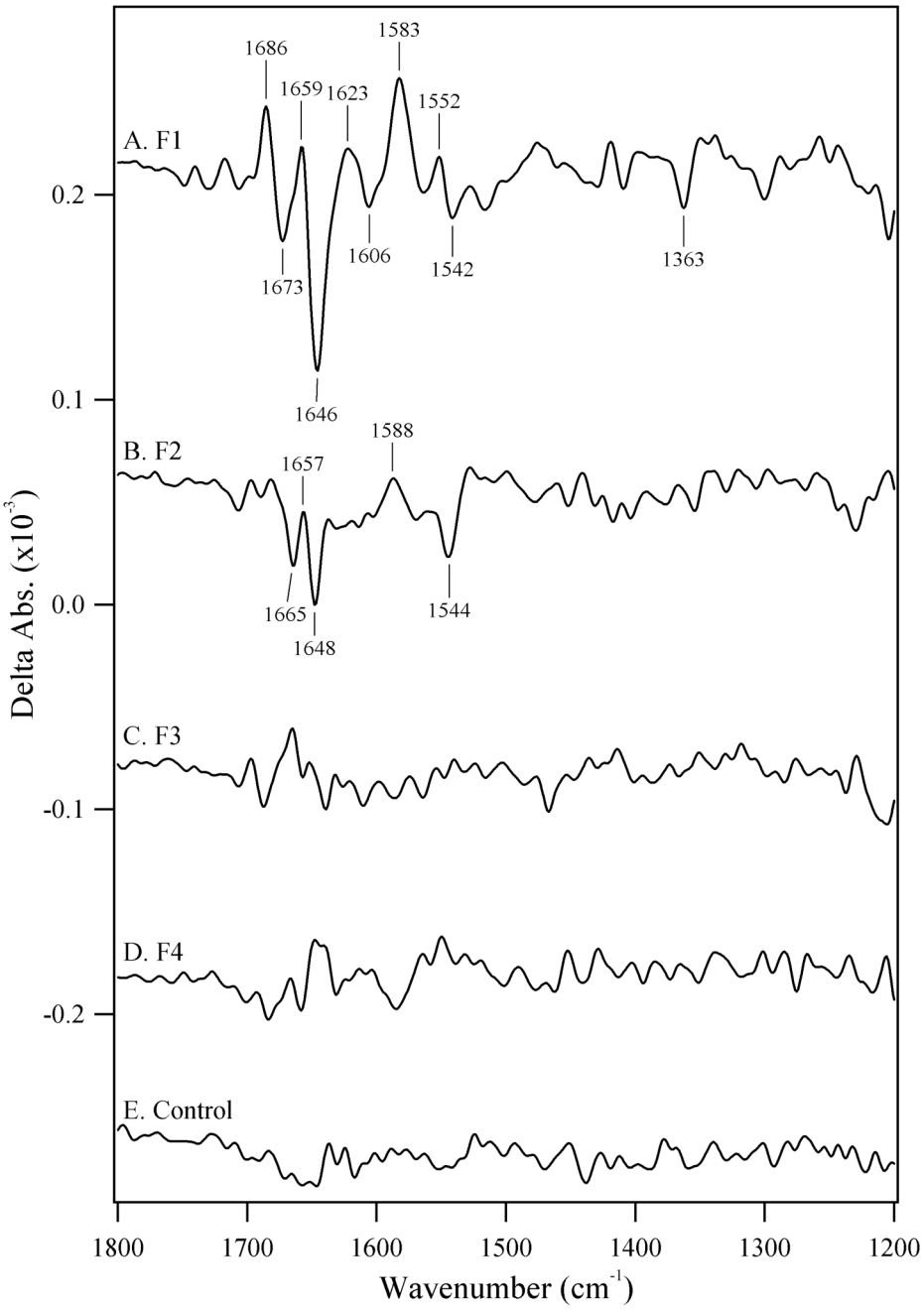

Figure 7. $^{2}H_2O$-edited double difference spectra constructed from the data in figure 6 ($^{1}H_2O$-minus-$^{2}H_2O$). The spectra are associated with the first (A), second (B), third (C), and fourth (D) flashes to a dark-adapted sample in the S_1 state. In (E), a representative double difference control is presented in which no vibrational bands are expected. This control was constructed from the dataset acquired with the first flash in the $^{1}H_2O$-containing sample.

example, see [74]). In our case, the ^2H_2O exchange protocol involved resuspension and centrifugation from ^2H_2O buffers and was designed to probe exchange at readily accessible sites.

Figure 6A-D compares the 2200-1200 cm^{-1} region of difference spectra generated from chloride-exchanged PSII in ^1H_2O (green line) and ^2H_2O (black line) buffers as a function of flash number. Control difference spectra are shown in figure 6E. Double difference spectra were then constructed to identify the extent of solvent exchange (figure 7). Significant features are observed in the double difference spectra constructed on the first and second flash (figure 7A and B). As described above, these spectral features, between 1690-1600 and 1590-1540 cm^{-1}, are most likely assignable to protein amide I and II bands. On the other hand, on the third and fourth flash (figure 7C and D), no significant spectral features are observed, compared to the control (figure 7E). This result suggests that a change in protein dynamics occurs during or after the S_3 transition.

Discussion

In our experiments, chloride was removed from the PSII reaction center by sulfate incubation at pH 7.5. Reconstitution either of chloride or bromide in this preparation restores oxygen evolution activity. Sulfate is a non-activating anion [29, 38, 44]. Comparison of vibrational frequencies in a chloride-exchanged sample with bromide-exchanged and chloride-depleted PSII identifies structural changes at the OEC chloride site. Using this approach, we report S state dependent perturbations of the PSII chloride site on each S state transition. We also provide evidence for significant changes in protein dynamics during the S state cycle, using ^2H_2O exchange as a probe. The detected

structural changes occur on long time scales compared to the water splitting reactions; however, the conformational changes are tightly coupled to water oxidation, because their vibrational spectra exhibit period four oscillations in frequency and amplitude [49, 50].

Previous work on the transmembrane halide pump, halorhodopsin, used bromide editing to identify arginine guanidino groups, which bind chloride [70]. In this protein, a chloride ion participates in hydrogen bonding interactions with the protonated Schiff base chromophore and a conserved arginine residue. The difference in ionic radii for chloride and bromide resulted in frequency shifts for the hydrogen-bonded arginine, and the vibrational bands of the arginine were observed to be perturbed when the photoproduct was formed. Vibrational spectroscopy of model compounds has also revealed halide dependent frequency shifts [71]. In this previous work, the frequency shifts, which were observed upon bromide substitution, were attributed to a weakening of a hydrogen bonding interaction with the bound arginine. Similarly, the origin of the bromide-induced frequency shifts in our spectra may also be due to changes in the hydrogen bonding of chloride ligands.

Optical spectroscopy in the UV has been used previously to investigate the role of chloride [31, 32, 38]. In this previous work, it was shown that, while the formation of the S_2 and S_1 states does not require chloride, the S_3 to S_0 and S_2 to S_3 transitions do require chloride [31]. Bromide reconstitution was shown to slow the S_3 to S_0 reaction, and it was suggested that bromide and chloride adjust the activation barrier of this step [38]. It has also been suggested that changes in chloride binding affinity occur during the S_1 to S_2 and S_2 to S_3 transitions [32]. A change in binding affinity is consistent with an alteration

in the structure of the OEC chloride site. If S state-induced structural changes *did not* occur at the chloride site, then bromide substitution would give the same bromide-edited spectrum on each flash. However, we obtain a distinct bromide-edited spectrum on each S state transition. Therefore, our data support the interpretation that structural changes occur at the chloride site on each S state transition. These structural changes could either be due to an electrostatic effect on the chloride-binding site or to a more long-range conformational rearrangement, caused by carboxylate shifts or changes in hydrogen bonding and protonation, for example.

In the absence of chloride, evidence from multiple laboratories suggests that manganese oxidation occurs during the S_1 to S_2 transition (reviewed in [1]), but not during the S_2 to S_3 transition [31, 63-65]. However, chloride-depleted PSII exhibits no S_2 multiline signal [75]. Thermoluminesence measurements show a reversible decrease in the S_2/S_1 midpoint potential after removal of chloride [76], and the recombination rate of the S_2 state is also slower in the absence of chloride [75]. These results suggest that the S_2 state is structurally modified in the absence of chloride. Such a change in the ligand environment of manganese with chloride removal is consistent with our results on chloride-depleted PSII, in which the FT-IR spectrum of the S_1' to S_2' transition exhibits frequency and amplitude shifts throughout the 1800-1200 cm^{-1} region, when compared to the chloride-exchanged control.

As expected on the basis of previous work, we have shown here that chloride-depleted PSII exhibits no significant FT-IR signals on the third and fourth flashes, i.e., from the S_3 to S_0 and S_0 to S_1 transitions. However, a difference FT-IR signal is observed on the second flash, in spite of the fact that the chloride-depleted PSII samples exhibit no

residual oxygen evolution under the same conditions (table 1), and that no FT-IR signal is observed on the third and fourth flash. Assignment of this spectrum to a photooxidation-induced perturbation of manganese ligands on this transition is then problematic. Instead, we favor the assignment of this spectrum to a conformational relaxation in the coordination of the manganese cluster.

Solvent isotope exchange provides a method to probe protein dynamics and conformational flexibility [77, 78]. Solvent exchange rates are determined by protein dynamics and by the intrinsic exchange rate of the exchanging group. Reaction-induced FT-IR spectroscopy detects ^2H_2O-induced shifts in the frequencies of the peptide bond, when spectra are constructed from chloride-exchanged PSII with one and two flashes. However, when three and four flashes are given to the same chloride-exchanged sample,there is no significant ^2H_2O-induced change in the FT-IR spectrum. Assuming no change in intrinsic exchange rates, these results suggest S state dependent changes in the flexibility of the OEC. Previous work has shown ^2H_2O isotope-dependent changes in the reaction-induced difference FT-IR spectra of intact, cyanobacterial PSII [79]. In that study, no double difference spectra were reported, but the effects of ^2H_2O exchange appeared to be small and were similar on each flash. Comparison of this previous result with our data suggests that the chloride-exchange process may induce additional conformational flexibility in the OEC. Note that the bromide-edited and ^2H_2O-edited spectra both exhibit bands in the 1690-1620 cm^{-1} region of the spectrum, indicating that both procedures alter the frequencies of peptide bond, arginine, and/or lysine side chains near the OEC.

The effect of bromide replacement and chloride depletion on the S_2'-minus-S_1' spectrum has been reported previously [80, 81]. In that previous study, chloride was removed by salt washing and dialysis, not by sulfate treatment, as employed here. In spite of this difference in chloride removal method, the effects of bromide exchange and chloride removal on the S_2'-minus-S_1' spectrum (first flash) appear to be similar in [80] and this work. To our knowledge, the effect of bromide substitution and chloride depletion on the other S state transitions has not been previously reported.

Summary

Our results show that the chloride site is altered by redox reactions at the OEC, suggesting that it is in close proximity to the Mn cluster. We also present evidence that chloride depletion causes structural changes in the OEC, which may contribute to the inhibition of oxygen evolution in the absence of chloride. Finally, we have obtained evidence for flash-induced changes in solvent isotope exchange, which are indicative of alterations in protein conformational flexibility during the water oxidizing cycle.

References

1. Britt, R.D., *Oxygen evolution*, in *Oxygenic Photosynthesis: The Light Reactions*, D.R. Ort and C.F. Yocum, Editors. 1996, Kluwer Academic Publisher: Dordrecht. p. 137-164.

2. Barry, B.A., *Tyrosyl radicals in photosystem II.* Methods Enzymol, 1995. **258**: p. 303-319.

3. Barry, B.A. and G.T. Babcock, *Tyrosine radicals are involved in the photosynthetic oxygen-evolving system.* Proc Natl Acad Sci USA, 1987. **84**: p. 7099-7103.

4. Boerner, R.J. and B.A. Barry, *Isotopic labeling and EPR spectroscopy show that a tyrosine residue is the terminal electron donor, Z, in manganese-depleted photosystem II preparations.* J Biol Chem, 1993. **268**: p. 17151-17154.

5. Babcock, G.T. and K. Sauer, *Electron paramagnetic resonance signal II in spinach chloroplasts.* Biochim Biophys Acta, 1973. **325**: p. 483-503.

6. Babcock, G.T. and K. Sauer, *Electron paramagnetic resonance signal in spinach chloroplasts II. Alternative spectral forms and inhibitor effects on the kinetics of signal II in flashing light.* Biochim Biophys Acta, 1973. **325**: p. 504-519.

7. Faller, P., et al., *Rapid formation of the stable tyrosyl radical in photosystem II.* Proc Natl Acad Sci USA, 2001. **98**: p. 14368-14373.

8. Ananyev, G.M., et al., *A functional role for tyrosine-D in assembly of the inorganic core of the water complex of photosystem II and the kinetics of water oxidation.* Biochemistry, 2002. **41**: p. 974-980.

9. Joliot, P. and B. Kok, *Oxygen evolution in photosynthesis*, in *Bioenergetics of Photosynthesis*, Govindjee, Editor. 1975, Academic Press: New York. p. 388-412.

10. Gerken, S., et al., *Optical characterization of the immediate donor to chlorophyll a_{II}^{+} in O_2-evolving photosystem II complexes.* FEBS Lett, 1988. **237**: p. 69-75.

11. Babcock, G.T., R.E. Blankenship, and K. Sauer, *Reaction kinetics for positive charge accumulation on the water side of chloroplast photosystem II.* FEBS Lett, 1976. **61**: p. 286-289.

12. Dekker, J.P., et al., *Kinetics of manganese redox transitions in the oxygen-evolving apparatus of photosynthesis.* Biochim Biophys Acta, 1984. **767**: p. 176-179.

13. Razeghifard, M.R. and R.J. Pace, *EPR kinetic studies of oxygen release in thylakoids and PSII membranes: a kinetic intermediate in S_3 to S_0 transition.* Biochemistry, 1999. **38**: p. 1252-1257.

14. Haumann, M., et al., *Photosynthetic O_2 formation tracked by time-resolved X-ray experiments.* Science, 2005. **310**: p. 1019-1021.

15. Clausen, J. and W. Junge, *Detection of an intermediate of photosynthetic water oxidation.* Nature, 2004. **430**: p. 480-483.

16. Barry, B.A., et al., *Time-resolved vibrational spectroscopy detects protein-based intermediates in the photosynthetic oxygen-evolving cycle.* Proc Natl Acad Sci USA, 2006. **103**: p. 7288-7291.

17. Zouni, A., et al., *Crystal structure of photosystem II from Synechococcus elongatus at 3.8 Å resolution.* Nature, 2001. **409**: p. 739-743.

18. Kamiya, N. and J.-R. Shen, *Crystal structure of oxygen-evolving photosystem II from Thermosynechococcus vulcanus at 3.7 Å resolution.* Proc Natl Acad Sci USA, 2003. **100**: p. 98-103.

19. Biesiadka, J., et al., *Crystal structure of cyanobacterial photosystem II at 3.2 Å resolution: a closer look at the Mn-cluster.* Phys Chem Chem Phys, 2004. **6**: p. 4733-4736.

20. Ferreira, K.N., et al., *Architecture of the photosynthetic oxygen-evolving center.* Science, 2004. **303**: p. 1831-1837.

21. Loll, B., et al., *Towards complete cofactor arrangement in the 3.0 Å resolution structure of photosystem II.* Nature, 2005. **438**: p. 1040-1044.

22. Yano, J., et al., *X-ray damage to the Mn_4Ca complex in single crystals of photosystem II: A case study for metalloprotein crystallography.* Proc Natl Acad Sci USA, 2005. **102**: p. 12047-12052.

23. Grabolle, M., et al., *Rapid loss of structural motifs in the manganese complex of oxygenic photosynthesis by X-ray irradiation at 10-300 K.* J Biol Chem, 2006. **281**: p. 4580-4588.

24. Yocum, C.F., *The calcium and chloride requirements for photosynthetic water oxidation*, in *Manganese Redox Enzymes*, V.L. Pecoraro, Editor. 1992, VCH Publishers: New York. p. 71-83.

25. Olesen, K. and L.-E. Andreasson, *The function of the chloride ion in photosynthetic oxygen evolution.* Biochemistry, 2003. **42**: p. 2025-2035.

26. Lindberg, K., T. Vanngard, and L.-E. Andreasson, *Studies of the slowly exchanging chloride in photosystem II of higher plants.* Photosynth Res, 1993. **38**: p. 401-408.

27. Clemens, K.L., D.A. Force, and R.D. Britt, *Acetate binding at the photosystem II oxygen evolving complex: an S_2-state multiline signal ESEEM study.* J Am Chem Soc, 2002. **124**: p. 10921-10933.

28. Yu, H., et al., *Evidence that azide occupies the chloride binding site near the manganese cluster in photosystem II.* Biochemistry, 2005. **44**: p. 12022-12029.

29. Sandusky, P.O. and C.F. Yocum, *The mechanism of amine inhibition of the photosynthetic oxygen evolving complex. Amines displace functional chloride from a ligand site on manganese.* FEBS Lett, 1983. **162**: p. 339-343.

30. Beauregard, M., L. Morin, and R. Popovic, *Sulfate inhibition of photosystem II oxygen evolving complex.* Appl Biochem Biotech, 1987. **16**: p. 109-117.

31. Wincencjusz, H., H.J. van Gorkom, and C.F. Yocum, *The photosynthetic oxygen evolving complex requires chloride for its redox state $S_2 \rightarrow S_3$ and $S_3 \rightarrow S_0$ transitions but not for $S_0 \rightarrow S_1$ or $S_1 \rightarrow S_2$ transitions.* Biochemistry, 1997. **36**: p. 3663-70.

32. Wincencjusz, H., C.F. Yocum, and H.J. van Gorkom, *S-state dependence of chloride binding affinities and exchange dynamics in the intact and polypeptide-depleted O_2 evolving complex of photosystem II.* Biochemistry, 1998. **37**: p. 8595-8604.

33. Haddy, A., R.A. Kimel, and R. Thomas, *Effects of azide on the S_2 state EPR signals from photosystem II.* Photosynth Res, 2000. **63**: p. 35-45.

34. Jajoo, A., S. Bharti, and A. Kawamori, *EPR characteristics of chloride-depleted photosystem II membranes in the presence of other anions.* Photochem Photobiol Sci, 2005. **4**: p. 459-462.

35. Kawamoto, K., J. Mano, and K. Asada, *Photoproduction of the azidyl radical from the azide anion on the oxidizing side of photosystem II and suppression of tyrosine Z by the azidyl radical.* Plant Cell Physiol, 1995. **36**: p. 1121-1129.

36. Haddy, A., et al., *Azide as a competitor of chloride in oxygen evolution by photosystem II.* Biochemistry, 1999. **38**: p. 6104-6110.

37. Kuhne, H., V.A. Szalai, and G.W. Brudvig, *Competitive binding of acetate and chloride in photosystem II.* Biochemistry, 1999. **38**: p. 6604-6613.

38. Wincencjusz, H., C.F. Yocum, and H.J. van Gorkom, *Activating anions that replace Cl^- in the O_2-evolving complex of photosystem II slow the kinetics of the terminal step in water oxidation and destabilize the S_2 and S_3 states.* Biochemistry, 1999. **38**: p. 3719-3725.

39. Putnam-Evans, C. and T.M. Bricker, *Site-directed mutagenesis of the CP47 protein of photosystem II: alteration of the basic residue ^{448}R to ^{448}G prevents the assembly of functional photosystem II centers under chloride-limiting conditions.* Biochemistry, 1994. **33**: p. 10770-10776.

40. Tichy, M. and W. Vermaas, *Functional analysis of combinatorial mutants altered in the conserved region in loop E of the CP47 protein in Synechocystis sp. PCC 6803.* Biochemistry, 1998. **37**: p. 1523-1531.

41. Bricker, T.M., et al., *Alterations of the oxygen-evolving apparatus in a ^{448}Arg-^{448}Ser mutant in the CP47 protein of photosystem II under normal and low chloride concentrations.* Biochemistry, 2001. **40**: p. 11483-11489.

42. Young, A., et al., *Alterations of the oxygen-evolving apparatus induced by a ^{305}Arg-^{305}Ser mutation in the CP43 protein of photosystem II form Synechocystis sp. PCC 6803 under chloride limiting conditions.* Biochemistry, 2002. **41**: p. 15747-15753.

43. Popelkova, H., et al., *Mutagenesis of basic residues R151 and R161 in manganese-stabilizing protein of photosystem II causes inefficient binding of chloride to the oxygen-evolving complex.* Biochemistry, 2006. **45**: p. 3107-3115.

44. Sandusky, P.O. and C.F. Yocum, *The chloride requirement for photosynthetic oxygen evolution. Analysis of the effects of chloride and other anions on amine inhibition of the oxygen evolving complex.* Biochim Biophys Acta, 1984. **766**: p. 603-611.

45. Boussac, A. and A.W. Rutherford, *Electron transfer events in chloride-depleted photosystem II.* J Biol Chem, 1994. **269**: p. 12462-12467.

46. McEvoy, J.P. and G.W. Brudvig, *Structure-based mechanism of photosynthetic water oxidation.* Phys Chem Chem Phys, 2004. **6**: p. 4754-4763.

47. Hasegawa, K., Y. Kimura, and T.-a. Ono, *Oxidation of the Mn cluster induces structural changes of NO_3^- functionally bound to the Cl^- site in the oxygen-evolving complex of photosystem II.* Biophys J, 2004. **86**: p. 1042-1050.

48. Haumann, M., et al., *Bromide does not bind to the Mn_4Ca complex in its S_1 state in Cl^--depleted and Br^--reconstituted oxygen-evolving photosystem II: Evidence from X-ray absorption spectroscopy at the Br K-edge.* Biochemistry, 2006. **45**: p. 13101-13107.

49. Hillier, W. and G.T. Babcock, *S-state dependent Fourier transform infrared difference spectra for the photosystem II oxygen evolving complex.* Biochemistry, 2001. **40**: p. 1503-1509.

50. Noguchi, T. and M. Sugiura, *Flash-induced Fourier transform infrared detection of the structural changes during the S-state cycle of the oxygen-evolving complex in photosystem II.* Biochemistry, 2001. **40**: p. 1497-1502.

51. Kimura, Y., et al., *FTIR detection of structural changes in a histidine ligand during S-state cycling of photosynthetic oxygen-evolving complex.* Biochemistry, 2005. **44**: p. 16072 -16078.

52. Strickler, M.A., et al., *Evidence from biosynthetically incorporated strontium and FTIR difference spectroscopy that the C-terminus of the D1 polypeptide of photosystem II does not ligate calcium.* Biochemistry, 2005. **44**: p. 8571-8577.

53. DeRiso, A., D.L. Jenson, and B.A. Barry, *Calcium exchange and structural changes during the photosynthetic oxygen evolving cycle.* Biophys J, 2006. **91**: p. 1999-2008.

54. Barry, B.A., et al., *Calcium ligation in photosystem II under inhibiting conditions.* Biophys J, 2005. **89**: p. 393-401.

55. Berthold, D.A., G.T. Babcock, and C.F. Yocum, *A highly resolved, oxygen-evolving photosystem II preparation from spinach thylakoid membranes.* FEBS Lett, 1981. **134**: p. 231-234.

56. Krimm, S. and J. Bandekar, *Vibrational spectroscopy and conformation of peptides, polypeptides, and proteins*, in *Advances in Protein Chemistry*, C.B. Anfinsen, J.T. Edsall, and F.M. Richards, Editors. 1986, Academic Press: New York. p. 181-364.

57. Kim, S. and B.A. Barry, *The protein environment surrounding tyrosyl radicals $D^{\bullet}$ and $Z^{\bullet}$ in photosystem II: a difference Fourier-transform infrared spectroscopic study.* Biophys J, 1998. **74**: p. 2588-2600.

58. Pujols-Ayala, I., C.A. Sacksteder, and B.A. Barry, *Redox-active tyrosine residues: Role for the peptide bond in electron transfer.* J Am Chem Soc, 2003. **125**: p. 7536-7538.

59. Ghanotakis, D.F., G.T. Babcock, and C.F. Yocum, *Calcium reconstitutes high rates of oxygen evolution in polypeptide depleted photosystem II preparations.* FEBS Lett, 1984. **167**: p. 127-130.

60. Ghanotakis, D.F., et al., *Water-soluble 17 and 23 kDa polypeptides restore oxygen evolution activity by creating a high-affinity binding site for Ca^{+2} on the oxidizing side of photosystem II.* FEBS Lett, 1984. **170**: p. 169-173.

61. Ghanotakis, D.F., J.N. Topper, and C.F. Yocum, *Structural organization of the oxidizing side of photosystem II. Exogenous reductants reduce and destroy the Mn-complex in photosystem II membranes depleted of the 17 and 23 kDa polypeptides.* Biochim Biophys Acta, 1984. **767**: p. 524-531.

62. Suzuki, H., et al., *Structural perturbation of the carboxylate ligands to the manganese cluster upon Ca^{2+}/Sr^{2+} exchange in the S-state cycle of photosynthetic oxygen evolution as studied by flash-induced FTIR difference spectroscopy.* Biochemistry, 2006. **45**: p. 13454-13464.

63. Itoh, S., et al., *Effects of chloride depletion on electron donation from the water-oxidizing complex to the photosystem II reaction center as measured by the microsecond rise of chlorophyll fluorescence in isolated pea chloroplasts.* Biochim Biophys Acta, 1984. **766**: p. 612-622.

64. Deak, Z., I. Vass, and S. Strying, *Redox interaction of tyrosine-D with the S-states of the water-oxidizing complex in intact and chloride-depleted photosystem II.* Biochim Biophys Acta, 1994. **1185**: p. 65-74.

65. Ono, T.-a., et al., *XANES spectroscopy for monitoring intermediate reaction states of Cl^--depleted Mn cluster in photosynthetic water oxidation enzyme.* J Am Chem Soc, 1995. **117**: p. 6386-6387.

66. Ma, C. and B.A. Barry, *Electron paramagnetic resonance characterization of tyrosine radical, M^+, in site-directed mutants of photosystem II.* Biophys J, 1996. **71**: p. 1961-1972.

67. Halverson, K.M. and B.A. Barry, *Evidence for spontaneous structural changes in a dark-adapted state of photosystem II.* Biophys J, 2003. **85**: p. 2581-2588.

68. Messinger, J., *Evaluation of different mechanistic proposals for water oxidation in photosynthesis on the basis of Mn_4O_xCa structures for the catalytic site and spectroscopic data.* Phys Chem Chem Phys, 2004. **6**: p. 4764-4771.

69. Suydam, I.T. and S.G. Boxer, *Vibrational Stark effects calibrate the sensitivity of vibrational probes for electric fields in proteins.* Biochemistry, 2003. **42**: p. 12050-12055.

70. Braiman, M.S., T.J. Walter, and D.M. Briercheck, *Infrared spectroscopic detection of light-induced changes in chloride-arginine interaction in halorhodopsin.* Biochemistry, 1994. **33**: p. 1629-1635.

71. Braiman, M.S., D.M. Briercheck, and K.M. Kriger, *Modeling vibrational spectra of amino acid side chains in proteins: effects of protonation state, counterion, and solvent on arginine C-N stretch frequencies.* J Phys Chem B, 1999. **103**: p. 4744-4750.

72. Barth, A., *The infrared absorption of the amino acid side chains.* Prog Biophys Mol Biol, 2000. **74**: p. 141-173.

73. Jackson, M. and H.H. Mantsch, *The use and misuse of FTIR spectroscopy in the determination of protein structure.* Crit Rev Biochem Mol Biol, 1995. **30**: p. 95-120.

74. Rath, P., W.J. DeGrip, and K.J. Rothschild, *Photoactivation of rhodopsin causes an increased hydrogen-deuterium exchange of buried peptide groups.* Biophys J, 1998. **74**: p. 192-198.

75. Ono, T.-a., et al., *EPR evidence for a modified S state transition in chloride-depleted photosystem II.* Biochim Biophys Acta, 1986. **851**: p. 193-201.

76. Vass, I., T. Ono, and Y. Inoue, *Stability and oscillation properties of thermoluminescent charge pairs in the O_2-evolving system depleted of Cl^- or the 33-kDa extrinsic protein.* Biochim Biophys Acta, 1987. **892**: p. 224-235.

77. Simmons, D.A., S.D. Dunn, and L. Konermann, *Conformational dynamics of partially denatured myoglobin studied by time-resolved electrospray mass spectrometry with online hydrogen-deuterium exchange.* Biochemistry, 2003. **42**: p. 5896-5905.

78. Xiao, H., et al., *Mapping protein energy landscapes with amide hydrogen exchange and mass spectrometry: I. A generalized model for a two-state protein and comparison with experiment.* Protein Sci, 2005. **14**: p. 543-557.

79. Noguchi, T. and M. Sugiura, *Flash-induced FTIR difference spectra of the water oxidizing complex in moderately hydrated photosystem II core films: effect of hydration extent on S-state transitions.* Biochemistry, 2002. **41**: p. 2322-2330.

80. Hasegawa, K., Y. Kimura, and T.-a. Ono, *Chloride cofactor in the photosynthetic oxygen-evolving complex studied by Fourier transform infrared spectroscopy.* Biochemistry, 2002. **41**: p. 13839-13850.

81. Kimura, Y., et al., *Studies on photosynthetic oxygen-evolving complex by means of Fourier transfer infrared spectroscopy: calcium and chloride cofactors.* Photosynth Res, 2005. **84**: p. 245-250.

CHAPTER 5

AZIDE AS A PROBE OF PROTON TRANSFER REACTIONS IN PHOTOSYNTHETIC OXYGEN EVOLUTION

by

Ian B. Cooper and Bridgette A. Barry

School of Chemistry and Biochemistry and the Petit Institute for Bioengineering and Bioscience, Georgia Institute of Technology, Atlanta, GA 30332

Abstract

In oxygenic photosynthesis, photosystem II (PSII) is the multi-subunit membrane protein responsible for the oxidation of water to O_2 and the reduction of plastoquinone to plastoquinol. One electron charge separation in the PSII reaction center is coupled to sequential oxidation reactions at the oxygen-evolving complex (OEC), which is composed of four manganese ions and one calcium ion. The sequentially oxidized forms of the OEC are referred to as the S_n states. S_1 is the dark-adapted state of the OEC. Flash-induced oxygen production oscillates with period four and occurs during the S_3 to S_0 transition. Chloride plays an important, but poorly understood role in photosynthetic water oxidation. Chloride removal is known to block manganese oxidation during the S_2 to S_3 transition. In this work, we have used azide as a probe of proton transfer reactions in PSII. PSII was sulfate-treated, in order to deplete chloride, and then treated with azide. Steady state oxygen evolution measurements demonstrate that azide inhibits oxygen evolution in a chloride-dependent manner and that azide is a mixed or non-competitive inhibitor. This result is consistent with two azide binding sites, one at which azide

competes with chloride and one at which azide and chloride do not compete. At pH 7.5, the K_i for the competing site was estimated as 1 mM, and the K_i' for the uncompetitive site was estimated as 8 mM. Vibrational spectroscopy was then used to monitor perturbations in the frequency and amplitude of the azide antisymmetric stretching band. These changes were induced by laser-induced charge separation in the PSII reaction center. The results suggest that azide is involved in proton transfer reactions, which occur before manganese oxidation, on the donor side of chloride-depleted PSII.

Introduction

Photosystem II (PSII) is a chlorophyll-containing protein complex found in the thylakoid membrane of cyanobacteria, algae, and higher plants. PSII catalyzes the light-induced oxidation of water and reduction of plastoquinone (reviewed in [1, 2]). The water-splitting reactions provide molecular oxygen, which is necessary for the maintenance of aerobic life on earth. Chlorophyll (chl) is the primary donor during the light-induced electron transfer reactions, which lead to the production of a transmembrane, charge-separated state. Two plastoquinone acceptors, Q_A and Q_B, are sequentially reduced on the stromal side of the PSII reaction center. On the PSII lumenal side, a chl cation radical, P_{680}^+, oxidizes tyrosine 161 (Y_Z) of the D1 polypeptide to produce a tyrosyl radical ($Y_Z^\bullet$). $Y_Z^\bullet$ then oxidizes the oxygen-evolving complex (OEC), which is composed of four manganese and one calcium ion. X-ray diffraction has been used to determine the structure of PSII at 3.8-3.0 Å [3-7]. However, X-ray induced damage to the OEC complicates interpretation of the manganese ligand environment in the current structures [5, 8, 9].

Four sequential light-induced charge separations are required to produce one oxygen molecule from two water molecules. These sequential reactions are stored as oxidation reactions at the OEC. Accordingly, the Mn_4Ca cluster cycles among five oxidation states in the production of molecular oxygen [10]. The oxidation states are labeled S_0 - S_4, where the subscript describes the number of oxidizing equivalents stored. The rate of OEC oxidation slows as charge is accumulated, and there is a period four pattern of oxygen release [11, 12]. Oxygen release occurs during the S_3 to S_0 transition, in which the transient S_4 state is formed. Information about the S_4 state has been obtained by X-ray absorption spectroscopy [12], electron paramagnetic resonance (EPR) spectroscopy [13], and transient infrared spectroscopy [14]. UV spectroscopy has been used to probe the identity of S state intermediates accumulated at high oxygen pressure [15].

Chloride is required to achieve the maximum rate of PSII oxygen evolution activity [16-19]. Although chloride is known to bind near the OEC [20, 21], chloride has not yet been located in the PSII X-ray structures and is not an identified component in the Mn_4Ca cluster [3-7]. Previously, chloride has been proposed to bind to amino acid side chains [22-24] or directly to metal ions [16].

Chloride depletion alters the functional properties of the OEC. Chloride-depletion changes the S_2 state EPR signals [25, 26], and S state transition-associated FT-IR spectra [24, 27]. Chloride removal also inhibits manganese oxidation [28-34]. Previously, chloride has been proposed to have a role in structural maintenance of the OEC [35], as a manganese ligand [16], as a facilitator of proton transfer [19], as an adjustor of the OEC midpoint potential [36], and/or as an activator of substrate [37].

In PSII, azide has been shown to be a reversible inhibitor [38]. Evidence has been presented for azide interactions with both the PSII donor-side chloride site and the PSII acceptor-side. Evidence for a donor-side azide binding site near the OEC includes perturbation of the S_2 state EPR [26] and electron spin-echo envelope modulation (ESEEM) [39] signals. In addition, azide-induced inhibition of semiquinone anion (Q_A^-) oxidation is partially reversed by bicarbonate [40]. This result suggests a second, low affinity azide binding site on the PSII acceptor side.

It has been proposed that proton transfer precedes manganese oxidation on some of the S state transitions [12-14]. To gain more insight into proton transfer reactions occurring in the OEC, we have used azide as a vibrational spectroscopic probe. The antisymmetric stretching vibration of azide is sensitive to changes in protonation and hydrogen bonding, because these interactions stabilize the triple-bonded, valence bond structures [41]. In our experiments, PSII was chloride-depleted by treatment with sulfate [24, 32] and was then treated with azide. Reaction-induced, rapid scan FT-IR spectroscopy and flash excitation were then used to step PSII through the accessible S state transitions, and the effect of light-induced electron transfer on the azide vibrational spectrum was assessed. Previous FT-IR studies (for previous examples, see [42-46]) have shown that long-lived conformational changes occurring during the S state cycle can be monitored, even on the slow (seconds) time scale of rapid scan FT-IR spectroscopy [47]. Our work provides evidence that azide inhibition is due to changes in proton transfer reactions on the PSII donor side.

Materials and Methods

PSII membranes were isolated from market spinach as previously described [48]. Activity was measured with a Clark-type electrode and either recrystallized 2,6-dichlorobenzoquinone (DCBQ) or recrystallized paraphenylbenzoquinone (PPBQ) as an electron acceptor [49]. Chloride-depleted samples were prepared by sulfate treatment as previously described [24, 32]. Immediately before the experiment, PSII membranes were exchanged into pH 7.5 buffer (400 mM sucrose, 50 mM HEPES-NaOH, pH 7.5) by centrifugation and resuspension. Exchanged samples were incubated in sulfate buffer (400 mM sucrose, 50 mM HEPES-NaOH, pH 7.5, and 50 mM Na_2SO_4) for 15 minutes while shaking on ice and in darkness. After centrifugation, the chloride-depleted samples were suspended again in pH 7.5 buffer. Manganese-depleted samples were prepared as previously described using alkaline tris(hydroxymethyl)aminomethane (Tris) [50]. Manganese-depleted samples were exchanged into pH 7.5 buffer, displayed no oxygen-evolving capability, and were stored at –70°C until use. The final Tris concentration for the manganese-depleted samples was estimated to be $\leq$ 6 mM. Azide-exchanged samples were prepared by suspension of chloride-depleted or manganese-depleted PSII into buffer containing 400 mM sucrose, 50 mM HEPES-NaOH, pH 7.5, and indicated concentrations of sodium ^{14}N-azide or terminally labeled ($^{15}N^{14}N^{14}N$) sodium ^{15}N-azide (98% ^{15}N enriched, Cambridge Isotope Laboratories, Andover, MA). Solvent isotope exchange was achieved by performing each step of the chloride depletion protocol in ^2H_2O-containing buffers (99.8% ^{2}H enriched, Isotec, Miamisburg, OH). The p^{2}H is reported as the uncorrected pH meter reading [51].

Reaction-induced FT-IR difference spectroscopy was performed at pH 7.5 as previously described [24, 46, 47]. Chloride-depleted samples were concentrated with dry nitrogen gas to give an O-H stretching absorbance (3370 cm^{-1}) to amide II absorbance ratio of ≥ 3. Manganese-depleted samples were concentrated with nitrogen for ten minutes. Data acquisition parameters were as follows: 8 cm^{-1} resolution; four levels of zero filling; Happ-Genzel apodization function; 60 KHz mirror speed; Mertz phase correction. Samples were given a single saturating 532 nm laser flash followed by 20 minutes of dark adaptation in order to set all reaction centers in the S_1 state. Each subsequent flash was followed by 15 seconds of rapid scan data collection at 4°C. S state difference spectra were created by ratio of data taken before and after flash excitation, followed by conversion to absorbance. All data were normalized to an amide II intensity of 0.5 absorbance units (AU) in order to eliminate differences in sample pathlength [24, 46, 47]. The amide II band intensity was determined from an infrared absorption spectrum, which was generated through the use of a blank background scan.

Results

Table 1 presents representative steady state oxygen evolution rates for sulfate-treated PSII (see also [24]). Sulfate treatment is known to dissociate the 24 and 18 kDa extrinsic subunits and to decrease the chloride binding affinity, allowing for quantitative ion release [18, 20, 24, 32, 52]. When assayed at pH 6.0 and pH 7.5 in the presence of DCBQ, untreated PSII had oxygen rates of > 750 μmol O_2 (mg chl-h)$^{-1}$ and > 500 μmol O_2 (mg chl-h)$^{-1}$, respectively. Sulfate treatment resulted in a complete suppression of

Table 1. Oxygen evolving activity of sulfate-treated PSII at pH 6.0 and 7.5.[a]

10 mM Ca^{+2}	10 mM Cl^-	pH 6.0[b]	pH 7.5[c]
–	–	60 ± 30	30 ± 10
+	+	460 ± 60	240 ± 3
–	+	370 ± 60	200 ± 20
+	–	46 ± 7	9 ± 1

[a] Oxygen evolving activity measured at 25°C and listed with units of μmol O_2 (mg chl-h)$^{-1}$ [24]. Values are reported plus or minus one standard deviation. All measurements are an average of at least three individual experiments. Each measurement performed with 1 mM ferricyanide and 0.5 mM DCBQ.
[b] Conditions were 400 mM sucrose and 50 mM MES-NaOH (pH 6.0).
[c] Conditions were 400 mM sucrose and 50 mM HEPES-NaOH (pH 7.5).

oxygen evolution activity at pH 7.5 ($\leq$ 30 μmol O_2 (mg chl-h)$^{-1}$). Table 1 demonstrates that addition of chloride resulted in the reconstitution of the majority of oxygen-evolving activity at pH 6.0 (460 μmol O_2 (mg chl-h)$^{-1}$) and pH 7.5 (240 μmol O_2 (mg chl-h)$^{-1}$). As expected [32], calcium addition had little effect on oxygen-evolving activity in sulfate-treated PSII (table 1). Thus, sulfate treatment allows the effect of chloride depletion to be studied separately from the effects of calcium depletion [24, 32]. In addition, sulfate-treated samples reconstituted with chloride are known to produce a higher flash yield of the S state transitions, compared to other methods of chloride depletion [32].

Figures 1 and 2 demonstrate that azide inhibits PSII oxygen evolution in a chloride-dependent manner, both at pH 6.3 (figures 1A and 2A) and 7.5 (figures 1B and 2B). The direct plots (figure 2) and the Lineweaver-Burk double reciprocal plots ($1/v_o$ versus $1/[Cl^-]$; figure 1) give the dependence of the initial oxygen evolution velocity on the azide concentration. The color coded, superimposed lines were generated with V_{max}, K_m, K_i, and K_i' values, derived from fits to the hyperbolic oxygen evolution plots (figure

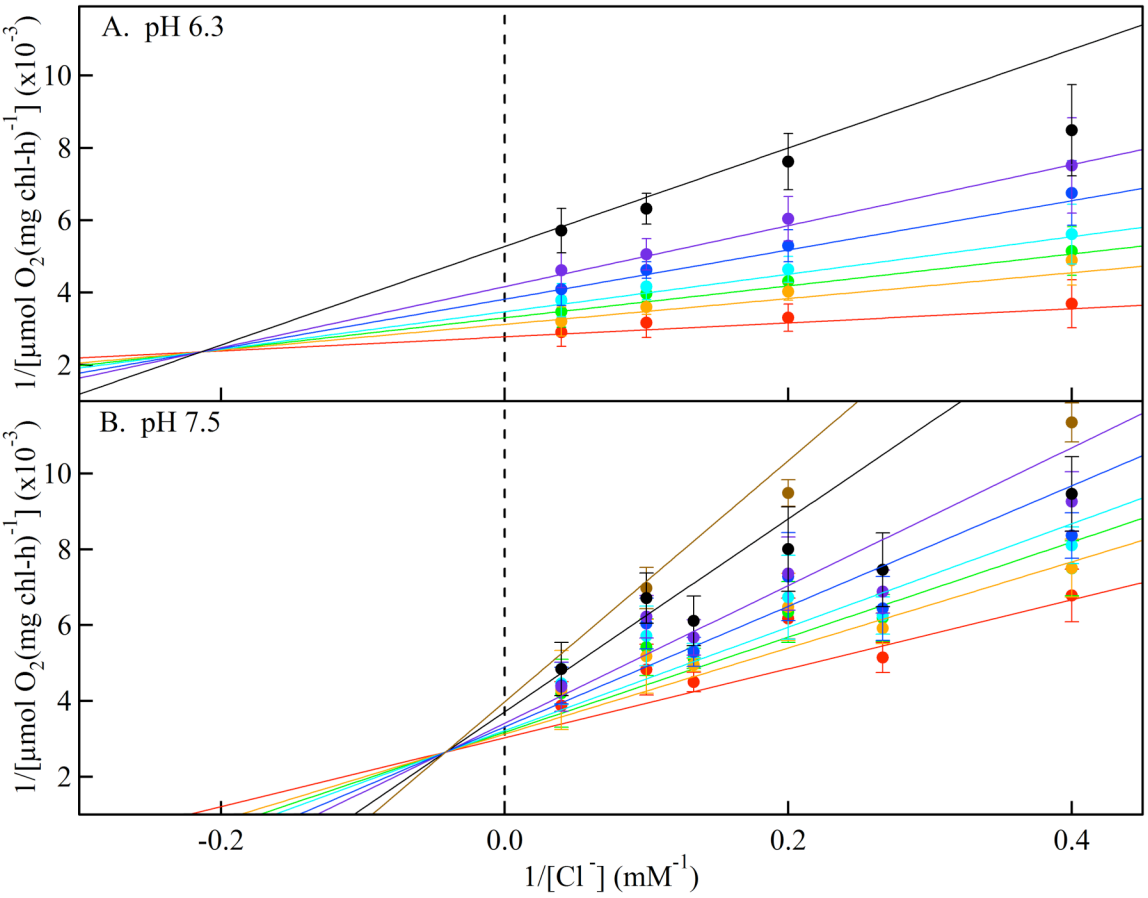

Figure 1. Lineweaver-Burk double-reciprocal plots, considering chloride as the substrate and showing the inhibitory effect of azide on PSII oxygen evolution activity. PSII was treated with sulfate in order to deplete chloride, and the PSII sample was then treated with 0 (red), 0.25 (orange), 0.38 (green), 0.50 (light blue), 0.75 (dark blue), or 1.0 (purple), 1.8 (black), and 2.5 (brown; pH 7.5 only) mM N_3^-. In (A), the assay conditions were taken from reference [38] and employed 400 mM sucrose, 50 mM MES-NaOH, pH 6.3, and 2 mM recrystallized PPBQ. In (B), the assay conditions were 400 mM sucrose, 50 mM HEPES-NaOH, pH 7.5, and 2 mM recrystallized PPBQ. The concentrations of chloride and azide were adjusted by addition from 1 M NaCl and 100 mM NaN_3 stock solutions, respectively, in the appropriate assay buffer. Error bars represent one standard deviation.

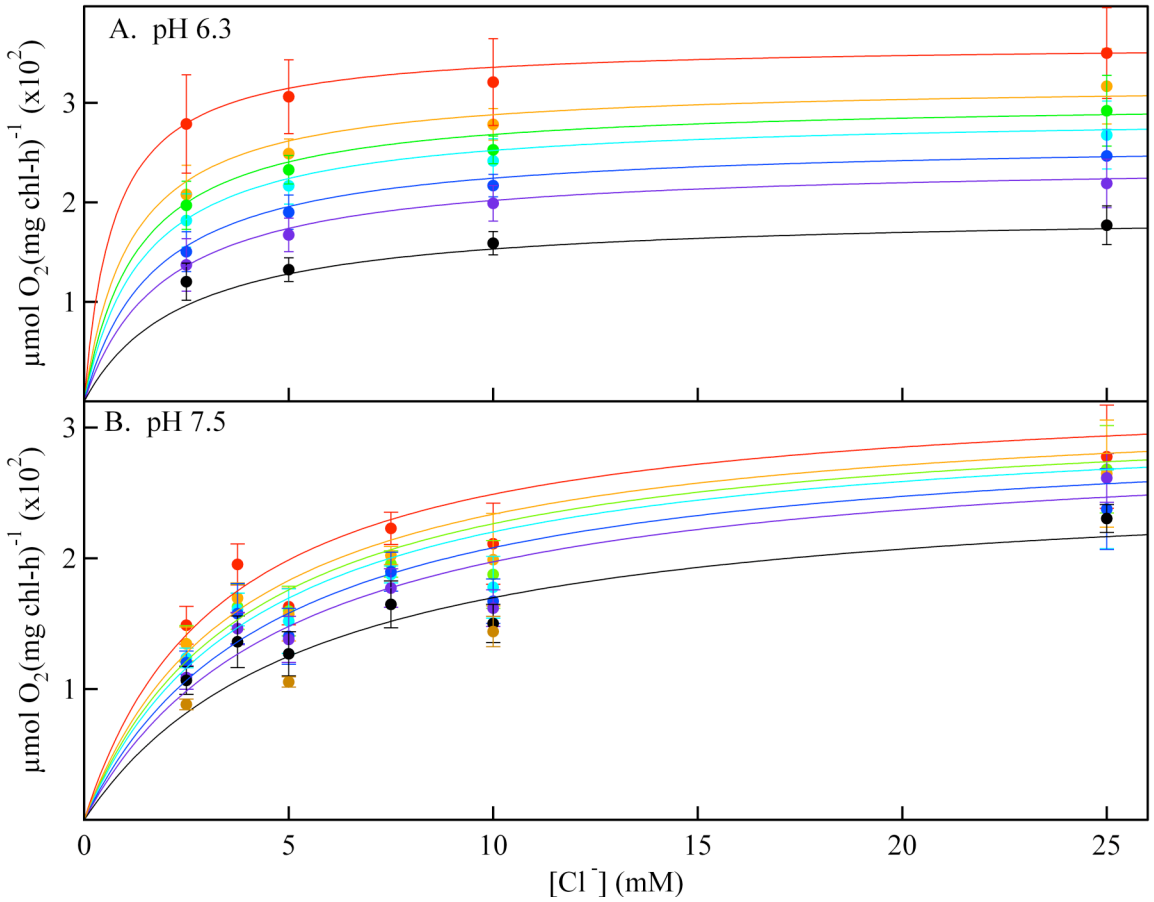

Figure 2. Michaelis-Menten plots, considering chloride as the substrate, and showing the effect of azide inhibition on PSII oxygen evolution activity. PSII was treated with sulfate in order to deplete chloride, and the PSII sample was then treated with 0 (red), 0.25 (orange), 0.38 (green), 0.50 (light blue), 0.75 (dark blue), or 1.0 (purple), 1.8 (black), and 2.5 (brown; pH 7.5 only) mM N_3^-. In (A), the assay conditions were taken from reference [38] and employed 400 mM sucrose, 50 mM MES-NaOH, pH 6.3, and 2 mM recrystallized PPBQ. In (B), the assay conditions were 400 mM sucrose, 50 mM HEPES-NaOH, pH 7.5, and 2 mM recrystallized PPBQ. The concentrations of chloride and azide were adjusted by addition from 1 M NaCl and 100 mM NaN_3 stock solutions, respectively, in the appropriate assay buffer. Error bars represent one standard deviation.

2). The double reciprocal pots were fit with the equation:

$$\frac{1}{v_0} = \frac{\left(1 + \frac{[N_3^-]}{K_i}\right)K_m}{V_{\max}}\left(\frac{1}{[Cl^-]}\right) + \frac{\left(1 + \frac{[N_3^-]}{K_i'}\right)}{V_{\max}},$$

where K_i is the azide inhibition constant for the competitive site and K_i' is the azide inhibition constant for the uncompetitive site. At pH 6.3, the Lineweaver-Burk results (figure 1A) are consistent with a family of lines that intersect to the left of the $1/v_o$ axis. This pattern provides evidence for reversible, non-competitive (or mixed) inhibition between azide and chloride, in agreement with an earlier report [38]. In a Michaelis-Menten interpretation, this type of inhibition occurs if azide simultaneously competes at the chloride site both in the enzyme (competitive site) and in the enzyme-substrate complex (uncompetitive site). Assuming that azide is a mixed inhibitor, fits to the direct plots (figure 2A) were used to yield kinetics constants. The data were fit using the Michealis-Menten equation for mixed inhibition,

$$v_0 = \frac{\left(V_{\max}[Cl^-]\right)}{K_m\left(1 + \frac{[N_3^-]}{K_i}\right) + [Cl^-]\left(1 + \frac{[N_3^-]}{K_i'}\right)}.$$

At pH 6.3, the K_m for chloride was derived as 0.7 mM, and the V_{max} was derived as 360 μmol O_2 (mg chl-h)$^{-1}$. The K_i for azide binding to the competitive site was derived as 0.3 mM and the K_i for the uncompetitive site was derived as 2 mM. Note that the uncompetitive azide site may correspond to an acceptor side binding event (see discussion below). Previously, Dixon and Cornish-Bowden plots were used to estimate the azide inhibition constants for the competitive and uncompetitive sites at pH 6.3 in sodium chloride treated PSII samples [38], and indistinguishable kinetic constants were obtained.

When pH 6.3 (figures 1A and 2A) and pH 7.5 (figures 1B and 2B) data were compared, a similar pattern of mixed inhibition was observed. Fits to the direct plots were again used to derive kinetic constants (figure 2B). At pH 7.5, the K_m for chloride was derived as 3 mM, the V_{max} was derived as 330 μmol O_2 (mg chl-h)$^{-1}$, the K_i for azide binding to the competitive site was derived as 1 mM, and the K_i for the uncompetitive site was derived as 8 mM. The Lineweaver-Burk plots exhibit some non-linearity at high azide concentrations (figure 1; $\geq$ 2.5 mM azide). Azide inhibition was found to be reversible at pH 7.5 (data not shown), as previously reported at pH 6.3 [38]. Taken together with previous work [38], figure 1 illustrates that the azide inhibition constant is similar in sulfate-treated PSII (figure 1) and other PSII preparations [38].

Figure 1 suggests that azide can be used as a spectroscopic probe, which will bind on the donor side of sulfate-treated PSII. The azide antisymmetric stretching band has been used previously to monitor protonation reactions in other enzymes, including bacteriorhodopsin [53] and sensory rhodopsin [54]. The frequency of the antisymmetric azide band falls outside the normal range of peptide and biological cofactor infrared absorption (1800-1200 cm^{-1}), facilitating detection of azide even in complex biological systems [53, 55].

In order to probe proton transfer reactions at the PSII azide site, we employed reaction-induced difference FT-IR spectroscopy. Figure 3A and B show the results of three consecutive 532 nm laser pulses (red, 1 flash; green, 2 flashes; blue, 3 flashes) on the azide antisymmetric stretching vibration in oxygen-evolving PSII at pH 6.0 and 7.5, respectively. Chloride was not depleted in these samples before the addition of 15 mM

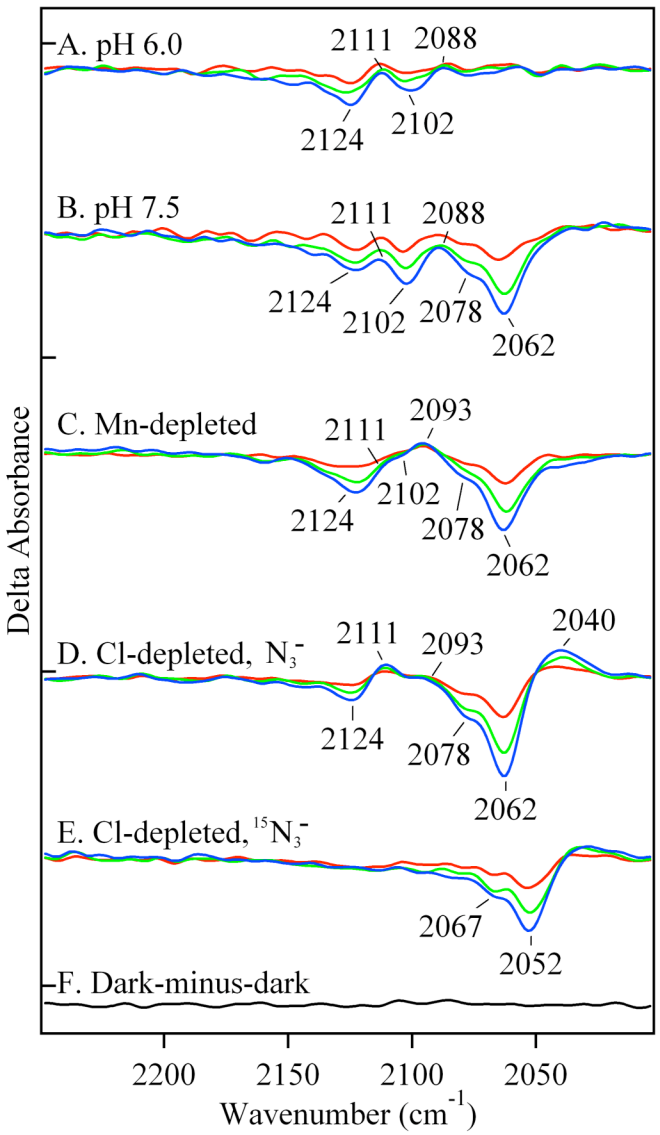

Figure 3. Difference FT-IR spectra showing flash-induced perturbation of the azide antisymmetric stretching band in untreated, manganese-depleted, or chloride-depleted PSII samples. Difference spectra were created by ratio of data taken before and after flash excitation, followed by conversion to absorbance. In (A-E), the results of three consecutive 532 nm laser flashes to a preflashed, dark-adapted PSII sample are presented in red (flash 1), green (flash 2), and blue (flash 3). In (A), untreated PSII contained 400 mM sucrose, 50 mM MES-NaOH, pH 6.0, and 15 mM NaCl (avg. of 12). In (B), untreated PSII contained in 400 mM sucrose, 50 mM HEPES-NaOH, pH 7.5 (pH 7.5 buffer) (avg. of 15). In (C), manganese-depleted PSII contained pH 7.5 buffer (avg. of 38). In (D), chloride-depleted PSII contained pH 7.5 buffer (avg. of 39). In (A-D), the sample also contained 15 mM N_3^-. In (E), chloride-depleted PSII in pH 7.5 buffer contained 15 mM $[^{15}N(^{14}N)_2]^-$ (avg. of 21). In F, a dark-minus-dark control was generated from the data set in (D). Delta absorbance on the y-axis indicates that the spectra show changes in absorbance. All samples contained 1.5 mM recrystallized DCBQ. The tick marks on the y-axis represent $5x10^{-4}$ AU.

azide. The difference spectra were constructed using data acquired following each flash and data acquired before the three laser flashes. In oxygen-evolving PSII, these spectra correspond to the S_1 to S_2 (one flash), S_1 to S_3 (two flashes), and S_1 to S_0 (three flashes) transitions. Our previously published work, analyzing the mid-infrared region of the spectrum, demonstrates that S state advancement is detectable under these conditions [24]. Azide bands were not observed in PSII without flash excitation (figure 3F) or in mixtures of azide, DCBQ acceptor and other buffer components, which did not contain PSII, but received flash excitation (data not shown).

Figure 3A and B show that PSII charge separation perturbs bands assignable to the azide antisymmetric stretching mode either at pH 6.0 (figure 3A) or at pH 7.5 (figure 3B). In both data sets, two band shifts at 2124 (–) /2111 (+) cm^{-1} and 2102 (–) /2088 (+) cm^{-1} are observed. These bands are significant compared to the noise in the measurement, as assessed by comparison to a dark-minus-dark spectrum (figure 3F). The pH 7.5 spectrum (figure 3B) displays additional negative bands at 2078 and 2062 cm^{-1}, which are not present at pH 6.0 (figure 3A). In the PSII samples used in figure 3A and B, chloride has not been depleted. Therefore, we assign azide bands, observed under these conditions, to a PSII acceptor side binding site. In agreement with this interpretation, similar perturbations of azide bands were also observed in manganese-depleted PSII at pH 7.5 (figure 3C). These manganese-depleted samples do not contain a chloride-binding site, because the OEC has been removed by Tris treatment [20, 52]. The small increase in azide band amplitude on each flash in (figure 3A-C) may be due to a light-induced conformational change, which allows increased access to the acceptor side binding site.

Figure 3D reveals the effect of PSII charge separation on azide bands in chloride-depleted samples. Reaction-induced FT-IR spectra were recorded at pH 7.5. While the S_1 to S_2 transition (first flash) proceeds in chloride-depleted PSII, the S_2 to S_3 transition (second flash) is blocked at the level of manganese oxidation [28-34]. Thus, in chloride-depleted samples, two flashes generate the $S_2Y_Z^{\bullet}$ state. This $S_2Y_Z^{\bullet}$ or S_3' state has a halftime of ~ 0.5 s [32]. Previous FT-IR studies of chloride-depleted samples have shown that structural changes occur in the OEC during the S_2 to S_3' transition, even though manganese oxidation is blocked [24]. These structural changes are long-lived and occur on the seconds time scale [24], as are other rapid-scan, FT-IR-detected structural changes during the normal S state cycle [46, 47].

The reaction-induced spectra obtained with a single flash (S_1 to S_2 transition) (figure 3D, red) are similar to data acquired in manganese-depleted PSII (figure 3C, red). This can be ascertained in figure 4A, in which these spectra subtract to give a flat baseline (compare to figure 4C). This result suggests that there is no significant perturbation of the azide donor-side binding site on the first flash. Spectra acquired with a second (figure 3D, green) and third (figure 3D, blue) flash (S_1 to S_3' transition) are similar to each other and exhibit new positive bands at 2111 and 2040 cm^{-1} and increased negative intensity at ~ 2062 cm^{-1}, compared to manganese-depleted PSII. In these samples, both the second and third flashes correspond to the inhibited S_1 to ($S_2Y_Z^{\bullet}$) S_3' transition, because charge recombination occurs in the time between the flashes [56]. The frequencies of all observed bands were downshifted when terminally ^{15}N labeled azide (figure 3E) was employed, confirming the spectral assignment to the azide

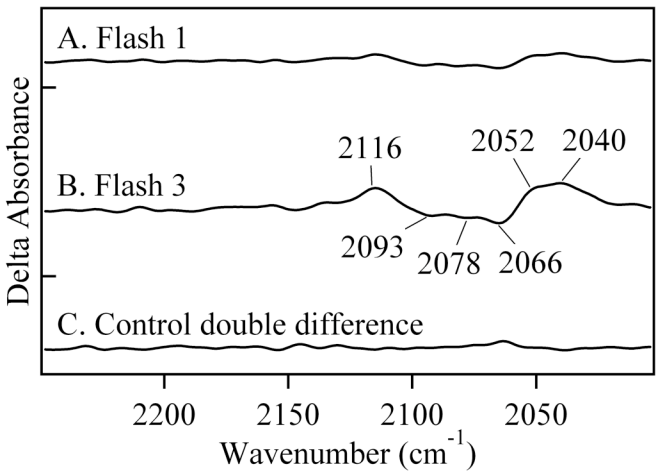

Figure 4. Double difference FT-IR spectra showing perturbations of azide antisymmetric stretching bands. To identify any structural changes at the OEC azide site, manganese-depleted PSII data were subtracted from chloride-depleted PSII data. Double difference spectra were created by subtraction of data shown in figure 2C and D. In (A), subtracted spectra were acquired with one laser flash (figure 2C and D, red). In (B), subtracted spectra were acquired with three laser flashes (figure 2C and D, blue). In (C), a control double difference spectrum, in which no vibrational bands are expected, was generated by subtraction of one half of the data in (figure 2D, red) from the other half of the data set and dividing by the square root of two. Delta absorbance on the y-axis indicates that the spectra show changes in absorbance. All samples contained 1.5 mM recrystallized DCBQ. The tick marks on the y-axis represent $5x10^{-4}$ AU.

antisymmetric stretching band.

A double difference spectrum (figure 4B), chloride-depleted-minus-manganese-depleted, can be used to remove acceptor-side and any other non-OEC azide contributions. This method will identify azide bands, which are due to binding at the OEC azide site and which are perturbed on the second and third flash. This double difference spectrum reveals three negative bands, at 2093, 2078, and 2066 cm^{-1}, which shift both to higher and lower frequency with three flash excitation. The positive bands are observed at 2116, 2052, and 2040 cm^{-1}. The intensities are significant compared to a control double difference spectrum, in which no vibrational bands are expected (figure

4C). The observation of these unique azide spectral features demonstrates that light-induced charge separation perturbs the OEC azide binding site during the S_1 to ($S_2Y_Z^{\bullet}$) S_3' transition in chloride-depleted PSII. The observation of multiple bands may be consistent with multiple azide orientations in its PSII binding site. In the presence of buried charges, the orientation of azide can influence the vibrational frequency through a Stark effect. Alternatively, sulfate treatment or extrinsic subunit removal may introduce heterogeneity at the PSII donor side. Such heterogeneity may cause the structure of the azide binding site to vary slightly from one PSII complex to another.

In the double difference spectrum (figure 4B), negative bands correspond to bound azide in the dark-adapted S_1 state. The antisymmetric stretching vibration of azide is expected at 2050 cm^{-1} in water [53]. In hydrophobic solvents, such as dimethyl sulfoxide, the band shifts down to 2018 cm^{-1} [53]. Protonation of azide upshifts these bands into the 2148-2129 cm^{-1} region [41, 53, 55]. Hydrogen bonding is also expected to upshift the antisymmetric stretching vibration [41]. Therefore, the characteristic frequencies of the observed negative bands in figure 4B, at 2093, 2078, and 2066 cm^{-1}, suggest that azide is bound in the S_1 state in a hydrogen-bonded, but deprotonated form, consistent with the expected azide pK_A of ~ 4.7 [57].

The data acquired with a single flash (figure 3D, red) show that no significant azide frequency perturbation occurs at the azide donor-side site during the S_1 to S_2 transition (see also double difference spectrum, figure 4A). However, the second and third flashes, which generate the S_1 to ($S_2Y_Z^{\bullet}$) S_3' transition (figure 4B), produce two new

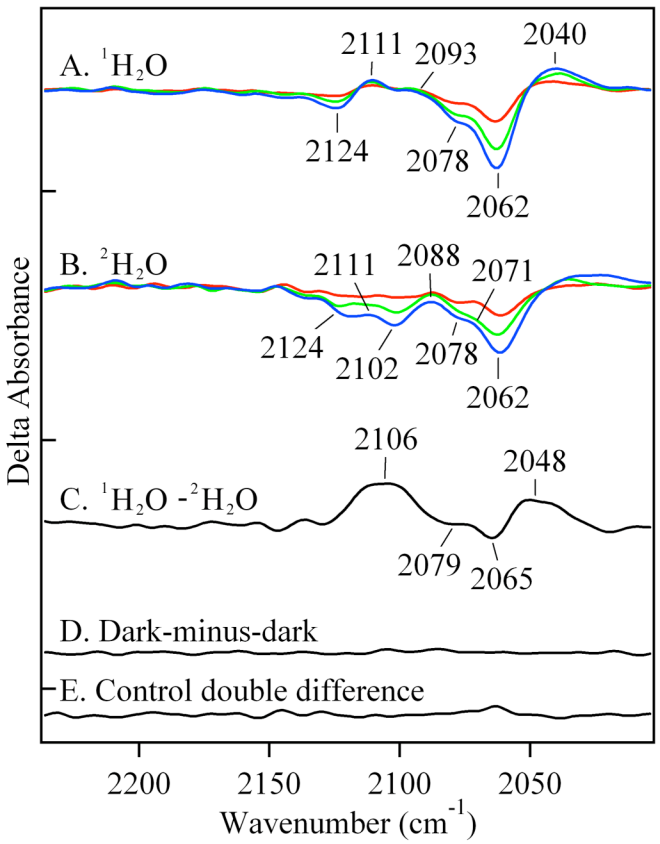

Figure 5. Difference FT-IR spectra showing the effect of solvent isotope exchange on the azide antisymmetric stretching band in chloride-depleted PSII samples. Difference spectra were created by ratio of data taken before and after flash excitation, followed by conversion to absorbance. In (A) and (B), the results of three consecutive 532 nm laser flashes to a preflashed, dark adapted PSII sample are presented in red (flash 1), green (flash 2), and blue (flash 3). In (A), chloride-depleted PSII in ^1H_2O p^{1}H 7.5 buffer contained 15 mM N_3^- (avg. of 39). In (B), chloride-depleted PSII in ^2H_2O p^{2}H 7.5 buffer contained 15 mM N_3^- (avg. of 26). In (C), an isotope-edited, ^1H_2O-minus-^2H_2O, double difference spectrum was generated by subtracting (B, flash 3, blue) from (A, flash 3, blue). In (D), a dark-minus-dark control was generated from the data set in (A). In E, a control double difference spectrum, in which no vibrational bands are expected, was generated by subtraction of one half of the data in (A) from the other half of the data set and dividing by the square root of two. Delta absorbance on the y-axis indicates that the spectra show changes in absorbance. All samples contained 1.5 mM recrystallized DCBQ. The tick marks on the y-axis represent $5x10^{-4}$ AU.

populations of azide, which are reflected as positive spectral bands. Based on the frequencies, both a protonated form (2116 cm^{-1}) and non-hydrogen bonded, anionic forms (2052 and 2040 cm^{-1}) are generated.

To test this interpretation, reaction-induced FT-IR spectra were acquired in azide-containing, chloride-depleted PSII, either in $^{1}H_2O$ (figure 5A) or $^{2}H_2O$ buffers (figure 5B). Solvent isotope exchange is expected to downshift the frequencies of protonated and hydrogen bonded forms of azide [58-60]. The effect of solvent isotope exchange is shown in a double difference, $^{1}H_2O$-minus-$^{2}H_2O$, spectrum (figure 5C). A positive band at ~ 2106 cm^{-1} is observed to shift to 2079 cm^{-1} and a negative band at 2065 cm^{-1} is observed to shift to 2048 cm^{-1}. These shifts are consistent with assignment of the positive 2116 cm^{-1} band (figure 4B) to protonated azide and the negative 2066 cm^{-1} band (figure 4B) to hydrogen-bonded azide, as described below. The isotope shifts for the other positive and negative bands are not discernable from the isotope-edited spectrum. These results suggest that, during the S_1 to ($S_2Y_Z^{\bullet}$) S_3' transition, azide acts both as a proton acceptor and a proton donor at the OEC azide site.

Discussion

Azide has been used previously in order to study proton transfer reactions in enzymes. In PSII, azide acts as an inhibitor [38]. In other proteins, azide addition may be stimulatory, due to effects on hydrogen bonding networks in proton transfer pathways [61]. For example, azide has been observed to stimulate proton transfer in site-directed mutants of bacteriorhodopsin, halorhodopsin, and hydroxysteroid dehydrogenase [53, 62-

67]. Previously, azide has also been shown to promote electron and proton transfer to the quinone acceptors in photosynthetic reaction center mutants [57].

We have used the azide antisymmetric stretching vibration as a vibrational probe [53, 55]. The antisymmetric stretching frequency is perturbed by changes in hydrogen bonding, polarity, and metal coordination [41, 53, 55]. Azide vibrational band frequencies are also sensitive to changes in electric fields [68]. Previously, azide has been used as a vibrational probe in bacteriorhodopsin. An increase in 2132 cm^{-1} amplitude was attributed to the transient protonation of azide during proton transfer [53]. Also, in metmyoglobin, shifts in azide bands at 2046 cm^{-1} and 2023/2018 cm^{-1} led to an estimation of the thermal spin equilibrium for high- and low-spin heme, respectively [69, 70].

In our work, reaction-induced difference FT-IR spectra show that the antisymmetric stretching mode of azide is perturbed by PSII charge separation. These data provide evidence for two azide binding sites in PSII. At pH 7.5, perturbation of azide gave rise to derivative-shaped bands, with both positive and negative components, at 2124 (–) /2111 (+), 2102 (–) /2088 (+) cm^{-1} and negative bands at 2078 and 2062 cm^{-1}. We attribute these bands to an acceptor side or other non-OEC azide binding site. These bands were observed both in manganese-depleted PSII, in which the OEC has been removed by Tris treatment, and in oxygen-evolving preparations, which had not been depleted of chloride.

Previous EPR and ESEEM measurements demonstrate that azide also binds to the chloride site near the OEC [26, 39]. In chloride-depleted PSII, we have detected unique azide vibrational bands when a second or third flash induces the S_1 to $(S_2Y_Z^{\bullet})$ S_3'

transition. We assign these bands to donor-side bound azide, because the vibrational frequencies are not observed in manganese-depleted PSII or in PSII, which has not been depleted of chloride. The azide species, which are present in the S_1 state, absorb at 2093 (–), 2078 (–), and 2066 (–) cm^{-1}. These are frequencies characteristic of hydrogen bonded, anionic azide. When the S_3' state is formed, three positive bands are observed. The frequency of the 2116 cm^{-1} band suggests assignment to protonated azide, and the frequencies of the 2052 and 2040 cm^{-1} bands suggest assignment to non-hydrogen bonded or weakly hydrogen bonded anionic azide. Solvent isotope exchange identified a 27 cm^{-1}, 17 cm^{-1}, and non-detectable isotope shift for the positive 2116, negative 2066, and positive 2040 cm^{-1} bands. Previous studies of azide have revealed a deuterium isotope shift of ~ 30 cm^{-1} for the protonated species [59, 60] and a ~ 8 cm^{-1} shift for the hydrogen bonded, anionic species [58]. Therefore, the results of solvent isotope exchange are consistent with the attribution of the 2116, 2066, and 2040 cm^{-1} bands to protonated azide, hydrogen-bonded anionic azide, and non-hydrogen bonded (or weakly hydrogen bonded) anionic azide, respectively.

These results suggest that a heterogeneous proton-coupled electron transfer reaction occurs at the OEC azide site during the S_1 to ($S_2Y_Z^{\bullet}$) S_3' transition. Bound, hydrogen-bonded azide molecules both protonate and deprotonate. While manganese oxidation does not occur on the second flash or third flash in chloride-depleted samples [28-34], the proton transfer reactions may be driven by conformational changes, linked to Y_Z oxidation. Therefore, our results are consistent with the conclusion that proton transfer reactions occur before the manganese oxidation reaction, as previously suggested [12, 14]. During the S_1 to S_2 transition, bands attributable to protonation of azide are not

observed in our chloride-depleted samples. This result is consistent with previous suggestions that the S_1 to S_2 transition involves uncompensated electron transfer and no net proton transfer [37, 71, 72].

Taken together, our results suggest that azide may establish a perturbed hydrogen bond network near the OEC. We propose that azide inhibits oxygen evolution by disruption or rearrangement of the normal hydrogen bond network, which is necessary for proton-coupled electron transfer reactions in the OEC. Because azide exhibits mixed inhibition and competes at the chloride site, this interpretation may also imply a role for chloride in PSII proton transfer reactions. Finally, our data support the interpretation that proton transfer reactions at the OEC azide site precede manganese oxidation reactions [12, 14, 24], at least in chloride-depleted PSII.

References

1. Nelson, N. and C.F. Yocum, *Structure and function of photosystems I and II.* Annu Rev Plant Biol, 2006. **57**: p. 521-565.

2. Yocum, C.F., *The calcium and chloride requirements of the O_2 evolving complex.* Coord Chem Rev, 2008. **252**: p. 296-305.

3. Zouni, A., et al., *Crystal structure of photosystem II from Synechococcus elongatus at 3.8 Å resolution.* Nature, 2001. **409**: p. 739-743.

4. Kamiya, N. and J.-R. Shen, *Crystal structure of oxygen-evolving photosystem II from Thermosynechococcus vulcanus at 3.7 Å resolution.* Proc Natl Acad Sci USA, 2003. **100**: p. 98-103.

5. Biesiadka, J., et al., *Crystal structure of cyanobacterial photosystem II at 3.2 Å resolution: a closer look at the Mn-cluster.* Phys Chem Chem Phys, 2004. **6**: p. 4733-4736.

6. Ferreira, K.N., et al., *Architecture of the photosynthetic oxygen-evolving center.* Science, 2004. **303**: p. 1831-1837.

7. Loll, B., et al., *Towards complete cofactor arrangement in the 3.0 Å resolution structure of photosystem II.* Nature, 2005. **438**: p. 1040-1044.

8. Yano, J., et al., *X-ray damage to the Mn_4Ca complex in single crystals of photosystem II: A case study for metalloprotein crystallography.* Proc Natl Acad Sci USA, 2005. **102**: p. 12047-12052.

9. Grabolle, M., et al., *Rapid loss of structural motifs in the manganese complex of oxygenic photosynthesis by X-ray irradiation at 10-300 K.* J Biol Chem, 2006. **281**: p. 4580-4588.

10. Kok, B., B. Forbush, and M. McGloin, *Cooperation of charges in photosynthetic O_2 evolution-I. A linear four step mechanism.* Photochem Photobiol, 1970. **11**: p. 457-475.

11. Dekker, J.P., et al., *Absorbance difference spectra of the successive redox states of the oxygen-evolving apparatus of photosynthesis.* Biochim Biophys Acta, 1984. **767**: p. 1-9.

12. Haumann, M., et al., *Photosynthetic O_2 formation tracked by time-resolved X-ray experiments.* Science, 2005. **310**: p. 1019-1021.

13. Razeghifard, M.R. and R.J. Pace, *EPR kinetic studies of oxygen release in thylakoids and PSII membranes: a kinetic intermediate in S_3 to S_0 transition.* Biochemistry, 1999. **38**: p. 1252-1257.

14. Barry, B.A., et al., *Time-resolved vibrational spectroscopy detects protein-based intermediates in the photosynthetic oxygen-evolving cycle.* Proc Natl Acad Sci USA, 2006. **103**: p. 7288-7291.

15. Clausen, J. and W. Junge, *Detection of an intermediate of photosynthetic water oxidation.* Nature, 2004. **430**: p. 480-483.

16. Sandusky, P.O. and C.F. Yocum, *The chloride requirement for photosynthetic oxygen evolution. Analysis of the effects of chloride and other anions on amine inhibition of the oxygen evolving complex.* Biochim Biophys Acta, 1984. **766**: p. 603-611.

17. Sandusky, P.O. and C.F. Yocum, *The chloride requirement for photosynthetic oxygen evolution: Factors affecting nucleophilic displacement of chloride from the oxygen-evolving complex.* Biochim Biophys Acta, 1986. **849**: p. 85-93.

18. Lindberg, K. and L.-E. Andreasson, *A one-site, two-state model for the binding of anions in photosystem II.* Biochemistry, 1996. **35**: p. 14259-14267.

19. Olesen, K. and L.-E. Andreasson, *The function of the chloride ion in photosynthetic oxygen evolution.* Biochemistry, 2003. **42**: p. 2025-2035.

20. Lindberg, K., T. Vanngard, and L.-E. Andreasson, *Studies of the slowly exchanging chloride in photosystem II of higher plants.* Photosynth Res, 1993. **38**: p. 401-408.

21. Clemens, K.L., D.A. Force, and R.D. Britt, *Acetate binding at the photosystem II oxygen evolving complex: an S_2-state multiline signal ESEEM study.* J Am Chem Soc, 2002. **124**: p. 10921-10933.

22. Hasegawa, K., Y. Kimura, and T.-a. Ono, *Oxidation of the Mn cluster induces structural changes of NO_3^- functionally bound to the Cl^- site in the oxygen-evolving complex of photosystem II.* Biophys J, 2004. **86**: p. 1042-1050.

23. Haumann, M., et al., *Bromide does not bind to the Mn_4Ca complex in Its S_1 state in Cl^--depleted and Br^--reconstituted oxygen-evolving photosystem II: Evidence from X-ray absorption spectroscopy at the Br K-edge.* Biochemistry, 2006. **45**: p. 13101-13107.

24. Cooper, I.B. and B.A. Barry, *Perturbations at the chloride site during the photosynthetic oxygen-evolving cycle.* Photosynth Res, 2007. **92**: p. 345-354.

25. van Vliet, P. and A.W. Rutherford, *Properties of the chloride-depleted oxygen-evolving complex of photosystem II studied by electron paramagnetic resonance.* Biochemistry, 1996. **35**: p. 1829-1839.

26. Haddy, A., R.A. Kimel, and R. Thomas, *Effects of azide on the S_2 state EPR signals from photosystem II.* Photosynth Res, 2000. **63**: p. 35-45.

27. Hasegawa, K., Y. Kimura, and T.-a. Ono, *Chloride cofactor in the photosynthetic oxygen-evolving complex studied by Fourier transform infrared spectroscopy.* Biochemistry, 2002. **41**: p. 13839-13850.

28. Itoh, S., et al., *Effects of chloride depletion on electron donation from the water-oxidizing complex to the photosystem II reaction center as measured by the microsecond rise of chlorophyll fluorescence in isolated pea chloroplasts.* Biochim Biophys Acta, 1984. **766**: p. 612-622.

29. Ono, T.-a., et al., *EPR evidence for a modified S state transition in chloride-depleted photosystem II.* Biochim Biophys Acta, 1986. **851**: p. 193-201.

30. Deak, Z., I. Vass, and S. Strying, *Redox interaction of tyrosine-D with the S-states of the water-oxidizing complex in intact and chloride-depleted photosystem II.* Biochim Biophys Acta, 1994. **1185**: p. 65-74.

31. Ono, T.-a., et al., *XANES spectroscopy for monitoring intermediate reaction states of Cl^--depleted Mn cluster in photosynthetic water oxidation enzyme.* J Am Chem Soc, 1995. **117**: p. 6386-6387.

32. Wincencjusz, H., H.J. van Gorkom, and C.F. Yocum, *The photosynthetic oxygen evolving complex requires chloride for its redox state $S_2 \rightarrow S_3$ and $S_3 \rightarrow S_0$ transitions but not for $S_0 \rightarrow S_1$ or $S_1 \rightarrow S_2$ transitions.* Biochemistry, 1997. **36**: p. 3663-70.

33. Wincencjusz, H., C.F. Yocum, and H.J. van Gorkom, *S-state dependence of chloride binding affinities and exchange dynamics in the intact and polypeptide-depleted O_2 evolving complex of photosystem II.* Biochemistry, 1998. **37**: p. 8595-8604.

34. Wincencjusz, H., C.F. Yocum, and H.J. van Gorkom, *Activating anions that replace Cl^- in the O_2-evolving complex of photosystem II slow the kinetics of the terminal step in water oxidation and destabilize the S_2 and S_3 states.* Biochemistry, 1999. **38**: p. 3719-3725.

35. Homann, P.H., *The relations between chloride, calcium, and polypeptide requirements of photosynthetic water oxidation.* J Bioenerg Biomembr, 1987. **19**: p. 105-123.

36. Boussac, A. and A.W. Rutherford, *Electron transfer events in chloride-depleted photosystem II.* J Biol Chem, 1994. **269**: p. 12462-12467.

37. McEvoy, J.P. and G.W. Brudvig, *Structure-based mechanism of photosynthetic water oxidation.* Phys Chem Chem Phys, 2004. **6**: p. 4754-4763.

38. Haddy, A., et al., *Azide as a competitor of chloride in oxygen evolution by photosystem II.* Biochemistry, 1999. **38**: p. 6104-6110.

39. Yu, H., et al., *Evidence that azide occupies the chloride binding site near the manganese cluster in photosystem II.* Biochemistry, 2005. **44**: p. 12022-12029.

40. Cao, J. and Govindjee, *Anion effects on the electron acceptor side of photosystem II in a transformable cyanobacterium Synechocystis 6803*, in *Current Research in Photosynthesis*, M. Baltscheffsky, Editor. 1990, Kluwer Academic Publishers: Dortrecht. p. 515-518.

41. Garcia-Viloca, M., et al., *Solvent and protein effects on the vibrational frequency shift and energy relaxation of the azide ligand in carbonic anhydrase.* J Phys Chem B, 2004. **108**(35): p. 13501-13512.

42. Noguchi, T. and M. Sugiura, *Flash-induced Fourier transform infrared detection of the structural changes during the S-state cycle of the oxygen-evolving complex in photosystem II.* Biochemistry, 2001. **40**: p. 1497-1502.

43. Hillier, W. and G.T. Babcock, *S-state dependent Fourier transform infrared difference spectra for the photosystem II oxygen evolving complex.* Biochemistry, 2001. **40**: p. 1503-1509.

44. Yamanari, T., et al., *Mid- to low-frequency Fourier transform infrared spectra of S-state cycle for photosynthetic water oxidation in Synechocystis sp. PCC 6803.* Biochemistry, 2004. **43**: p. 7479-7490.

45. Debus, R.J., et al., *No evidence from FTIR difference spectroscopy that aspartate-170 of the D1 polypeptide ligates a manganese ion that undergoes oxidation during the S_0 to S_1, S_1 to S_2, or S_2 to S_3 transitions in photosystem II.* Biochemistry, 2005. **44**: p. 1367-1374.

46. Barry, B.A., et al., *Calcium ligation in photosystem II under inhibiting conditions.* Biophys J, 2005. **89**: p. 393-401.

47. DeRiso, A., D.L. Jenson, and B.A. Barry, *Calcium exchange and structural changes during the photosynthetic oxygen evolving cycle.* Biophys J, 2006. **91**: p. 1999-2008.

48. Berthold, D.A., G.T. Babcock, and C.F. Yocum, *A highly resolved, oxygen-evolving photosystem II preparation from spinach thylakoid membranes.* FEBS Lett, 1981. **134**: p. 231-234.

49. Barry, B.A., *Tyrosyl radicals in photosystem II.* Methods Enzymol, 1995. **258**: p. 303-319.

50. Yamamoto, Y., et al., *Release of polypeptides from highly active O_2-evolving photosystem-2 preparation by tris treatment.* FEBS Lett, 1981. **133**: p. 265-268.

51. Jenson, D.L., A. Evans, and B.A. Barry, *Proton-coupled electron transfer and tyrosine D of photosystem II.* J Phys Chem B, 2007. **111**: p. 12599-12604.

52. Lindberg, K., et al., *Slow release of chloride from ^{36}Cl-labeled photosystem II membranes.* FEBS Lett, 1990. **264**: p. 153-155.

53. Le Coutre, J., et al., *Experimental evidence for hydrogen-bonded network proton transfer in bacteriorhodopsin shown by Fourier-transform infrared spectroscopy using azide as catalyst.* Proc Natl Acad Sci USA, 1995. **92**: p. 4962-4966.

54. Guijarro, J., M. Engelhard, and F. Siebert, *Binding of anions to halorhodopsin from natronobacterium pharaonis studied by static and time-resolved FTIR spectroscopy.* Biophys J, 2003. **84**: p. 270A-270A.

55. Agrell, I., *The infra-red spectra of some inorganic azide compounds.* Acta Chem Scand, 1971. **25**: p. 2965-2974.

56. Ono, T.-a., et al., *Effect of preillumination on the P-680^{+} reduction kinetics in chloride-free photosystem II membranes.* FEBS Lett, 1986. **203**: p. 215-219.

57. Takahashi, E. and C.A. Wraight, *Small weak acids stimulate proton transfer events in site-directed mutants of the two ionizable residues, glu^{L212} and asp^{L213}, in the Q_B-binding site of Rhodobacter sphaeroides reaction center.* FEBS Lett, 1991. **283**: p. 140-144.

58. Li, M., et al., *Vibrational and rotational relaxation times of solvated molecular ions.* J Chem Phys, 1993. **98**: p. 5499-5507.

59. Bendtsen, J. and G. Guelachvili, *High-resolution infrared absorption spectrum of the v_2 band of hydrazoic acid (HN_3).* J Mol Spectrosc, 1994. **165**: p. 159-167.

60. Hansen, C.S., J. Bendtsen, and F.M. Nicolaisen, *Analyses of the high-resolution infrared absorption spectra of the v_2 and v_3 bands of deuterated hydrazoic acid (DN_3).* J Mol Spectrosc, 1996. **175**: p. 239-245.

61. Steinhoff, H.-J., et al., *Azide reduces the hydrophobic barrier of the bacteriorhodopsin proton channel.* Biophys J, 1999. **76**: p. 2702-2710.

62. Tittor, J., et al., *A defective proton pump, point-mutated bacteriorhodopsin asp96 → asn is fully reactivated by azide.* EMBO J, 1989. **8**: p. 3477-3483.

63. Váró, G., et al., *Proton transport by halorhodopsin.* Biochemistry, 1996. **35**: p. 6604-6611.

64. Misra, S., et al., *Proton uptake and release are rate-limiting steps in the photocycle of the bacteriorhodopsin mutant E204Q.* Biochemistry, 1997. **36**: p. 4875-4883.

65. Schmies, G., et al., *Sensory rhodopsin II from the haloalkaliphilic Natronobacterium pharaonis: light-activated proton transfer reactions.* Biophys J, 2000. **78**: p. 967-976.

66. Hein, M., et al., *Time-resolved FTIR studies of sensory rhodopsin II (NpSRII) from Natronobacterium pharaonis: Implications for proton transport and receptor activation.* Biophys J, 2003. **84**: p. 1208-1217.

67. Chang, Y.H., L.Y. Chuang, and C.C. Hwang, *Mechanism of proton transfer in the 3 alpha-hydroxysteroid dehydrogenase/carbonyl reductase from Comamonas testosteroni.* J Biol Chem, 2007. **282**: p. 34306-34314.

68. Suydam, I.T. and S.G. Boxer, *Vibrational Stark effects calibrate the sensitivity of vibrational probes for electric fields in proteins.* Biochemistry, 2003. **42**: p. 12050-12055.

69. Bogumil, R., et al., *FTIR analysis of the interaction of azide with horse heart myoglobin variants.* Biochemistry, 1994. **33**: p. 7600-7608.

70. Maurus, R., et al., *Structural and spectroscopic studies of azide complexes of horse heart myoglobin and the His-64→Thr variant.* Biochem J, 1998. **332**: p. 67-74.

71. Messinger, J., *Evaluation of different mechanistic proposals for water oxidation in photosynthesis on the basis of Mn_4O_xCa structures for the catalytic site and spectroscopic data.* Phys Chem Chem Phys, 2004. **6**: p. 4764-4771.

72. McEvoy, J.P. and G.W. Brudvig, *Water-splitting chemistry of photosystem II.* Chem Rev, 2006. **106**: p. 4455-4478.

CHAPTER 6

CONCLUSIONS

The energy needs of the earth's biosphere as well as the enrichment of oxygen in our atmosphere are provided by the membrane-bound, oxidoreductase protein complex known as photosystem II (PSII). PSII utilizes the sun's energy to oxidize water to molecular oxygen while providing electrons used for the fixation of carbon into sugars. Multiple investigations into the structure of PSII have revealed the electron transfer cofactors involved in water oxidation to 3.0 Å resolution [1-5]. Details of the structure have lead to speculation about the role each cofactor plays in water splitting chemistry.

We have shown that the kinetics of photosynthetic electron transfer can be monitored through the use of time-resolved vibrational spectroscopy. Focusing on flash-induced changes in infrared absorption at single wavelengths has allowed us to identify cofactors and amino acids involved in water oxidation. Among these intermediates, the transient S_4 state, during which oxygen release occurs, has been detected. This intriguing step in water oxidation has been studied by other techniques [6-8], and information about this step will lead to a better understanding of O-O bond formation. We have observed the classic perioud-four oscillation associated with oxygen release in our derived rate constants, and our results indicate that proton transfer may precede manganese oxidation during the S_2-to-S_3 and S_3-to-S_0 transitions. We assign the signal observed at 1483 cm^{-1} to perturbation of histidine near the OEC.

Having established the utility of time-resolved vibrational spectroscopy, we used the technique to study the mechanism of proton-coupled electron transfer (PCET) associated with the function of redox-active Y_Z. In Mn-depleted PSII, we observed microseond decay kinetics attributable to $Y_Z^{\bullet}$ decay. We also observed millisecond decay kinetics assignable to charge recombination between $Y_Z^{\bullet}$ and Q_A^{-}. Based on the solvent isotope effect calculated by comparing experiments in ^1H_2O and ^2H_2O, we suggest a concerted proton-electron transfer (CPET) pathway for $Y_Z^{\bullet}$ reduction. This study contrasts with a previous study monitoring PCET reactions involving tyrosine D (Y_D), another redox-active tyrosine in PSII [9]. In this study, coupled proton-electron transfer (CPET) was suggested at high pH while PTET was suggested at low pH. These two studies underscore the differences in the protein environments surrounding Y_Z and Y_D, and they address the different roles each residue plays in the function of PSII.

To summarize these new studies using time-resolved infrared spectroscopy, we have gained novel information about protein- and cofactor-based intermediates of photosynthetic water oxidation. Specifically, we have detected the elusive S_4 state and suggest that proton transfer reactions precede manganese oxidation. We have also shown that $Y_Z^{\bullet}$ reduction may follow a coupled proton-electron transfer mechanism, based on pL and solvent isotope effects.

Information gained from kinetic experiments using time-resolved vibrational spectroscopy is supplemented by the broad spectral resolution of Fourier-transform infrared (FT-IR) spectroscopic studies of PSII. Using reaction-induced difference spectroscopy, we have provided evidence for the potential binding site of chloride. Though chloride has not been identified in crystal structures [4, 5], it is a necessary

cofactor in water oxidation (reviewed in [10]). Comparing bromide-reconsituted and chloride-reconstituted PSII, vibrational band shifts were identified and attributed to arginine or lysine sidechains that may form the putative chloride binding site. Indeed, arginine 357 of the CP43 subunit is placed only 5 Å away from manganese in a recent crystal structure [5] and has been implicated in proton transfer events during water oxidation [11]. Future site-directed mutagenesis studies will test the hypothesis that CP43-R357 is the chloride binding site.

In another reaction-induced difference FT-IR study, we used azide (N_3^-) to probe proton transfer reactions at the oxygen-evolving complex (OEC). The asymmetric stretching vibration of azide is sensitive to protonation and hydrogen bonding [12]. The asymmetric stretching vibration falls outside the region of protein and cofactor infrared absorption [13]. Also, azide is an inhibitor of oxygen evolution [14] and has been shown to bind at the chloride site near the OEC [15]. This evidence shows that azide can be an ideal spectroscopic probe of proton transfer reactions. We show that when PSII is flashed, azide is transiently protonated and deprotonated at the OEC. Our results also indicate that proton transfer reactions may precede manganese oxidation in our PSII preparations and that rearrangement of necessary proton transfer pathways may be the mechanism of azide inhibition of PSII.

To summarize these new studies using reaction-induced difference FT-IR spectroscopy, we have shown that arginine or lysine sidechains may be perturbed by addition of bromide to chloride-depleted PSII. The data indicate that arginine or lysine may make up the chloride binding site in the OEC. In a similar study, we have shown that azide in transiently protonated and deprotonated when bound at the chloride site in

the OEC. From the data, we suggest that azide inhibits PSII by altering proton transfer networks required for water oxidation. The data also suggest a role for chloride in proton transfer reaction in the OEC.

In this body of work, the chemistry and mechanism of photosynthetic water oxidation have been investigated. Through the use of vibrational spectroscopy, insights into the details of inorganic cofactor involvment and proton-coupled electron transfer reactions have been elucidated. The studies presented here supplement and enhance the existing body of knowledge concerning the biological conversion of water to molecular oxygen, protons, and electrons. A deeper understanding of the physical mechanism, thermodynamic controls, and elegant precision of photosynthetic water oxidation can aid in the design of biomimetic systems. Such systems can harness the energy of the sun to provide energy alternatives to nuclear and fossil fuel sources of today.

References

1. Zouni, A., et al., *Crystal structure of photosystem II from Synechococcus elongatus at 3.8 Å resolution.* Nature, 2001. **409**: p. 739-743.

2. Kamiya, N. and J.-R. Shen, *Crystal structure of oxygen-evolving photosystem II from Thermosynechococcus vulcanus at 3.7 Å resolution.* Proc Natl Acad Sci USA, 2003. **100**: p. 98-103.

3. Biesiadka, J., et al., *Crystal structure of cyanobacterial photosystem II at 3.2 Å resolution: a closer look at the Mn-cluster.* Phys Chem Chem Phys, 2004. **6**: p. 4733-4736.

4. Ferreira, K.N., et al., *Architecture of the photosynthetic oxygen-evolving center.* Science, 2004. **303**: p. 1831-1837.

5. Loll, B., et al., *Towards complete cofactor arrangement in the 3.0 Å resolution structure of photosystem II.* Nature, 2005. **438**: p. 1040-1044.

6. Razeghifard, M.R. and R.J. Pace, *EPR kinetic studies of oxygen release in thylakoids and PSII membranes: a kinetic intermediate in S_3 to S_0 transition.* Biochemistry, 1999. **38**: p. 1252-1257.

7. Clausen, J. and W. Junge, *Detection of an intermediate of photosynthetic water oxidation.* Nature, 2004. **430**: p. 480-483.

8. Haumann, M., et al., *Photosynthetic O_2 formation tracked by time-resolved X-ray experiments.* Science, 2005. **310**: p. 1019-1021.

9. Jenson, D.L., A. Evans, and B.A. Barry, *Proton-coupled electron transfer and tyrosine D of photosystem II.* J Phys Chem B, 2007. **111**: p. 12599-12604.

10. Popelkova, H. and C.F. Yocum, *Current status of the role of Cl^- in the oxygen-evolving complex.* Photosynth Res, 2007. **93**: p. 111-121.

11. McEvoy, J.P. and G.W. Brudvig, *Structure-based mechanism of photosynthetic water oxidation.* Phys Chem Chem Phys, 2004. **6**: p. 4754-4763.

12. Le Coutre, J., et al., *Experimental evidence for hydrogen-bonded network proton transfer in bacteriorhodopsin shown by Fourier-transform infrared spectroscopy using azide as catalyst.* Proc Natl Acad Sci USA, 1995. **92**: p. 4962-4966.

13. Agrell, I., *The infra-red spectra of some inorganic azide compounds.* Acta Chem Scand, 1971. **25**: p. 2965-2974.

14. Haddy, A., et al., *Azide as a competitor of chloride in oxygen evolution by photosystem II.* Biochemistry, 1999. **38**: p. 6104-6110.

15. Yu, H., et al., *Evidence that azide occupies the chloride binding site near the manganese cluster in photosystem II.* Biochemistry, 2005. **44**: p. 12022-12029.

VITA

IAN BLAKE COOPER

COOPER was born in Atlanta, Georgia. He attended public schools in Dunwoody, Georgia. He received a B.S. in Chemistry from Berry College, Mount Berry, Georgia in 2002 before coming to Georgia Tech to pursue a doctorate in Physical Chemistry. When he is not working on his research, Mr. Cooper enjoys playing music, developing leadership in young adults, and hiking with his wife, Robyn.